# Design of supramolecular nanomaterials

**From molecular recognition to hierarchical self-assembly**

Inauguraldissertation

zur

Erlangung der Würde eines Doktors der Philosophie

vorgelegt der

Philosophisch-Naturwissenschaftlichen Fakultät

der Universität Basel

von

**Mohamed El Idrissi**

Aus Frankreich/Marokko

Basel 2017

Genehmight von der Philosophisch-Naturwissenschaftlichen Fakultät auf Antrag von


Prof. Dr. Wolfang Meier

Prof. Dr. Patrick Shahgaldian

Prof. Dr. Florent Perret


Basel, 21 February 2017


Prof. Dr. Martin Spiess

*It is not the critic who counts, nor the man who points out how the strong man stumbled, or where the doer of deeds could have done them better. The credit belongs to the man who is actually in the arena; whose face is marred by dust and sweat and blood; who strives valiantly; who errs and comes short again and again; who knows the great enthusiasms, the great devotions, and spends himself in a worthy cause; Who, at the best, knows in the end, the triumph of high achievement; and who, at the worst, if he fails, fails while daring greatly, so that his place shall never be with those cold and timid souls who know neither victory nor defeat.*

**-Theodore Roosevelt**
*From the speech "Citizenship in a Republic" delivered at the Sorbonne, Paris, 1910.*

*There is no shortcut to success.*

**- Unknown source**

*For my beloved parents,*
*who sacrificed their life for mine.*

# Acknowledgements

First and foremost I would like to express my sincere gratitude to my PhD supervisor Prof. Dr. Patrick Shahgaldian. He has been an excellent coach, a great adviser and a good friend for me. It has been a great pleasure working and learning on his side and I did appreciate the trust and confidence he placed in me throughout my PhD thesis. He knew how to get me out of my comfort zone and to do "better" when it was already "good". Thanks to him I learned a lot about chemistry and science. It has been a unique and wonderful experience where I have not only grown up as scientist but where I also learnt a lot on my person.

I would like also to thank my doctor father at the university of Basel, Prof. Dr. Meier, without who my PhD thesis would not have been possible. I want to thank him for the support, the trust and to allow me to work efficiently with great freedom.

I want to deeply thank the members of my doctoral committee, Prof. Dr. Palivan, Prof. Dr. Perret, Prof. Dr. Meier and Prof. Dr. Shahgaldian for the work and time they placed in the evaluation of my thesis and their contribution in the success of this PhD thesis.

I also want to thank Pr. Dr. Scott Dalgarno for his collaboration and scientific input on my work and I am grateful for the rigorous work he provided, along with Prof. Dr. Martin J. Paterson and Prof. Dr. Simon J. Teat, on the crystal structure of the pyrene derivative.

I would like to thank Dr. Aurora Molina for her kindness and efficient collaboration during our long hours spent working on the pilot plant and phenolic compounds. I would also want to thank Dr. Dario Frascari for his collaboration on the KillSpill project. I am as well grateful for the nice work SIMA-tec provided with the pilot plant.

I would like to thank also Prof. Dr. Philippe Corvini for his kind collaboration and for providing me with laboratory facilities, and all the members of his group with who I collaborated. I would like to thank especially Dr. Nora Corvini who carried out the experiments with bacteria.

# Abstract

In the present thesis, are reported new strategies for the design of nanostructures to partly address environmental issues. The work carried out has been divided into three parts: the design of cyclodextrin (CD)-based polymeric materials, the molecular engineering of a pyrene derivative for the formation of self-assembled nanostructures and the design of smart nanocarriers.

Considerable efforts have been devoted to the design of molecular receptors capable of specific recognition of a wide variety of targets ranging from small inorganic ions to large biomolecules. These molecular receptors have been widely used to produce (nano)materials with superior molecular recognition properties. While these materials have been extensively studied for biomedical applications, their use in environmental sciences or biotechnology has been, to some extent, neglected.

Supramolecular materials, because of their superior molecular recognition properties may find a wealth of new applications for the selective removal of harmful or valuable targets from industrial waste streams. While the specific recovery of valuable chemicals from waste streams represents an environmentally-friendly and potentially economically-relevant alternative to synthetic chemical productions, it remains a largely unmet challenge. This is partially explained by the complexity of designing sorption materials able to target one specific compound and able to function in complex matrices.

In this manuscript, is reported the synthesis of a series of CD-based polymers (CDPs) designed to selectively extract phenolic compounds from a complex organic matrix that is OMW. In order to endow these polymers with selective adsorption properties, several monomers and cross-linkers were screened and selected. The adsorption properties of the CDPs produced were first tested with selected phenolic compounds commonly found in OMW, namely syringic acid, *p*-coumaric acid, tyrosol (TY) and caffeic acid. The selected CDPs were subsequently tested for their ability to adsorb phenolic compounds directly from OMW, which is known to possess a high and complex organic content. Adsorption models and adsorption kinetics were studied and allowed to set a new method on a pilot plant. It was demonstrated through liquid chromatography-mass spectroscopy (LC-MS) analyses that efficient removal of phenolic compounds from OMW could be achieved but also that two compounds, namely TY and

hydroxytyrosol (HT), could be selectively extracted from OMW. The chemical oxygen demand (COD) level which is correlated to the amount of organic compounds was also reduced in the recovered fractions after extraction of the phenolic compounds, which makes the recovered waters relevant for irrigation purposes.

The use of CD-based polymeric materials for the removal of valued added molecules could represent a new approach that will benefit from the ease of production of CDP and cost.

Nature represents an inexhaustible source of inspiration for elegant hierarchically assembled structures and biology is replete with numerous examples of highly complex self-assembled structures. From cell membranes to proteins and viruses, the precise internal organisation of these biological structures is based on non-covalent interactions of subunits. Self-assembly strategies have been extensively exploited for the creation of supramolecular entities due to the complex synthesis of large structures through covalent synthetic strategies. Bottom-up approaches permit to build large and complex supramolecular assemblies through the interactions of building blocks.

The accurate molecular design of organic building blocks is of great importance for the creation of large supramolecular entities with precise dimensional organisation. In this PhD thesis, we report the synthesis and template-free hierarchical self-assembly of a novel pyrene derivative into well-defined nanorods. The formation and the three dimensional packing of this pyrene derivative into nanorods were studied by means of fluorescence and UV-Vis spectroscopy, scanning electron microscopy, single crystal and powder X-ray diffraction studies.

Nowadays oil and hydrocarbons cover most of our energy needs. In 2008, the world demand reached 85.62 million barrels/day.[1] Consequently spill accidents cause also considerable damages and water contamination by oil spills represents a major global problem. Several approaches for the degradation of oil spills are available including mechanical removal, wiping with absorbent materials or booming and skimming, but these techniques stay fairly limited in efficiency. Besides these methods, bioremediation has emerged as one of the most promising treatment for oil spill. Bioremediation is divided into two branches, biostimulation and bioaugmentation. We propose in this thesis an alternative way to overcome dilution related issues in biostimulation to degrade hydrocarbons through the stimulation of the microbial growth to increase the rate and efficiency of hydrocarbons degradation. The system

would be able then to target specifically the oil phase and avoid any dilution of the needed nutrients into the sea, which should lead to a higher performance of the bacteria.

We reported in this manuscript the synthetic strategy to produce what we named "Smart Gates Particles" (SGPs) that can act as nanocarriers and deliver specifically the nutrients to bacteria. The loading and kinetic releases of the nutrients contained in the SGPs have been studied in different environments, water and mixture oil/water. The design of such particles represents an alternative and ecological way to overcome the dilution or the non-targeted release of nutrients for oil-degrading bacteria.

# TABLE OF CONTENT

# List of figures

# Abbreviations

| | |
|---|---|
| 1D | one dimensional |
| AFM | atomic force microscopy |
| AIBN | azobisisobutyronitrile |
| APTES | (3-aminopropyl)triethoxysilane |
| AU | arbitrary unit |
| BET | Brunauer–Emmett–Teller |
| BOD | biochemical oxygen demand |
| CD | cyclodextrin |
| CDP | cyclodextrin based-polymer |
| CFU | colony forming unit |
| COD | chemical oxygen demand |
| CTAB | cetyltrimethylammonium bromide |
| DBTDL | dibutyltin dilaurate |
| DFT | density functional theory |
| DHBA | dihydroxybenzoic acid |
| DHNA | 1,4-dihydroxy-2-naphthoic acid |
| DHTA | 2,5-dihydroxyterephtalic acid |
| DLS | dynamic light scattering |
| DMPA | 2,2-bis(hydroxymethyl)propionic acid |
| EDC | 1-ethyl-3-(3-dimethylaminopropyl)carbodiimide |
| EPI | epichlorohydrin |
| FE-SEM | field emission scanning electron microscopy |

| FE-SEM | field-emission scanning electron microscopy |
|---|---|
| FTIR | Fourier-transform infrared spectroscopy |
| HDI | hexamethylene diisocyanate |
| HPLC | high performance liquid chromatography |
| HT | hydroxytyrosol |
| LC-MS | liquid chromatography-mass spectrometry |
| MALDI-TOF | matrix-assisted laser desorption/ionization time of flight mass spectroscopy |
| MDI | 4,4'-methylene diphenyl diisocyanate |
| Me-β-CD | methyl- β-cyclodextrin |
| MNP | magnetic nanoparticle |
| NMR | nuclear magnetic resonance |
| OMW | olive oil mill wastewater |
| OPV | oligo(*p*-phenylenevinylene) |
| PBA | pyrene butyric acid |
| PBI | perylene bisimide |
| PDI | 1,4-phenylene diisocyanate |
| PySi | N-(3-(triethoxysilane)propyl)pyrene butylamide |
| SDA | structure-directing agent |
| TD-DFT | time dependant-density functional theory |
| TEM | transmission electron microscopy |
| TEOS | tetraethoxysilane |
| TFA | trifluoroacetic acid |
| TY | tyrosol |

# Chapter 1

# Introduction

# 1. Supramolecular material

The plethora of chemical reactions identified over the years had led chemists to design molecules with an extremely precise control of reactivity. Over time and with a significant work from Linus Pauling in the 1930's,[2] a comprehensive understanding of the nature of covalent bonding has been established. However, the complete control of the interactions that govern the dynamic assembly of chemical entities is still an unmet challenge.

## 1.1 Supramolecular chemistry

Lehn coined the name "supramolecular chemistry" in 1978,[3] but breakthrough in this field came 20 year before, by Pedersen, with the synthesis of crown ethers.[4] Cram, with his work on cryptand,[5] and Lehn with the synthesis of ion selective receptors,[6-7] joined Pederson in winning the Nobel Prize in chemistry in 1987 for their development and use of molecules with structure-specific interactions of high selectivity. All together they allowed supramolecular chemistry to become a recognised and vivid domain of chemistry.

Before it was recognised as a field of study in its own, supramolecular chemistry was already making its way through the mind of chemists. It was first conceptualised by Emil Fisher in 1894 with the lock and key mechanism.[8] The concept was developed to explain enzyme binding to their substrates. A concept that is nowadays being exploited for molecularly imprinted polymers.[9] The structural complementary between enzyme and substrate is responsible for the high selectivity of binding, Figure 1. Half a century later, in 1958, Koshland proposed the "induced-fit" mechanism, a new concept that would correct and replace the lock and key mechanism, Figure 1.[10] In this new model, the interaction of the substrate with the enzyme induces conformational changes of the enzyme binding site before the biocatalytic reaction occurs. Supramolecular chemistry did not cease to evolve and to become more complex since then. Evidence of the fast development of the field: in the 1990s Stoddart introduced the concept of molecular machines based on noncovalent forces; he has been awarded in 2016 for his work together with Sauvage and Feringa.[11]
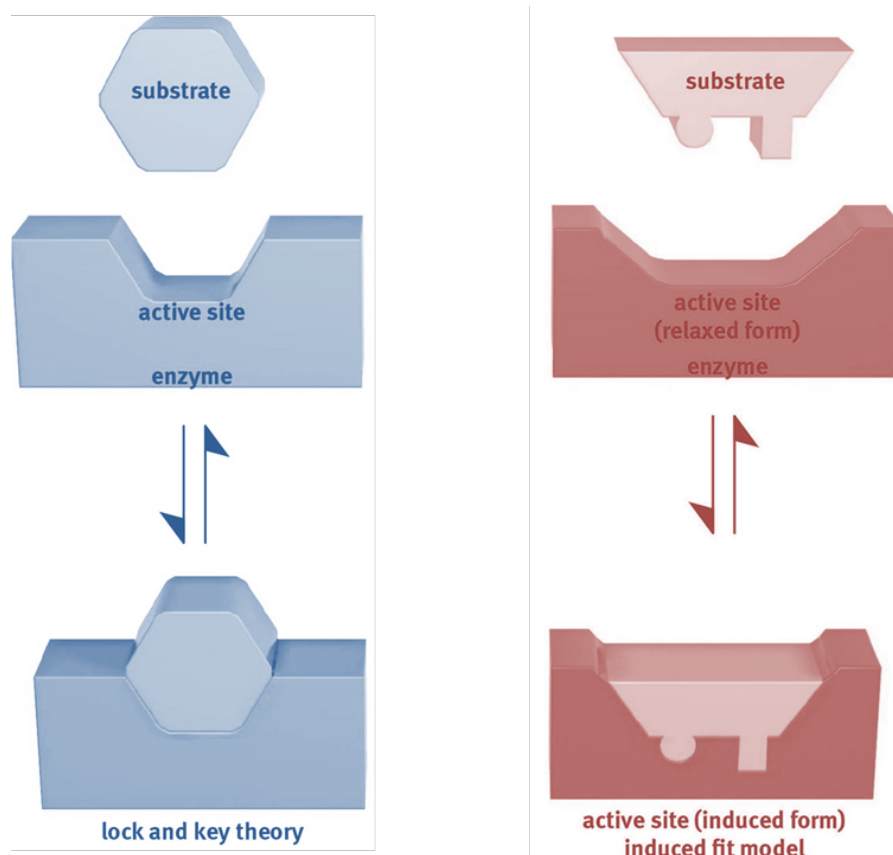
**Figure 1**. Graphical representation of the lock and key and induced fit mechanism.

Nowadays supramolecular chemistry cannot be reduced to the host and guest concept but comprises a broader use of noncovalent intermolecular forces that allow assembly of large and sophisticated entities. Development of bottom-up approaches can now lead to large structures in which building blocks have been designed to present specific features and interactions that synergistically interact to form the final assembly.

**1.2 Host-guest chemistry: molecular complexation**

Molecular complexation involves the complementary binding of a guest molecule and a host molecule through noncovalent interactions such as hydrogen bonding, ion pairing, van der Waals force or hydrophobic effect. The pioneering work of Cram, Lehn and Pedersen focused firstly on the binding of cations by synthetic macrocyclic ligands as crown ethers or cryptands. Cavitands, cucurbituril and carcerands were also studied, Figure 2. These molecules can form host-guest complexes by binding a variety of different guest molecules. For example, crowns ether are well-known to bind efficiently alkali metal cations.[12]
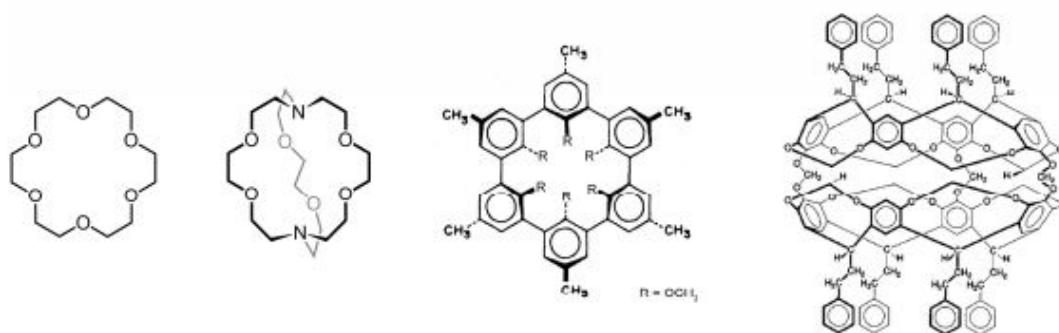
**Figure 2**. Host molecules; (from left to right) crown ether, cryptand, cavitands, carcerand.
[Reproduced with permission from ref. 13. Copyright 1991. WILEY-VCH Verlag GmbH & Co. KGaA.]

Cram and coworkers showed that a carcerand could encapsulate and stabilize a highly reactive cyclobutadiene compound, Figure 3.[13] The carcerand acted as a shell and prevented the guest from dimerization. The macrocycle also stopped large reactants to access the cavity. Furthermore, the synthesis and reactions of cyclobutadiene that had been carried out first in solution and in argon matrix had been also carried out successfully in the confined "inner phase" of the carcerand.
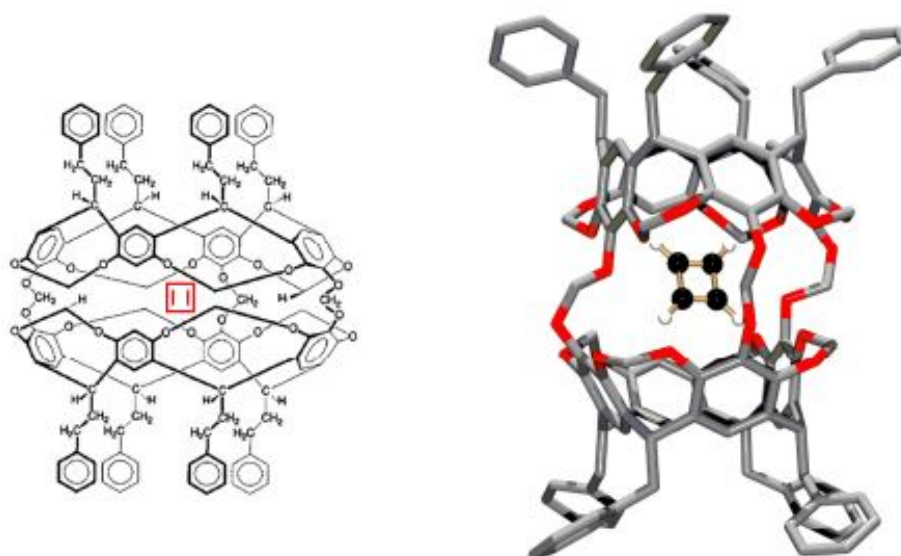


**Figure 3**. Host-Guest complex carcerand/cyclobutadiene.
[Reproduced with permission from ref. 13. Copyright 1991. WILEY-VCH Verlag GmbH & Co. KGaA.]

More recently, another example that illustrates the use of cryptand is the work of Huang and coworkers,[14] who introduced an azobenzene moiety as the third arm of a cryptand to construct a photodriven molecular switch, Figure 4.
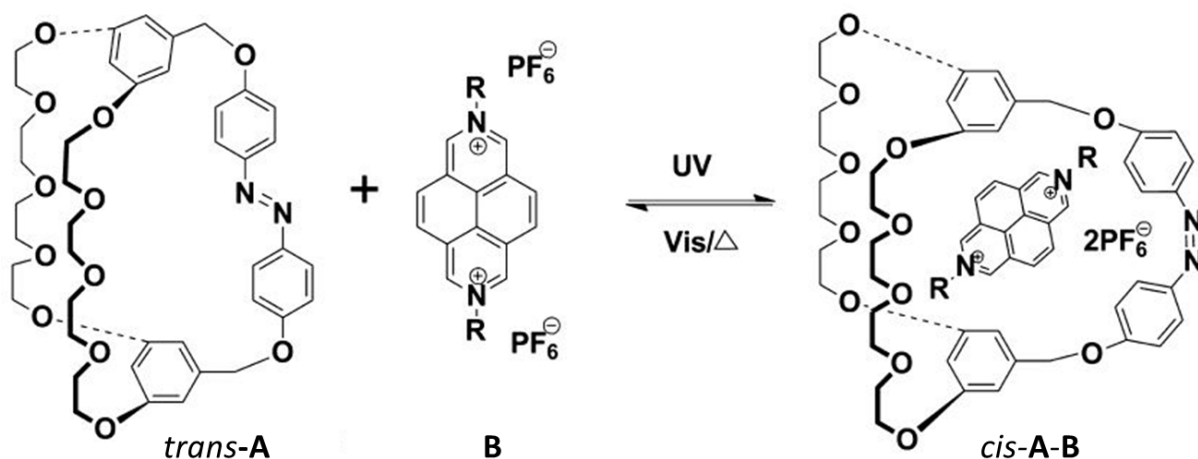
**Figure 4**. Structures and interconversion of photoresponsive cryptand hosts **A** containing an azobenzene and its corresponding guest molecule **B**.
[Adapted with permission from ref. 14. Copyright 2015. The American Chemical Society.]

In the original state, the azobenzene moiety of cryptand **A** exhibits a *trans* conformation state. This conformation prevents the cryptand to bind to the 2,7-diazapyrenium salt because of the relatively small cavity size. UV irradiation triggers the *trans*-to-*cis* isomerization of the azobenzene unit and bestow the cryptand with a good affinity for the guest molecule **B**. On the contrary, visible light or heating triggers the dissociation of the host-guest complex.

Calixarenes have been also studied for the complexation of guest molecules. They are known in different ring sizes and substitution patterns. These molecules can complex cations, anions and also neutral molecules, the broad possibility of guest complexation had made synthesis of calixarene an intensive subject of research.[15] For example calixarenes have been synthesized to include a crown ether moiety and form a calixcrown.[16] The main applications of calixcrowns have been focalised on ion recognition and sensing.

Another class of macrocycles, CDs, have been also studied for their ability to form complexes with a vast array of molecules and have been extensively studied as drug carrier systems. Their broad range of functionalization, low toxicity, and size range have made CDs excellent candidates for numerous applications, especially in pharmacy, cosmetic, chromatography, environment and food.[17-18] Thakkar and Demarco were the first in 1971 to bring direct evidence of the formation of inclusion complexes between several organic substances and β-CD using nuclear magnetic resonance (NMR) spectroscopy.[19] They described changes in the chemical shifts of the protons present in the inner cavity before and after complexation; consequence of the guest shielding. The functionalization of CDs allowed to further broaden

the field of applications to a larger extent. For example, Breslow and coworkers managed to catalysis a Diels-Alder cycloaddition that no natural enzyme and no common catalyst could, using a modified CD.[20] Mediation and catalysis of organic reactions using CDs has been also an intensive field of research.[21] Further properties and features of CDs will be discussed in Chapter 2.

## 1.3 Molecular and hierarchical self-assembly

More recently, other approaches have been developed where the non-covalent forces are used to build larger and more sophisticated structures. In hierarchical molecular self-assembly molecules adopt a defined arrangement and configuration to spontaneously form an organized supramolecular structure of increasing order and complexity.[22]

Nature is filled of examples of elegant hierarchically assembled structures. One of the major and particularly vital process of self-assembly, with the formation of the double-stranded DNA molecule, is protein folding, Figure 5.[23] The translation of a sequence of nucleobases from the messenger ribonucleic acid allows the synthesis of a peptide sequence made of amino acids. This primary structure is yet not an active protein. Creation of intramolecular hydrogen bonding between carbonyl oxygen atoms and amide groups constitute α-helices. Other intermolecular hydrogen bonds are responsible of the formation of β-sheets. The self-organisation mediated by α-helices and β-sheets yields to the tertiary structure and forms the subunit protein. At this stage of protein folding the catalytic activity is functional. Eventually, self-organisation of the subunits forms the quaternary structure of the protein.[23-24] It is the primary structure and the specific sequence of amino acids that gave the final structure of the protein. Following this model, chemists have been producing supramolecular structures with bottom-up approaches.
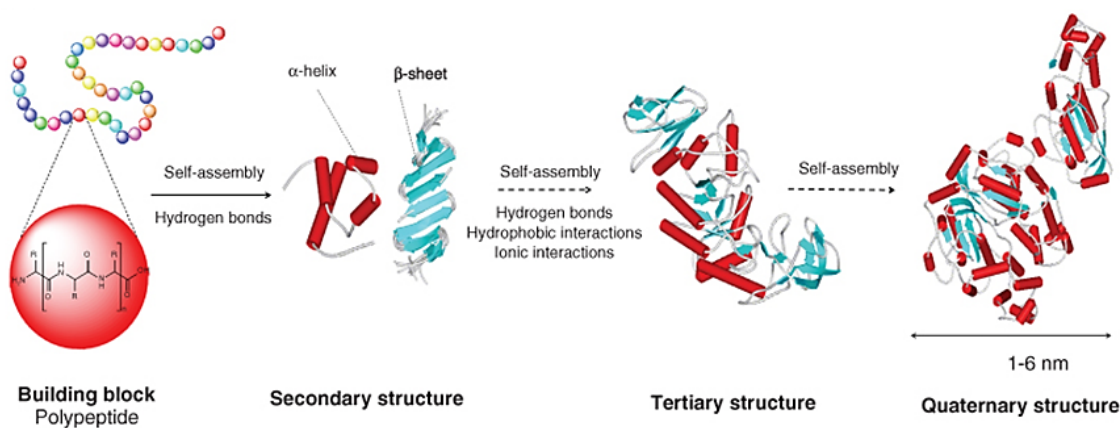


**Figure 5**. Interactions involved in the protein folding.
[Adapted with permission from ref. 23. Copyright 2013. WILEY-VCH Verlag GmbH & Co. KGaA.]

The most commonly used approach to produce hierarchical supramolecular polymers is based on the cooperative hydrogen bonding interactions and the combination of hydrogen bonding and π-π interactions.[25] In 2006, Meijer's group reported the hierarchical self-assembly of oligo(*p*-phenylenevinylene) (OPV) derivatives, Figure 6.[26] These OVP derivatives feature a peripheral trialkoxy group on one side and an ureidotriazine moiety on the other. The creation of hydrogen bonds between these ureidotriazines allowed the formation of dimers via quadruple hydrogen bonds. Decrease in temperature causes 10 to 15 dimers to interact together via an isodesmic pathway, forming a disordered stack. Upon further cooling, the OPV derivatives become more and more restricted via a cooperative process and undergo then a coil-helix transition to form aggregates of 28 dimers. From this point, the elongation process starts and clustering of the different assemblies occurs.
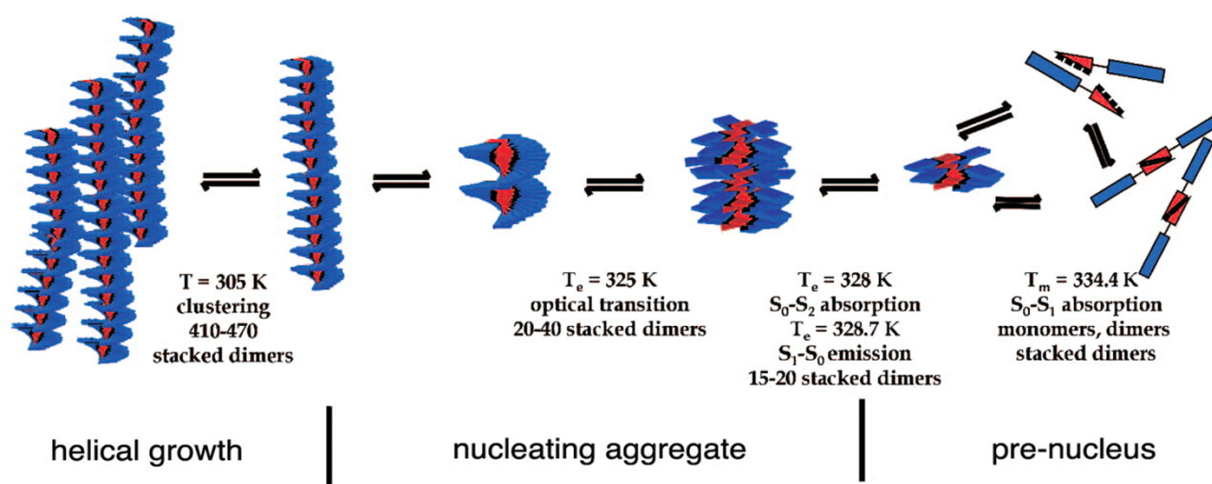


**Figure 6**. Schematic representation of the hierarchical self-assembly of OPV derivative in solution. [Reproduced with permission from ref. 26. Copyright 2006. American Association of the Advancement of Science.]

In self-assembled systems, the hierarchical organisation provides a high degree of complexity to the structure. The structure acquires its final complex arrangement after the assembly of subunits. The emergence of this complex (nano)structures and the ability to control and program their form is of high interest for fields like optics or optoelectronics. Aizenberg and coworkers used bottom-up strategies to build supramolecular structures.[27] The authors produced diverse high-order architectures assembled hierarchically by tuning environmental conditions such as pH, temperature, or salt concentration. The control of the different growth modes allowed the authors to dynamically sculpt evolving structures that mimic the shape of flowers, Figure 7.

**Figure 7**. Stack of different morphologies on top of each other. The scanning electron micrographs are false-colored to mark parts of the structure grown in different steps. $SrCO_3$-$SiO_2$ vases (purple) containing $SrCO_3$-$SiO_2$ stems (green) that were subsequently opened with a $CO_2$ pulse (blue).
[Adapted with permission from ref. 27. Copyright 2013. American Association of the Advancement of Science.]

## 1.4 Supramolecular template-directed synthesis

In supramolecular template-directed synthesis or directed self-assembly, an intrinsic self-assembling system is modulated or assisted using a template. This chemical template is present to force the building blocks to adopt a specific shape or position through noncovalent interactions. The removal of the template after completion of the self-assembly can be either thermodynamically favoured or triggered by external stimuli. The development of catenane, rotaxane and other interlocked molecular structures illustrates the intensive work carried out in supramolecular template-directed synthesis, Figure 8.[28] Catenanes consist in two or more interlocked rings; the name is derived from the Latin word *catena* (chain). Rotaxanes are comprised of linear dumbbell-shaped component encircled by one or more macrocycles, with the name derived from the Latin words *rota* (wheel) and *axis* (axle).



**Figure 8**. Different types of synthetically interlocked molecules (from left to right)— [2]catenane, [2]rotaxane, Borromean rings, Solomon links, and a trefoil knot.
[Reproduced with permission from ref. 28. Copyright 2008. IUPAC.]

In 1960, Wasserman described the first synthetic pathway for the production of catenane but the efficiency of the synthesis was low, the yield was less than 1%.[29] One year later, Wasserman and Frisch established in a landmark paper that mechanically interlocked systems are molecules rather than assemblies. They proposed to reconsider the definition of a molecule

as the definition was not sufficient for some chemical systems. This was the case for interlocked systems which are made of two entities that are not attached covalently. However, in such system at least one covalent bond has to be broken, as in a molecule, to clearly differentiate it from another molecule.[30] Thus the authors proposed to consider also the topology of the chemical compound rather than just the order in which given numbers of specific atoms are joined, type of bond or the spatial arrangement around asymmetric centres. In 1964, Lüttringhaus and Schill developed a strategy to direct the formation of catenane to increase the yield of the desired catenane. The synthetic pathway involved 14 steps with the formation of a cyclic compound as the first step followed by covalent functionalization to create another cyclic moiety. The final catenane was formed by breaking one covalent bond between these two cyclic moieties.[31] Despite the efficiency of the method, this approach was too tedious to be widely adopted by chemists. Concerning rotaxane, the first synthesis was achieved in 1967 by Harrison and Harrison.[32] This work was then followed by covalent-directed rotaxane synthesis by other chemists but always resulting in low rotaxane yield.

Template-directed synthesis revealed to be a good strategy to circumvent the poor yields of covalent strategies.[33] With this approach a template forms a complex with another component (*e.g.* macrocycle) through noncovalent interactions, Figure 9. Once the supramolecular entity is formed (pseudorotaxane), chemical reactions can be carried out on the extremity of the "host" molecule to produce the interlocked molecule. The real advantage of this strategy is the possibility to obtain high yields with few steps compared to covalent-directed synthesis methods.
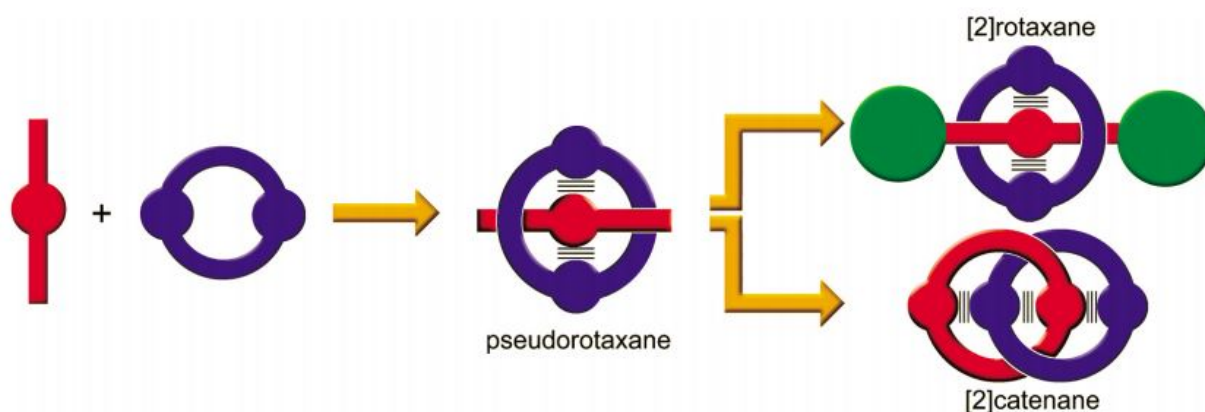


**Figure 9**. Formation of a rotaxane and catenane through template-directed synthesis.
[Reproduced with permission from ref. 28. Copyright 2008, IUPAC.]

In 1983, Sauvage and coworkers reported the first template-directed synthesis of a catenane.[34] In this seminal paper reported in French, the authors exposed an elegant method to build a catenane. The authors proposed a strategy where they formed an intermediate and stable complex from the complexation of a Cu(I) ion with a 1,10-phenanthroline-based thread and with a 1,10-phenanthroline-containing macrocycle. The reaction of the 1,10-phenanthroline-based thread in dimethylformamide (DMF) with an ether compound and cesium carbonate ($Cs_2CO_3$) formed a metallo-catenane complex that after decomplexation afforded the final catenane. Since this publication, numerous studies employed other noncovalent interactions (*e.g.*, hydrogen interactions or π–π stacking) to produce mechanically interlocked molecular compounds in high yields. This work carried out by Sauvage represented the premise of what we know today as molecular machines.

Molecular imprinting method also belongs to the supramolecular template-directed synthesis strategies as the targeted molecule (or enzyme, polymer, etc…) is used to produce the imprint.[9] We will adopt the definition of molecular imprinting proposed by Whitcombe and coworkers: "The construction of ligand-selective recognition sites in synthetic polymers where a template (atom, ion, molecule, complex or a molecular, ionic or macromolecular assembly, including micro-organisms) is employed in order to facilitate recognition site formation during the covalent assembly of the bulk phase by a polymerization or polycondensation process, with subsequent removal of some or all of the template being necessary for recognition to occur in the spaces vacated by the templating species."[35-36] This definition is illustrated in Figure 10. Different type of interactions are involved between the template and the polymerizable entity, it can be reversible covalent bonding, electrostatic interactions, hydrophobic, van der Waals interactions or coordination with a metal centre. The next step which consists in the polymerization reaction results in the formation of an insoluble matrix around the template. Template is then removed from the polymer through disruption of polymer-template interactions.
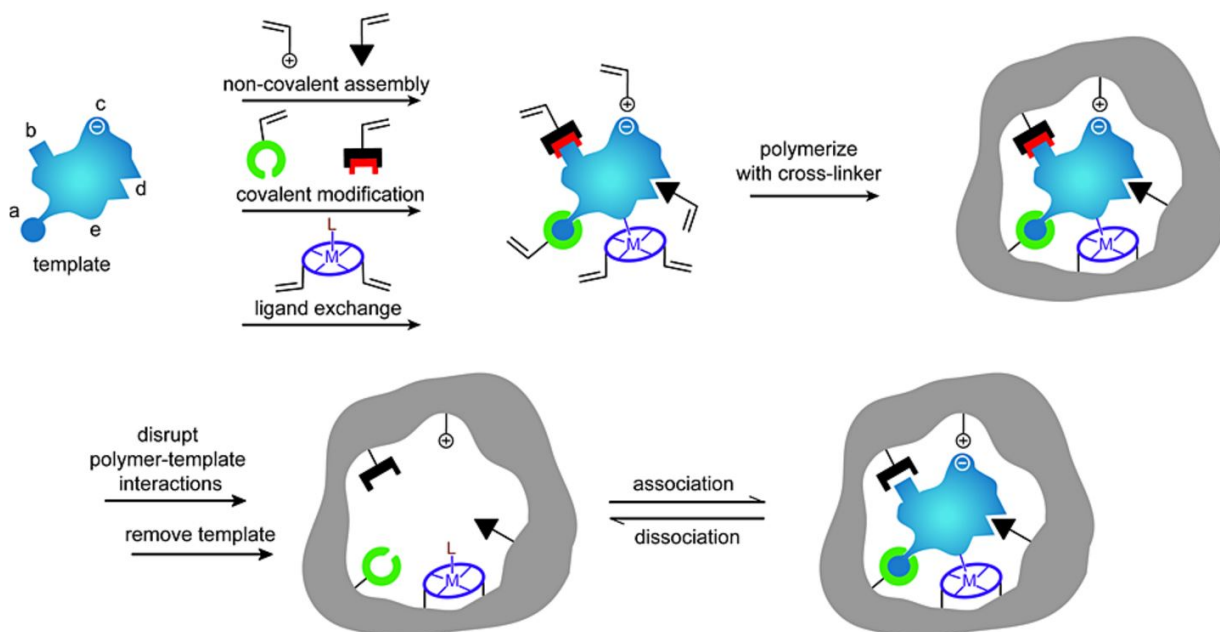
**Figure 10**. Schematic representation of the molecular imprinting process. While the representation here is specific to vinyl polymerization, the same basic scheme can equally be applied to sol-gel, polycondensation. [Reproduced with permission from ref. 35. Copyright 2014. WILEY-VCH Verlag GmbH & Co. KGaA ]

Following the pioneering work of Polyakov in the 1931,[37] where he reported for the first time an increase uptake of an organic compound (benzene, toluene or xylene) by silica particles over two structural analogues when the particles were prepared in the presence of the organic compound. The increasing number of publications on molecular imprinting as well as the improvement in imprinted polymers techniques over the past years has reflected the high interest for this technology.[38] In the same way, Shahgaldian and coworkers, reported a synthetic strategy to produce an artificial organic-inorganic nanoparticulate material possessing virus imprints on its surface.[39] The approach consisted in three steps: the binding of the template virus on the surface of silica nanoparticles, the incubation of the virus-modified nanoparticles with an organosilanes mixture to grow an organosilica recognition layer that would form a replica of the virus and the last step the removal of the immobilized virions to free the imprints, Figure 11. They demonstrated that they could control the kinetic of layer growth and tune the affinity of the virus imprinted material for the template by varying the thickness and composition of the recognition layer and consequently showed a high and specific binding to the targeted virus.
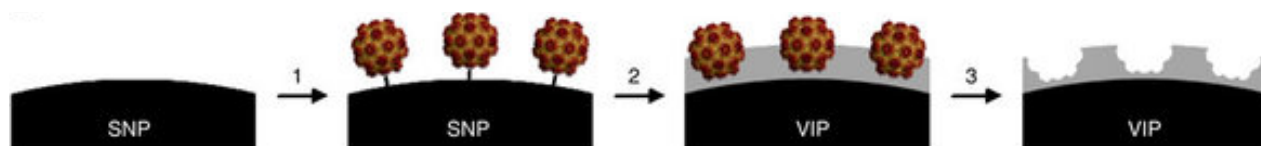
**Figure 11.** Overview of preparation and materials used in the synthesis. Step 1: immobilization of template virions at the surface of SNPs (in black); Step 2: addition of an organosilanes mixture to build the recognition layer (in grey); Step 3: removal of immobilized virions to free the virion imprints.
[Adapted with permission from ref. 39. Copyright 2013. The Nature publishing group]

The synthesis of mesoporous materials is also an intensive field of study among the template-directed synthesis methods; this will be discussed in details in Chapter 4.

## 2. Cyclodextrin based-polymers

This section will details the historical findings of CDs, the industrial production processes, the structural features of CDs and the ability of CDs to form host-guest complexes. The synthesis and production of CDPs will also be discussed. A third part will focus on the applications of CDPs.

### 2.1 Cyclodextrin

In the early 1890s, after experiments on the degradation and reduction of carbohydrates using the butyric ferment *Bacillus amylobacter*, the French chemist, Villiers, noticed the formation of unwanted elongated shinny crystals.[40] He reported his results to the French Academy of Sciences proposing the chemical formula: "$C^{12}H^{10}O^{10}+3HO$" for this product. This marked the beginning of research on CDs. At this time, Villiers called this substance "cellulosine" for its similarity to cellulose, also resistant to acids.

Later in 1903, the Austrian chemist and bacteriologist Schardinger managed to isolate the strain of bacteria responsible for the degradation of starch and the formation of the crystals. He has been able then to distinguish two types of dextrins using a simple colorimetric test with iodine: a solution of α-dextrin gave a yellowish-green and β-dextrin a reddish-brown color. These dextrins are now known as α- and β-CD. Between 1905 and 1911 he gave the first detailed description of preparation, separation and purification of the two cellulosine described previously by Villiers.[18]

From 1911 to 1935, the German chemist Pringsheim contributed significantly to the research on dextrins and was the first to discover that they can form complexes with various organic compounds.[41-42]

The Swiss Karrer was the first to propose a cyclic structure for CDs but it is only in 1936 that the German chemist Freudenberg started his research on the chemical structure of dextrins and demonstrated few years later that the molecule has a cyclic structure formed from maltose units bound together via 1→4 glucosidic linkages.[43]

Structural and physicochemical characteristics of CDs where intensively studied in several publications. French reported in 1942 the molecular weight of CDs but also the exact number of glucose unit for the different type of CDs.[44] In 1954, Cramer gathered the data on CDs and summarized the chemical and physical features of CDs in a book entitled *Inclusion Compounds*

(original German title *"Einschlussverbindungen"*).[45] More exhaustive history of the discovery and research on CDs has been reported in other manuscript and reviews since.[18, 46] Modern studies on CDs began in the 1970s and were mainly ushered by Osa in Japan and Szejtli in Hungary.[17]

If today, CDs are commercially available in ton quantities at a price of few USD/kg, it is because of tremendous effort made to understanding the process of synthesis and production.[47] There are two main processes of production: the "solvent process" which is the most widely used and the "non-solvent process"; both of them use starch as source and enzymes to convert starch into CDs, Figure 12.
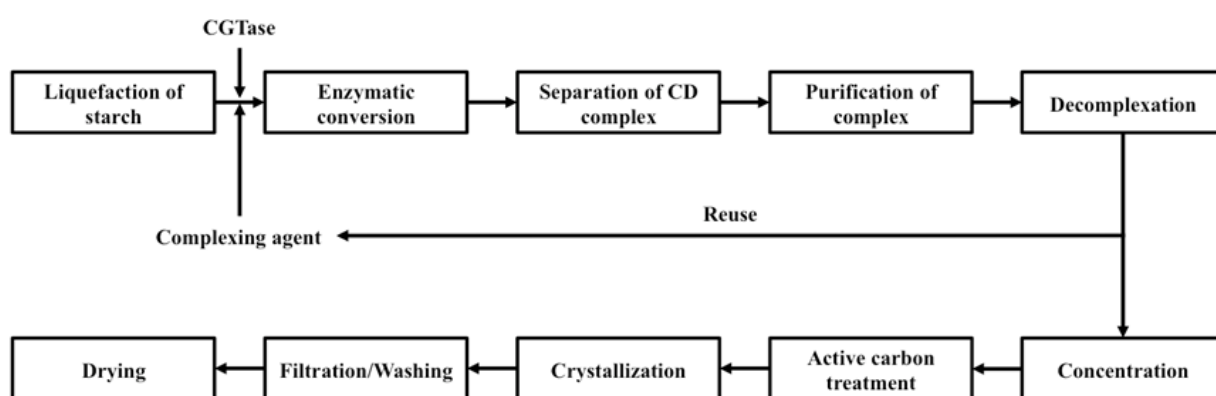


**Figure 12**. Diagram of solvent processes for industrial production of CDs.
[Reproduced with permission from ref. 47. Copyright 1996. Elsevier.]

Starch is first liquefied; the liquid is then cooled down to an optimum temperature to allow enzymes to begin the enzymatic conversion. The enzymatic conversion of starch or starch derivatives is carried out by CD glucosyl transferase enzyme (CGTases).[17, 48-49] CGTases are produced by various bacterial species such as *B. macerans or B. stearothermophilus*.[48, 50-51] To increase the enzymatic conversion, organic compounds are added to cause CD complexation and precipitation, and therefore equilibrium displacement. CDs are then heated in aqueous solution followed by a process of distillation and extraction to remove the organic additives. The mixture is then concentrated and treated with activated carbon. Eventually, CDs are isolated by crystallization and filtration.[47-48] The production of β-CD is nonetheless mainly achieved through the non-solvent process.[52-53]

Due to the abundant researches on CDs we can now have a comprehensive understanding of the chemical and physical features of CDs. Herein, we will focus mainly on the three main CDs type: α, β and γ-CDs. CDs are oligomeric macrocycles of glucosidic units, bound via α (1→4)

glucosidic linkages. They are composed of 6, 7 or 8 glucopyranose units, corresponding to α, β and γ-CD, respectively, Figure 13.
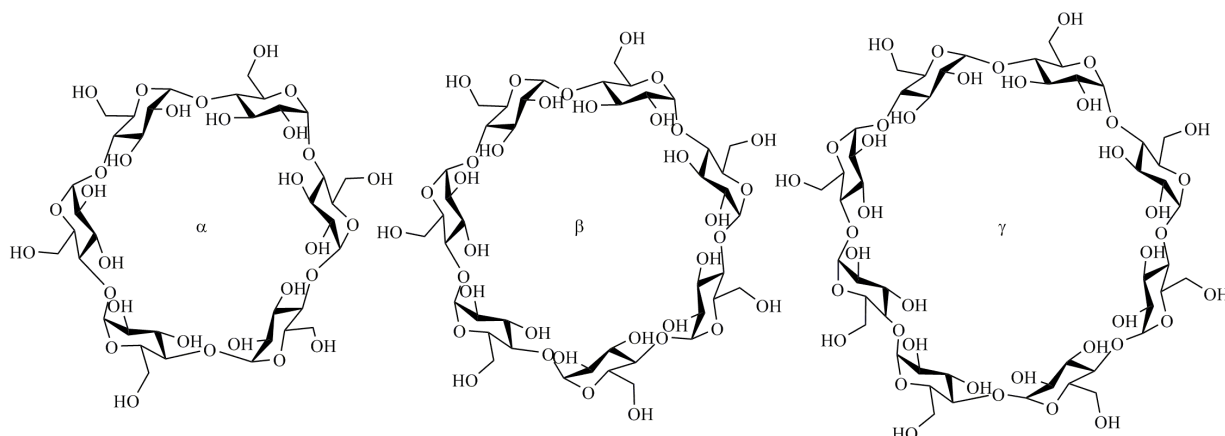


**Figure 13**. Chemical structures of α, β and γ-CDs.

CDs feature a toroidal shape (truncated cone) with a hydrophobic cavity. The primary hydroxyl groups are exposed and readily accessible at the narrow rim (the primary rim), and the secondary hydroxyl groups are exposed at the wide rim (the secondary rim), Figure 14. The differential positioning of the primary and secondary hydroxyl groups represents an attractive feature of this class of molecules, as it allows fairly easy regio (rim)-selective chemical modifications of the macrocycles. The main structural characteristics for α, β and γ-CDs are listed in Table 1.

CDs have relatively high water solubility values of 142, 18.5 and 232 g L$^{-1}$ for α, β and γ-CDs, respectively at 25°C. The relatively lower solubility of the β-derivative is explained by the geometry of the macrocycle, which favors the formation of a set of hydrogen bonds linking the hydroxyl groups together at the lower rim of the macrocycle, hence limiting their ability to interact with the surrounding water molecules. Nevertheless, the fairly good water solubility of all three CDs, combined with the presence of a hydrophobic cavity renders these macrocycles excellent candidate receptors for supramolecular host-guest chemistry. As the CD macrocycle is inherently chiral, CDs can also be used to form asymmetric inclusion complexes; this property is largely exploited to produce chiral stationary phases in chromatography[54-58] and chiral sensors.[59]
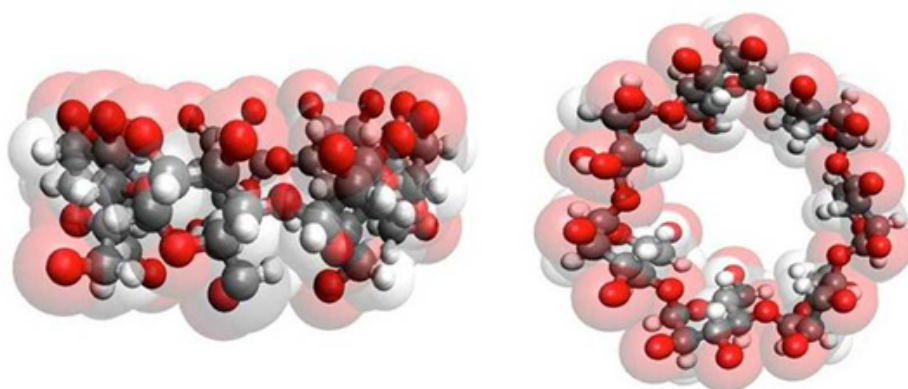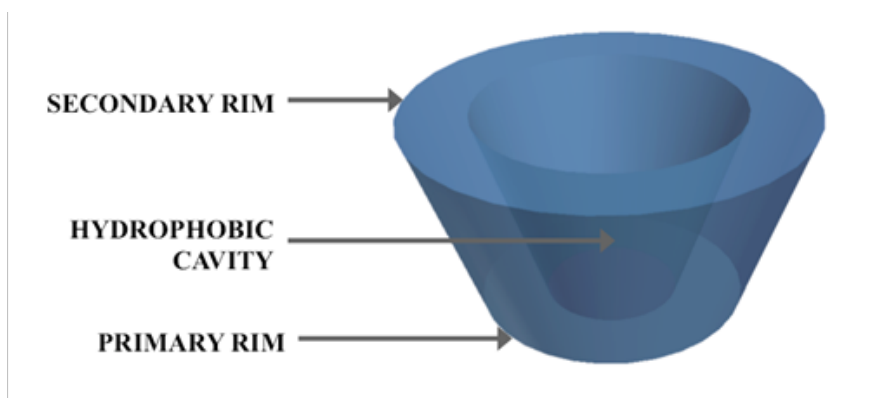
**Figure 14.** Schematic representation of a CD macrocycle (top) and X-ray crystal structure of β-CD, side view (left bottom) and top view (right bottom), water molecules are omitted for clarity.

**Table 1.** Main structural and physicochemical characteristics of CDs.

| Cyclodextrin | α | β | γ |
|---|---|---|---|
| Glucose monomers | 6 | 7 | 8 |
| Molecular weight | 972 | 1135 | 1297 |
| Height of torus, Å | 7.9 | 7.9 | 7.9 |
| Internal cavity volume, Å$^3$ | 174 | 262 | 427 |
| Internal cavity diameter, Å | 4.7-5.3 | 6.0-6.5 | 8 |
| Diameter of outer periphery, Å | 14.6 | 15.4 | 17.5 |
| $[\alpha]_D$ 25°C | 150 | 162 | 177 |
| Water solubility (g/L: 25° C) | 142 | 18.5 | 232 |
| Water molecules in cavity | 6 | 11 | 17 |

One of the most attractive features of CDs is their ability to form inclusion complexes with a large variety of guest molecules in solution.[60] Those complexes are formed by the inclusion of the guest molecules inside the hydrophobic cavity of CD macrocycles, Figure 15.
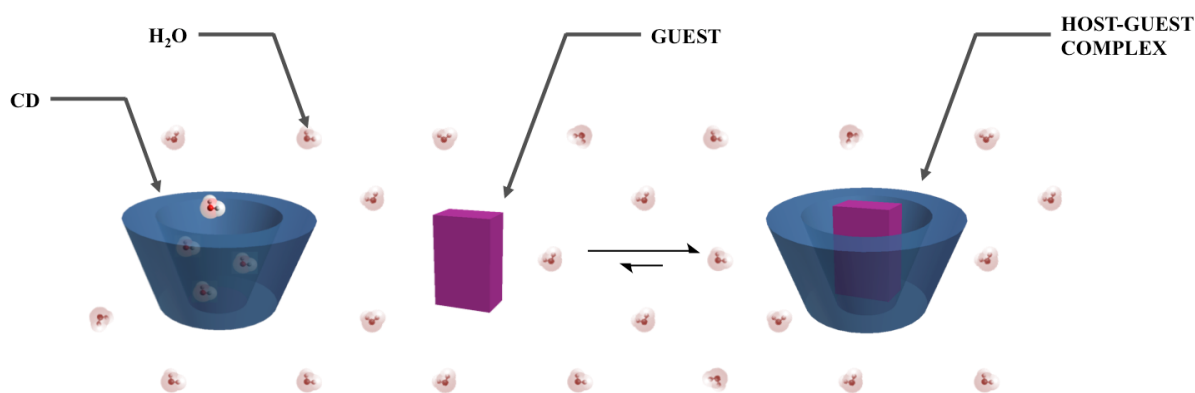


**Figure 15**. 1:1 inclusion complex of a hydrophobic guest molecule and a CD in water.

Water molecules occupy the cavity of the CDs under aqueous conditions, but as the cavity is hydrophobic the presence in solution of a guest molecule with poor polarity yields the formation of an inclusion complex, wherein the guest molecule replaces the bound water molecules with the *proviso* that the geometry of the guest molecule is compatible with the internal space of the host CD. Even though single crystal X-ray crystallography remains the method of choice in the study of CD inclusion compounds,[61] 2-dimensional NMR spectroscopy represents a good alternative for the study of inclusion complex formation in solution.[62-63] The presence of a guest molecule inside the cavity induces changes in the spectral properties of both the host and the guest, allowing a structural characterization of the complex. A number of additional characterization techniques have been applied to study the formation of complexes. These include thermogravimetric methods, polarimetry and infrared, fluorescence and UV-visible spectroscopy.[64]

Because of their ability to form inclusion complexes with hydrophobic compounds to yield water-soluble entities, CDs are widely used for the formulation of pharmaceuticals, and numerous drug formulations containing CDs are available on the market.[46, 65-66]

## 2.2 Cyclodextrin based-polymers

Several synthetic approaches have been developed in order to produce CDPs that exploit the outstanding molecular recognition and inclusion properties of CDs for the creation of functional

materials. CDPs can be produced as insoluble materials in the form of bulk or nanostructured polymers. CDPs can be classified according to their chemical structures, Figure 16.

Highly cross-linked CDPs are typically produced using the CD macrocycle as a multi-functional cross-linker. The synthesis of such CDPs can be carried out in two different ways. The first one, through the reaction of native CDs with hydroxyl-reactive monomers. The second one, through the introduction of chemical reactive functionalities on the macrocycle followed then by the polymerization reaction. Highly cross-linked CDPs can be produced in the form of hydrogels or micro- and nanoparticles.[67]

Linear CDPs are typically more laborious to produce, because the formation of linear CDPs requires the synthesis of CD monomers functionalized at only two positions. Tubular CDPs can also be considered as linear CDPs, in this special case the CDs are linked to each other through at least two covalent bonds on each rim, allowing the formation of a tubular architecture.[68-69]

Polymers with pendant CD units are produced either exploiting CDs possessing only one polymerizable functionality (typically with an additional co-monomer spacer) or by grafting CDs onto a preformed polymer backbone.[70]

Supramolecular CDPs and materials are produced using the inclusion properties of CDs. For supramolecular CDPs, monomeric unit or CD-based monomers interact together through the inclusion of one part of the monomeric unit into the cavity of another CD. For supramolecular CDP-based materials, non-covalent interactions occur between two or more CDPs and another chemical entity joining the two CDPs together.[71]

Solms and Egli published the first example of cross-linked CDP in 1965.[72] Produced by mixing α-, β- or γ-CDs with epichlorohydrin (EPI) under basic conditions, the resulting polymers were tested for their ability to bind a series of small organic and inorganic molecules (*e.g.,* benzaldehyde, aniline, *p*- and *o*-nitrophenol, pyridine, butyric acid and methyl-orange). The synthetic procedure, inspired by the production of epoxy resins, was fairly straightforward, as it did not necessitate any prior modification of the CD macrocycle, Figure 17.
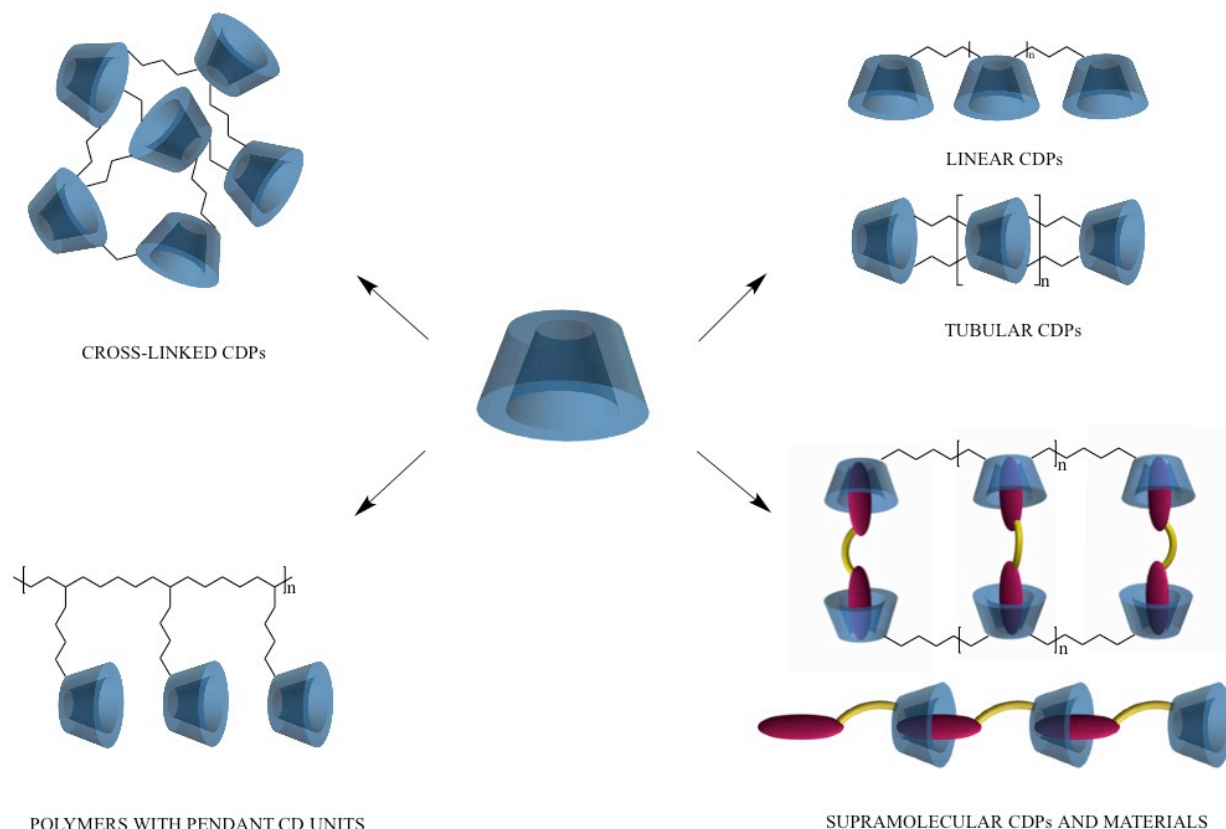
**Figure 16.** The different types of CDPs.

Under basic conditions, the hydroxyl group of the CD is deprotonated and the formed alkoxide group react with EPI via a nucleophilic substitution to form the epoxide derivative. In turn, another CD open the epoxide via a regioselective attack to give the cross linked product. It was demonstrated that the produced CDPs have greater binding capabilities than commercial, cross-linked dextran deprived of inclusion moieties.
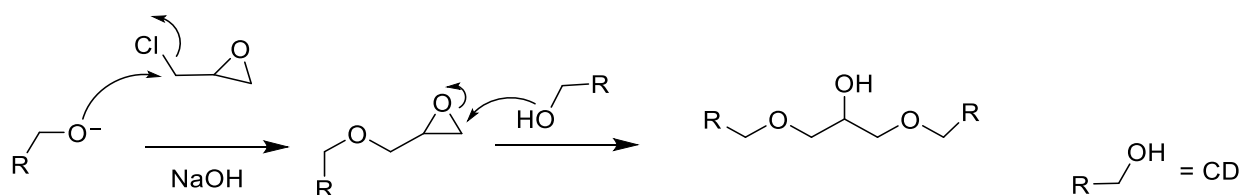


**Figure 17.** Mechanism of reaction of CD with EPI.

A large number of highly cross-linked CDPs have been prepared using other cross-coupling agents, *e.g.* citric acid, diisocyanates, succinic anhydride, glutaraldehyde, giving rise to a range of CDPs endowed with new binding properties compared to native CDs, due to the functional groups present in these polymers.[73-74] For example, Shahgaldian and coworkers developed a synthetic procedure that allows producing, in a high throughput fashion, more than 96 different

CDP polyurethanes with specific recognition properties. A study of the binding properties of the CDPs produced has revealed that the nature of the cross-linker has a great influence on the affinity of the CDPs for a series of target pharmaceuticals. The authors also demonstrated that the synthesis of the selected polymers can be scaled up without significantly changing the binding capabilities of the produced CDPs.[75-76]

Besides the above-mentioned methods, highly cross-linked CDPs have also been produced using modified CDs, which bear polymerizable functionalities. For example, acryloyl-modified CDs can be efficiently produced by reacting native CDs with acryloyl chloride,[77] Figure 18. However, this reaction is not rim-selective as both primary and secondary hydroxyl groups of CDs can react with the highly reactive acryloyl chloride, affording the acryloyl-CD monomers. The resulting product typically consists of a mixture of CDs with different degrees of substitution that can be controlled by changing the coupling reaction conditions. These acryloyl-esters can be used to produce CDPs with or without additional monomers. For instance, Shahgaldian and coworkers produced a series of CDPs, using acryloyl-CDs with a series of cross-linkers and co-monomers, by means of photopolymerization reactions.[78] They demonstrated that this high-throughput synthesis approach was efficient in tuning the molecular recognition properties of the produced CDPs.
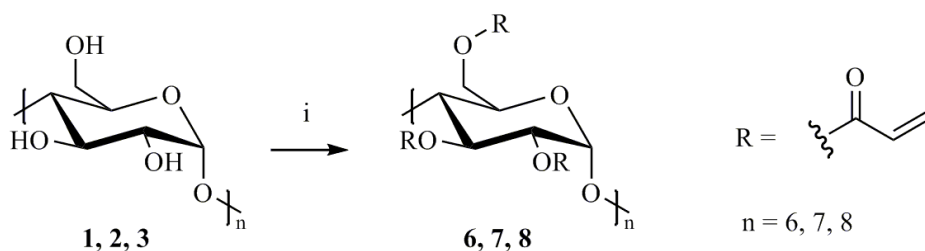


**Figure 18.** Synthesis of acryloyl-CD monomer. i) Acryloyl chloride, triethylamine.

A number of highly cross-linked CDPs have been shown to form gels. CDP-based gel systems were used by Harada to demonstrate macroscopic self-assembly through molecular recognition.[67] To that end, a series of acrylamide gels were produced, containing either α- or β-CD units or small organic moieties (*i.e.*, adamantyl, *n*-butyl or *t*-butyl) known to be guest functional groups for CD hosts. These gels were produced as millimetre-size cubes and doped with dyes to allow their differentiation. The study revealed that strong affinity exists between β-CD gel and adamantyl-gel in water, due to the complexation of the host and guest molecules. It was also shown that there is complementarity between the α-CDP gel and the gel containing *n*-butyl functionalities while β-CD gel binds *t*-butyl and adamantyl-containing gels, Figure 19.

Mohamed EL IDRISSI

The study of Harada certainly represents one of the first studies showing that recognition phenomena taking place at the molecular level can impact the assembly of millimetre-size objects.
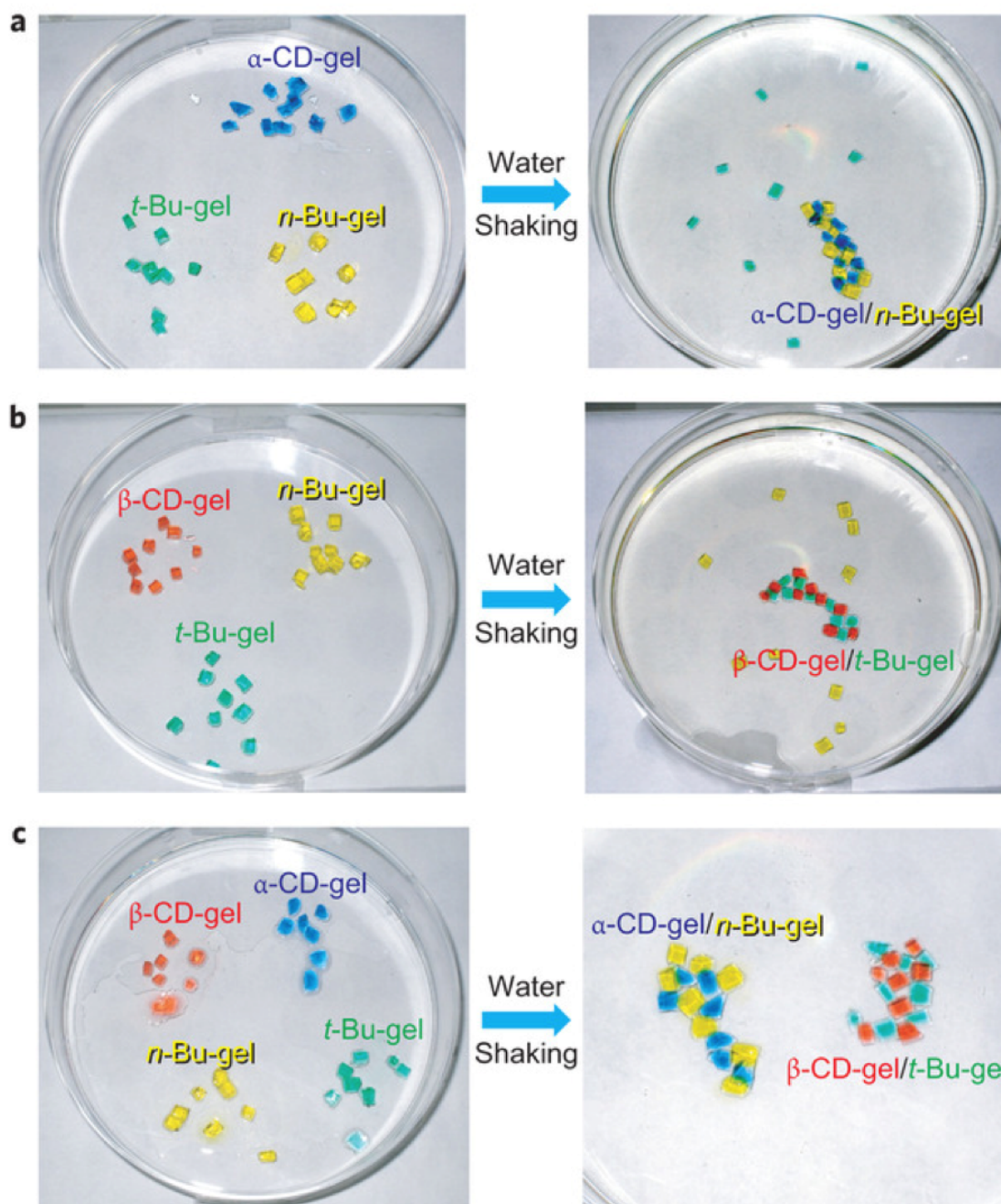


**Figure 19**. Specific molecular recognition visualized at macroscopic scale.
[Reproduced with permission from ref. 67. Copyright 2011. The Nature publishing group.]

## 2.3 Application of CDPs

As previously mentioned, due to their ability to form supramolecular inclusion complexes,[79] soluble native or chemically modified CDPs have been widely used in pharmaceutical

formulations to dissolve small organic drugs efficiently.[74] For example, Mura *et al.* demonstrated that EPI-cross-linked CDPs can be loaded with naproxen, a nonsteroidal anti-inflammatory drug, rendering it capable of exceeding its former maximum aqueous solubility by 30-fold.[80] Similarly, Rodriguez-Tenreiro *et al.* showed a 500-fold increase in solubility of estradiol, a poorly water-soluble steroid hormone, when the cross-linked CDP was added to the solution.[81] Cheng *et al.* produced a high molecular weight linear copolymer of a diaminocarboxy-derivative of β-CD condensed with di-functionalized PEG co-monomers.[82] This polymer was then conjugated, through its free carboxylate functions, to 20-*O*-trifluoroglycylcamptothecin and 20-*O*-trifluoroglycylglycylglycylcamptothecin to yield polymeric prodrugs, Figure 20. It was demonstrated that this system could increase the solubility of the camptothecin derivatives studied by more than three orders of magnitude, while keeping low toxicity to the cultured cells. These CDPs were tested on nude mice bearing human colon carcinoma tumors. Long-term therapeutic efficacy was observed due to the sustained release of camptothecin derivatives from these CDPs.[83]
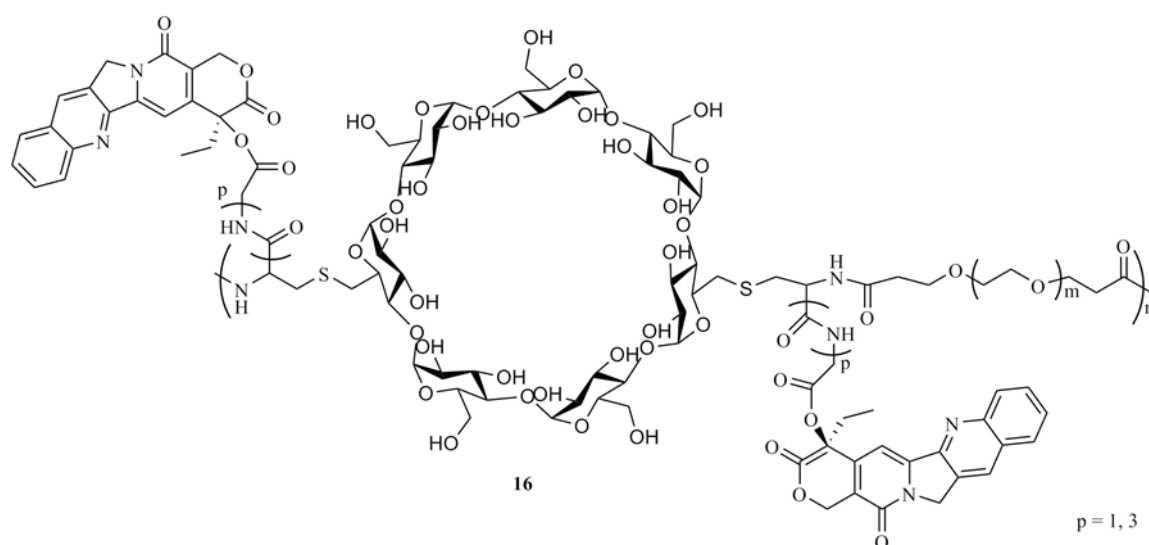


**Figure 20**. Linear, α-CDP-camptothecin prodrug.

While CDs have been widely used for agro-food applications, the use of CDPs has been much less developed. Su and Yang demonstrated that CDP gels can be employed to extract natural food components such as naringin, caffeine and theobromine from aqueous solution.[84] Appel and Jackson demonstrated that a CDP polyurethane can efficiently bind ochratoxin A, a major food-contaminating mycotoxin produced by *Aspergillus ochraceus*, *Aspergillus carbonarius* or *Penicillium verrucosum*.[85] CDPs were also shown to act as sorbents of naringin, a flavanone glycoside responsible for the bitter taste of grapefruit juice.[86-87] A CDP functionalized with 1-

(2-pyridylazo)-2-naphthol was applied in the determination of cobalt content in food by a direct, polymer phase spectrophotometry method.

A significant number of applications of EPI-based CDs as sorbent materials have been reported and reviewed recently.[88] They have been studied for their ability to bind targets such as nonylphenol ethoxylate,[89] naphthenic acids,[90] cinnamaldehyde,[91] benzaldehyde,[91] aniline,[92] fuchsine,[93] phenol,[94] and naphthalene.[95] For example, Orpecio *et al.* demonstrated that cross-linked CDP beads, packed in a column, were able to trap organic compounds in flowing water for remediation purposes. Considerable trapping of naphthalene and 2-naphthol has been achieved. Moon *et al.* showed that the process of extracting steroids was more efficient with CDPs than with commercial CD-based cartridges.[96] The new, solid phase extraction sorbent resulted in improved selectivity and better extraction efficiency due to the chemical interactions brought by the cross-linked network of CDPs. In another work, Sancey *et al.* chemically modified CDPs to enlarge the range of targeted compounds, and to capture metals in water.[97]

## 3. Design of 1D supramolecular nanomaterial

### 3.1 1D supramolecular structures

Molecular self-assembly strategies have been used to construct 1D supramolecular structure like nanofibers, nanotubes or nanorods. Although chemists can exploit a variety of non-covalent interactions to invoke the self-assembly of molecular building blocks into complex supramolecular structures, stable and directional interactions are preferred as they allow for a better control over the self-assembly process. In this context, π-π stacking is of high significance as, besides a relatively high energy of interaction (*ca*. 10-70 kJ mol$^{-1}$),[98] it is highly directional. Consequently, π-π stacking has been largely exploited to produce 1D organic nanostructures such as nanowires,[99] nanotubes or nanorods.[100-102] Porphyrins and pyrene derivatives have attracted substantial interest as building blocks capable of self-assembling through π-π stacking.[103-107] For instance, Meijer and coworkers introduced a zinc-porphyrin-based supramolecular polymer that self-assemble into 1D supramolecular aggregates with porphyrin units organized in a helical fashion.[108] Atomic-force microscopy (AFM) studies showed micrometer-long curled fribrillar nanostructures with typical height of 3 nm, while in solution, static and multi angle dynamic light scattering measurements indicated rod-like aggregates. Upon addition of pyridine, the aggregates disassemble to monomeric units because of the increased polarity of the solvent, breaking up the hydrogen bonds within the aggregates. Dilution experiments performed at a fixed pyridine-to-porphyrin ratio of 40, showed an almost full transition from complex pyridine-porphyrin to the aggregated state, Figure 21.
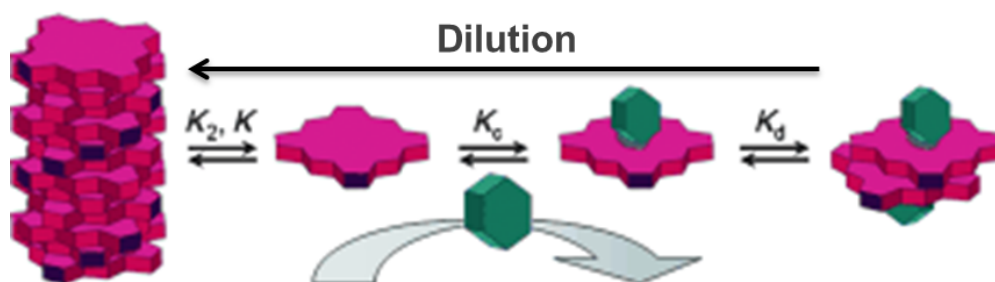


**Figure 21**. A model for aggregates formation. Monomers, and monomeric and dimeric porphyrin-pyridine adducts are connected by equilibrium constants.
[Reproduced with permission from ref. 108. Copyright 2010. WILEY-VCH Verlag.]

Guiseppone and coworkers investigated the self-assembly behaviour of a triarylamine derivative.[109] They demonstrated that the self-assembly into rod-like structures is triggered by

light irradiation, Figure 22. The self-assembly process started first by the formation of arylammonium cationic radicals. This radical is then turned into a neutral triarylamine through charge hopping during the supramolecular polymerization that contains a delocalized cationic radical. Electron paramagnetic resonance spectroscopy indicated that one radical was sufficient to stabilize the stacking of about 160 triarylamine units along the self-assembled wires. In addition to the charge-transfer phenomena responsible of the self-assembly of the supramolecular structure, π-π interactions played also a significant role as well as hydrogen bonding and van der Waals interactions on the lateral chains. These latter acted synergistically to ensure stability to the structures.
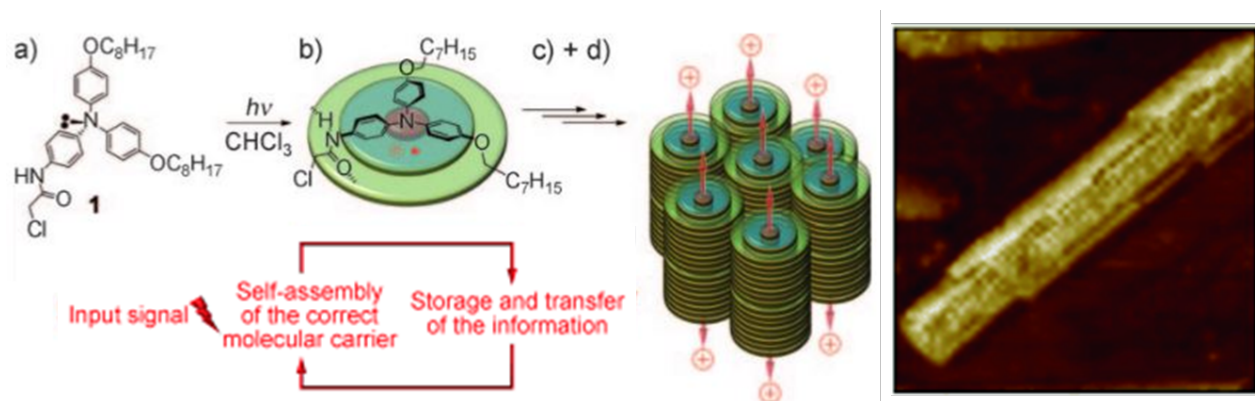


**Figure 22**. Hierarchical self-assembly processes that occur upon irradiation of the neutral triarylamine and AFM image (surface scale 50x50 nm) of a single self- assembled structure.
[Reproduced with permission from ref. 109. Copyright 2010. WILEY-VCH Verlag GmbH & Co.]

The range of functionalized pyrene derivatives available, their self-assembly behaviour, as well as their remarkable optical and electronic properties render these chromophores ideal candidates for several applications where control of molecular assembly into a defined structure is of high importance. Gao and coworkers reported  the first discovery of protrusion of nanotubes from microcapsules of poly(allylamine hydrochloride)-graft-pyrene (PAH-graft-pyrene) in solution.[110] The microcapsules were produced by the following process: first $CaCO_3$ particles were doped with PAH and then were further reacted with 1-pyrenecarboxaldehyde (Py-CHO). The $CaCO_3$ template was then removed with acidic solution, Figure 23.
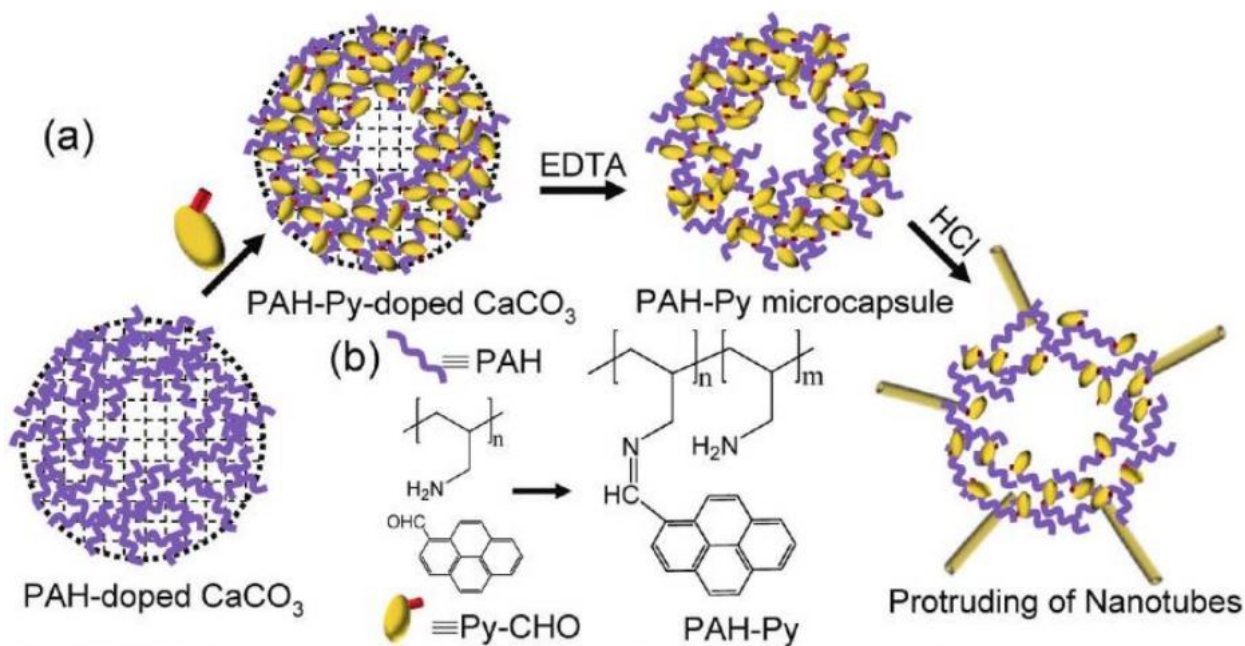
**Figure 23**. **a**)Schematic illustration of PAH-Py microcapsule fabrication and 1D-nanotube protrusion. **b**) Chemical structures of PAH, Py-CHO, and PAH-Py.
[Reproduced with permission from ref. 110. Copyright 2011. The American Chemical Society.]

When the microcapsules were incubated in HCl solution, protrusion of 1D nanotubes were observed. The nanotubes kept growing with incubation until eventually only nanotubes were visible, Figure 24. The final nanotubes were composed of Py-CHO only but not PAH-Py, suggesting that assembly of Py-CHO were forming the nanotubes through π-π interactions. The authors demonstrated with X-ray diffraction studies, circular dichroism and polarized microscopy that the built up of the nanotubes occurs indeed from the π-π stacking of Py-CHO in solution.
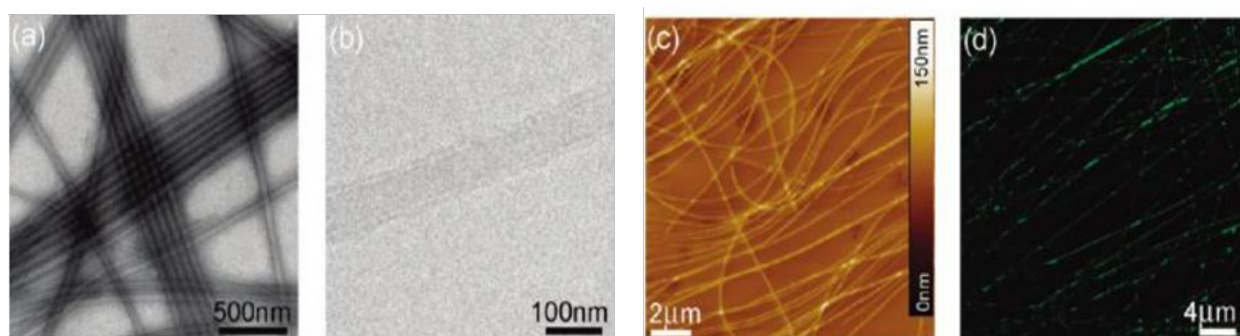


**Figure 24**. **a**) TEM, **b**) Cryo-TEM, **c**) SFM, and **d**) confocal laser scanning microscopy images of 1D-nanotube prepared from PAH-Py polymers after incubation in pH 0 HCl for 144 h.
[Reproduced with permission from ref. 110. Copyright 2011. The American Chemical Society.]

Another example of use of pyrene derivatives and π-π interactions for the formation of 1D supramolecular structures was exposed by Wang et al. who synthesized an amphiphilic

copolymer containing pyrene moieties linked through a light responsive ester bond.[111] The formation of nanorods was thus triggered through UV irradiation.

### 3.2 Formation of H- and J- type aggregates in organic 1D supramolecular structures

The first observation of H- and J-aggregates was made by Scheibe et al. and Jelley in 1936.[112] They worked independently and observed the uncommon behaviour of pseudoisocyanine chloride (PIC chloride) in aqueous solutions. In contrary to other solvent like ethanol, the absorption maximum of PIC chloride was shifted to a longer wavelength (solvatochromism effect) and upon increasing the concentration of the dye in aqueous solution the absorption band became more intense and sharper with large deviation from the Beer-Lambert law. Despite few differences in their interpretations, both Scheibe and Jelley found that the spectral changes were reversible upon heating and cooling of the dye solution, which indicated a self-assembly process of the PIC chloride.

Today, J-aggregates (named after Jelley) are defined with a narrow absorption band that is shifted to a longer wavelength than the monomer absorption band. They exhibit also a small Stokes shift with the fluorescence band. For the H-aggregates (H designates hypsochromic), the absorption band is shifted to shorter wavelength and is labelled as blue-shift or hypsochromic shift. H-aggregates often display low or no fluorescence, Figure 25.
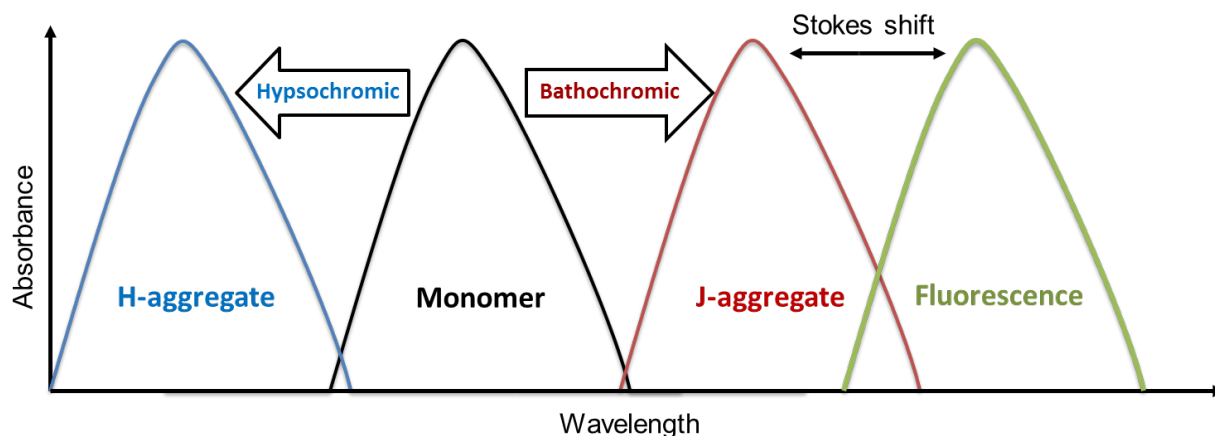


**Figure 25**. Schematic representation of the main spectral characteristics of H-and J-aggregates.

The structure of J-aggregate is characterized by a slipped face-to-face packing arrangement where the monomers are interacting through π-π interaction with an angle θ < 54.7°, Figure 26. In H-aggregates, the arrangement can be either face-to-face or slipped face-to-face with an angle θ > 54.7°.
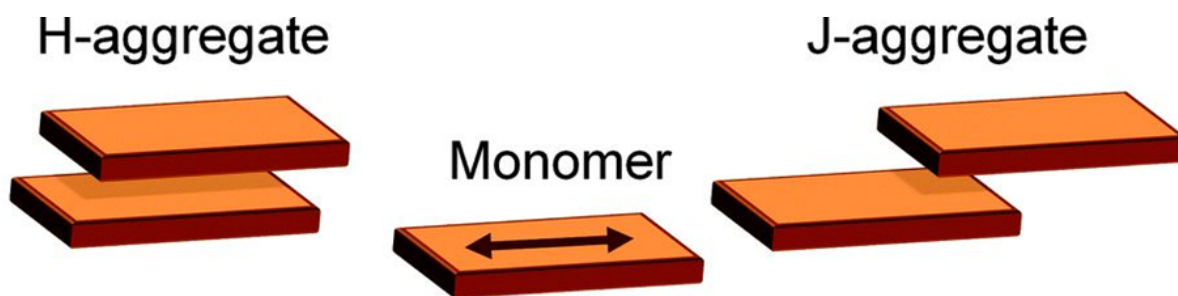
**Figure 26**. Typical arrangements of H- and J-aggregates for a π-conjugated molecule (dimer).

During the last 30 years, numerous dyes such as cyanines, perylene disimide (PBI), squaraines and pyrene or porphyrin derivatives,[113] had been the subject of studies to apprehend J-aggregates formation and structure. For instance, Würthner et al. showed that PBI derivatives with amide functionalities, and with trialkoxyphenyl groups at the imide positions, formed aggregates that exhibit either H- or J-type absorption spectra depending on the peripheral alkoxy chains. The PBIs could formed long fibers through hydrogen-bond-assisted self-assembly. One type of the PBI derivative with simple *n*-alkyl chains at the periphery formed H-aggregates, while the other PBI dye bearing chiral, branched alkyl chains exhibited a strongly bathochromically shifted broad J-band in solution.[114] The same group then investigated a broad series of PBIs with different alkyl chains at the periphery and demonstrated that sublte variations of the peripheral substituents could alter the aggregation mode, Figure 27.[115] Several other examples have been reported to exhibit in general broad J-bands where the self-organisation is formed through H-bonding and π-π interactions.[116]
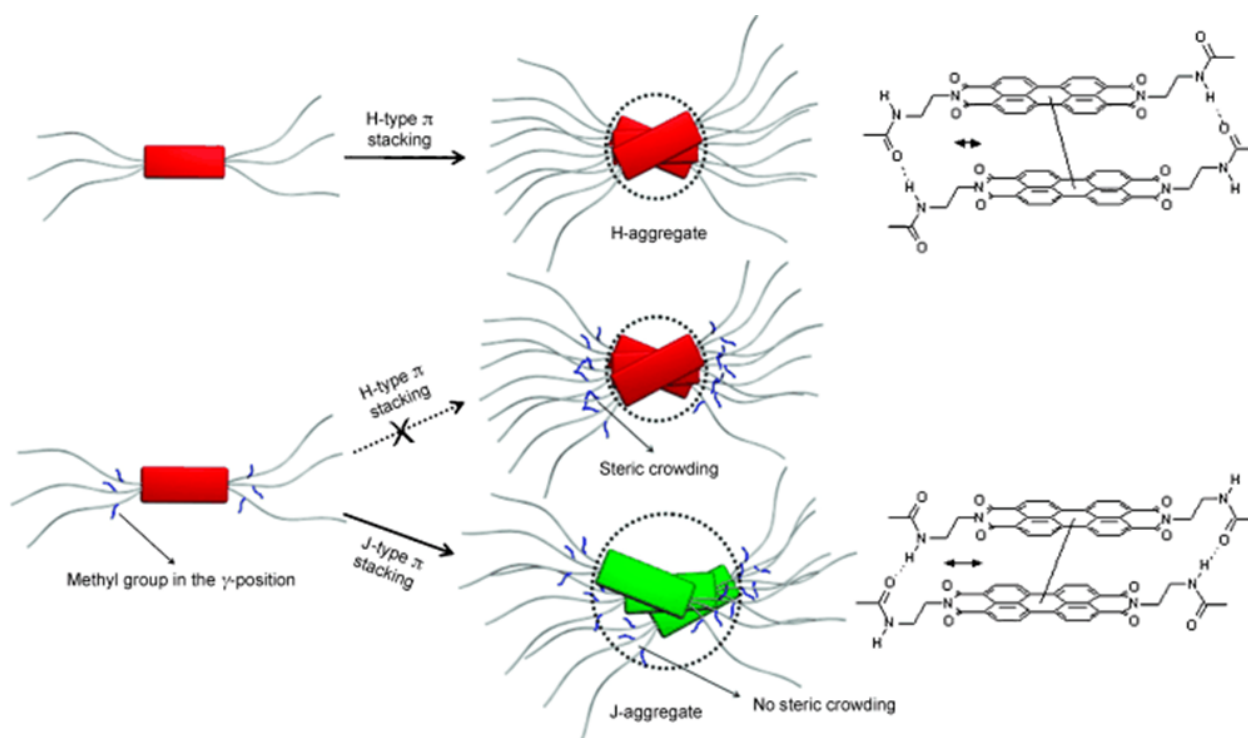
**Figure 27**. Left: schematic representation of PBI chromophores with linear (top) and branched (bottom) alkyl substituents. Middle: the transition from H- (top) to J-type (bottom) π stacking with increasing steric demand of the peripheral alkyl side chains. Right: Packing model for H- (top) and J-type (bottom) π-stacking. In both cases additional rotational offsets are needed to enable both close π-π contact and hydrogen bonding. [Reproduced with permission from ref. 115. Copyright 2008. WILEY-VCH Verlag GmbH & Co. KGaA.]

# 4 Supramolecular assistance to covalent synthesis

## 4.1 Templated synthesis for porous material

Porous materials possess attractive properties such as large surface areas and excellent gas sorption performances, and have been extensively studied and used as catalyst, adsorbent or for applications in energy conversion and storage.[117-118]

Since the first report on mesoporous silica in the 1990s,[119] a number of mesoporous materials emerged and illustrated the intense interest and need for such material. According to the definition given by the international union of pure and applied chemistry, a porous material can be categorized into three classes based on their pore diameter: microporous (< 2 nm); mesoporous (2-50 nm) and macroporous (> 50 nm).[120] Herein, we will focus mainly on mesoporous materials and their templated preparation methods.

The main advantage of using template-based strategies lies in the control of the (pore) size and morphology of the material. Template-based syntheses of mesoporous materials consist of three main steps: template preparation or preorganization of the template, directed synthesis of the material around the template and template removal. Various methods exist to produce mesoporous materials, Figure 28. We can classify them as soft-, hard- and multiple-templating method and *in situ*-templating pathway.

In soft-templating approaches, the formation of micelles with amphiphilic molecules creates the template before the precursors self-organize around the micelle through attractive interactions and start to react. After removal of the template, an ordered mesoporous material is obtained.

In hard-templating methods, the mesostructure is produced from a preformed hard template, such as mesoporous carbon and silica. The advantage of using a hard template resides in the fact that no control is needed for the hydrolysis, assembly and condensation of the precursors and assure thus a better ordered structure of the final material. The hard template offers a high resistance to high reaction temperatures but implies complex procedures.

The multiple-templating method is a combination of soft- and hard-templating approaches. The first step consists in the mixture of colloidal crystal with the precursor solution, followed by the infiltration of the precursor in the colloidal crystals. After a heat or chemical treatment a solid is obtained. The last step consists in the removal of the template yielding a mesoporous material.

For *in-situ* templating method, salts, ions or molecules contained in the precursor solution can act as template after phase separation, the route is then the same than the other methods. It is a straightforward method but it provides low control on the mesopores order.
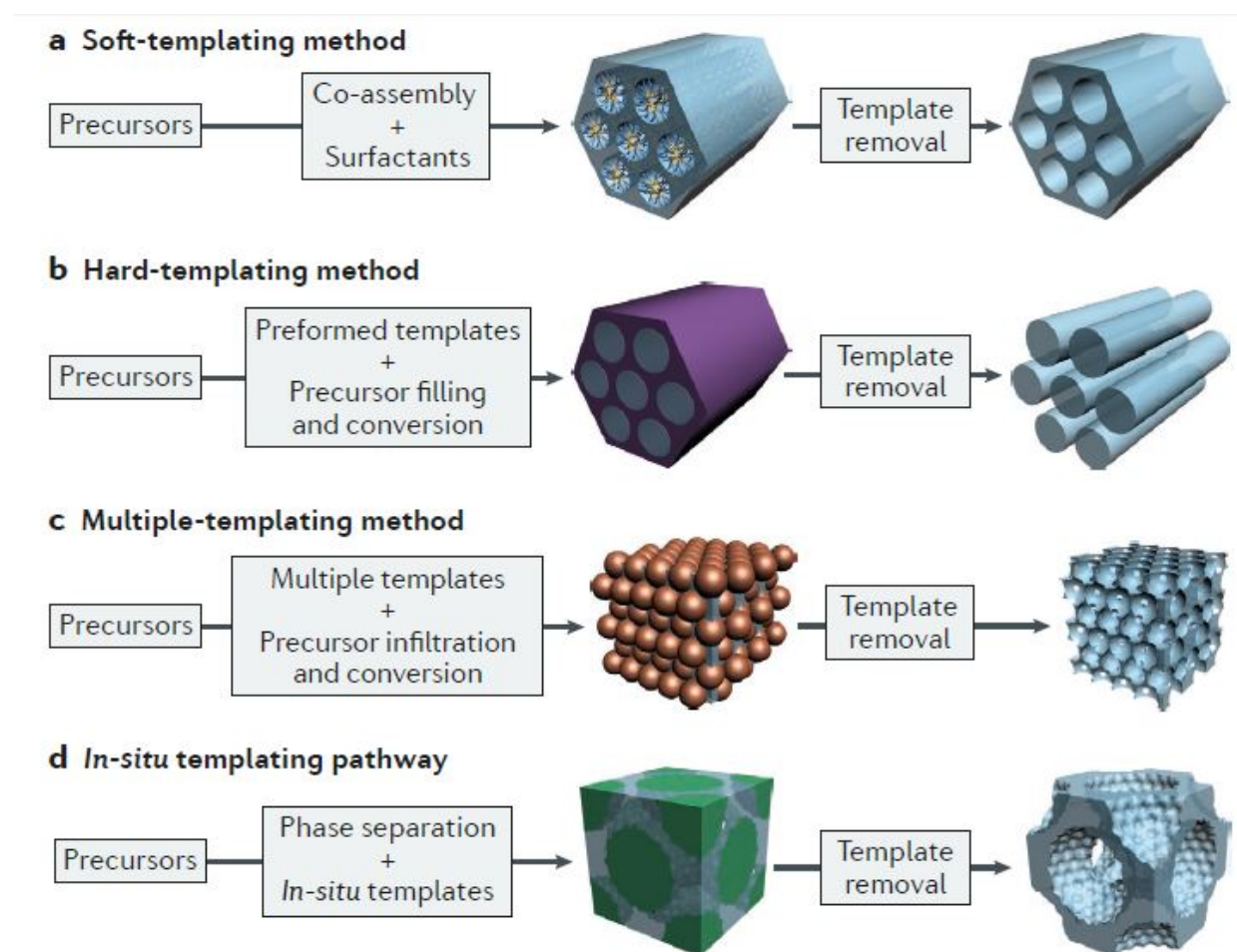


**Figure 28**. The principal methods for synthesizing mesoporous materials. **a)** Soft-templating method. **b)** Hard-templating method. **c)** Multiple-templating method. **d)** *In-situ* templating pathway.
[Reproduced with permission from ref. 118. Copyright 2016. The Nature publishing group.]

As depicted above, the physical properties of templates can vary significantly from soft to hard templating, both having their advantage and disadvantages, Table 2.

The last step common to all the previous methods consists in the removal of the template after the synthesis, which can be carried out with calcination or etching as long as the synthesized material is preserved. Mild methods have been developed to allow the recovery and the reuse of the organic template. The interactions between the framework and the surfactants are mainly of electrostatic nature, the removal of the template can be thus carried out by mild treatments such as liquid extraction with salt solutions or alcohols.[121]

**Table 2.** Comparison of soft- and hard-templating synthetic methods.
[Adapted with permission from ref. 118. Copyright 2016. The Nature publishing group.]

| Methods | Examples of mesoporous materials | Advantages | Disadvantages |
|---|---|---|---|
| **Soft-templating method** | • Silica<br>• Carbon<br>• Polymers<br>• Metals<br>• Organosilica | • Controllable mesostructured and pore sizes<br>• Tuneable morphologies<br>• High quality product<br>• Large scale production | • Uses surfactants<br>• Mesostructured formation<br>• Highly sensitive to the reaction conditions<br>• Relatively low crystallinity |
| **Hard-templating method** | • Carbon<br>• Metal oxides<br>• Zeolithes | • Low sensitivity to reactions conditions<br>• Highly crystalline product<br>• Ordered nanoarrays structure | • Uses preformed hard templates<br>• High cost<br>• Time consuming |

## 4.2 Porous siliceous material

The synthesis and development of methods for the production of silica-based porous material are currently an intensive area of research. An upsurge of interest for the porous material started in 1992 when the synthesis of mesoporous silica particles known as M41S material, carried out by Beck and Mobil's researchers was reported.[119, 122] It should be noted that the synthesis of micelle-templated mesoporous silica had been already published in a US patent 21 years before Beck's paper.[123]

Such as zeolites, which are natural mineral microporous materials, silica mesoporous materials are also characterized by a high surface area and an ordered pore system. Among silica solids of the M41S class material the MCM-41 (Mobil composition of matter n°41), MCM-48 and MCM-50 materials are some of the most studied.[124] Each of these silica mesoporous material features different mesopores arrangement, hexagonal for MCM-41, cubic for MCM-48 and laminar structure for MCM-50, Figure 29.
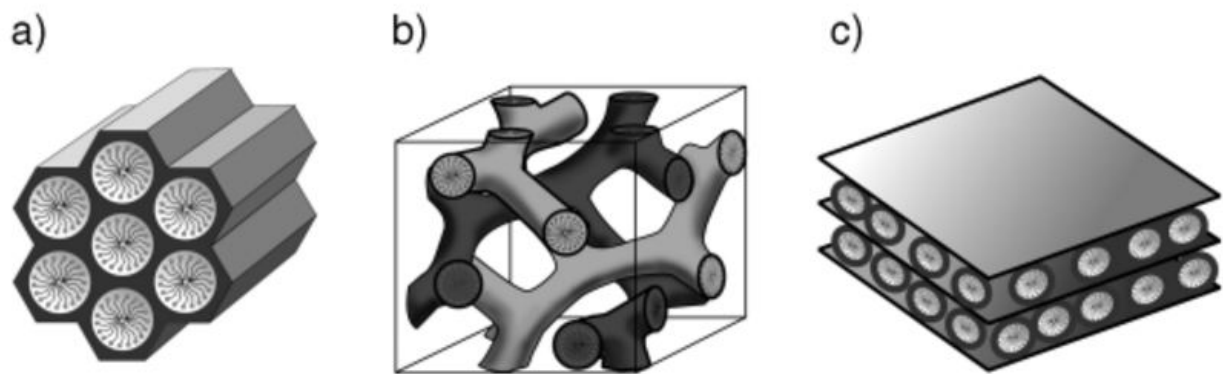
**Figure 29**. Structures of mesoporous M41S materials: **a**) MCM-41 (hexagonal), **b**) MCM-48 (cubic) and **c**) MCM-50 (lamellar).
[Reproduced with permission from ref. 124. Copyright 2006. WILEY-VCH Verlag GmbH & Co. KGaA.]

Two mechanisms have been reported for the formation process of the composite material (silica + template), Figure 30. One involves a true liquid crystal templating, in that case the concentration of surfactant is high enough to form, under the prevailing conditions of temperature and pH, a lyotropic liquid phase without the requirement of the inorganic precursor framework (*e.g.* tetraethyl orthosilicate). The other pathway involves the formation of a liquid-crystal phase at lower concentration of surfactant and in the presence of the inorganic precursors. The cooperative self-assembly of the structure directing agent (SDA) and inorganic precursors leads to the assembly of ordered mesostructured composite during the condensation of the silica precursors.
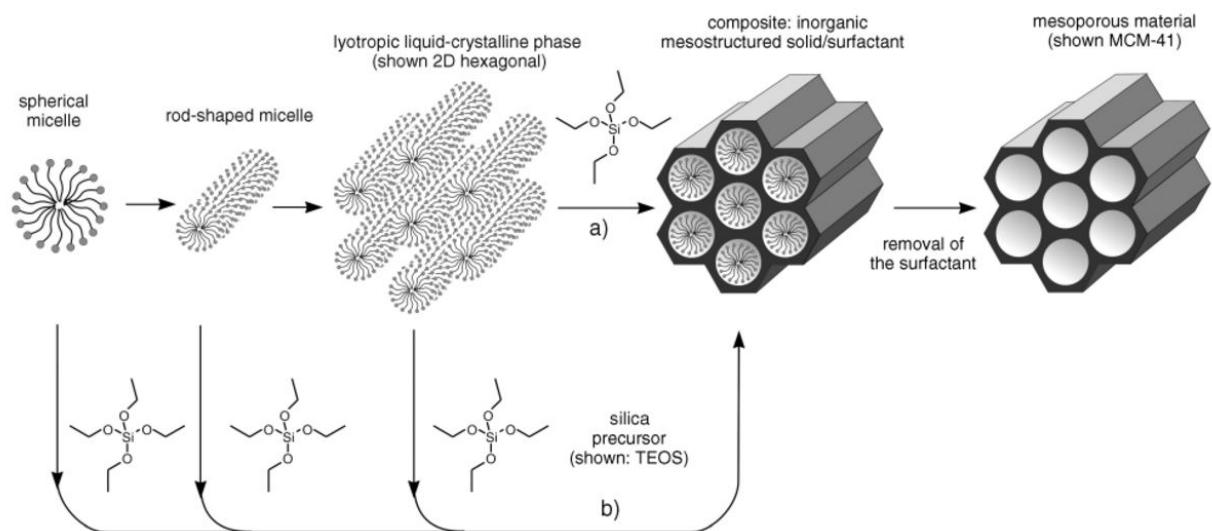


**Figure 30**. Formation of mesoporous materials by SDA: **a**) true liquid-crystal template mechanism, **b**) cooperative liquid-crystal template mechanism.
[Reproduced with permission from ref. 124. Copyright 2006. WILEY-VCH Verlag GmbH & Co. KGaA.]

A prerequisite for the viability of the method is that the template presents characteristic chemical functions to create with the silica precursor attractive interactions to ensure that no phase separation occurs. Different interactions can take place between the polar head of the surfactant and the inorganic precursor. Huo et al. proposed a classification for the different type of interactions, Figure 31.[124-125]
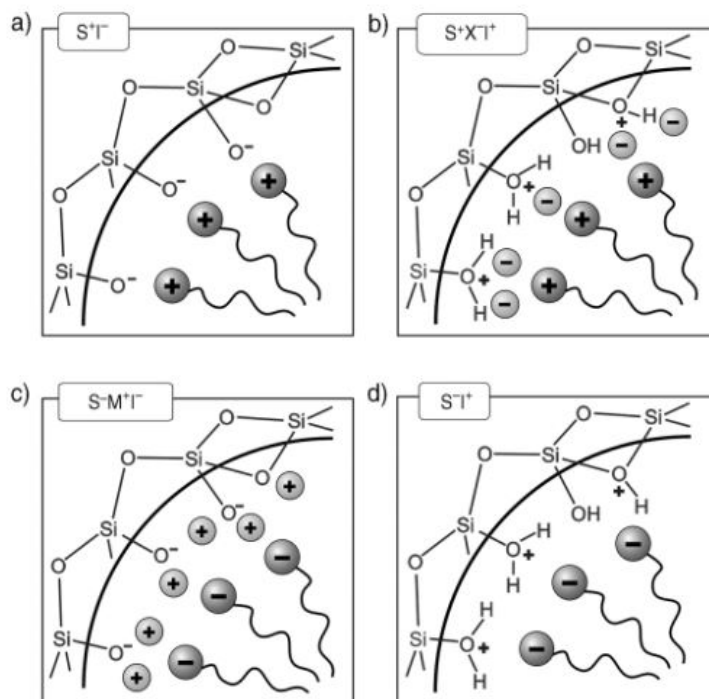


**Figure 31**. Interactions between the inorganic species and the head group of the surfactant for the possible synthetic pathway in **a**), **c**) basic and **b**), **d**) acidic media. (S: surfactant; I: inorganic species, $X^+$ and $M^-$: mediators). [Adapted with permission from ref. 124. Copyright 2006. WILEY-VCH Verlag GmbH & Co. KGaA.]

The authors proposed two direct pathways. One takes place under basic conditions where the silica species are present as anion and the cationic quaternary ammonium surfactants are used as SDA, the synthetic pathway is termed $S^+I^-$, (**a**). The other direct pathway takes place under acidic conditions. Negatively charged surfactants interact with the positively charged hydroxyl groups of the silica species, (**d**).

Two mediated pathways are also proposed by the authors where interactions are mediated by counterions of opposite charge to that of the surfactant, (**b** and **c**). In acidic conditions the silica species are positively charged. In the presence of cationic surfactant, the negatively charged mediators $X^-$ (e.g. halide) interact directly with the positively charged surfactants and allow to keep the attractive electrostatic forces with the positively charged hydroxyl groups of the silica species, (**b**).

On the contrary, when negatively charged surfactants are used as SDA in basic conditions, positively charged mediators ion $M^+$ interact with the negatively charged surfactants and ensure thus interactions with the negatively charged silica species, (**c**).

The authors showed that changes in the pH to adjust the charge density of different oxide species affect directly the final structure of the mesoporous material. Nonetheless, they did not study the effect of counterions at same pH neither the catalytic effect of quaternary ammonium surfactant on the silica polymerization rate.

## 4.3 Smart gate system in mesoporous silica particles

The high versatility of functionalization makes mesoporous silica particles a convenient tool for several applications. One of the advantages of mesoporous silica particles is the possibility to functionalize specifically one part of the particles. Three sites of functionalisation are available on mesoporous silica particles: the external surface of the particles, the entrance of the pores and the interior of the pores. Herein, we will focus mainly on the functionalisation of the pores gates. This type of functionalization allows to produce "smart gate" systems.

One of the first work carried out on the functionalization of the pore entrances was done by Fujiwara and coworkers.[126] Successful functionalization required uncalcined mesoporous particles with pores still filled with the surfactant molecules to ensure that the reactive molecules react preferentially at the pore outlets rather than inside of the pores. To create an access control to the pores, Fujiwara and coworkers used a coumarin derivative, 7-[(3-triethoxysilyl)propoxy]coumarin, as a gate. Before photo-irradiation the coumarin substituents were present as monomers, the gates were opened and allowed access to the interior of the pores. After photo-irradiation of the material at wavelengths longer than 310 nm, dimerization of the coumarin substituents occurred and the formation of cyclobutane dimers spanned the pore entrances obstructing the access to the pores. Subsequently, SDAs were removed by extraction leaving the pores empty. The authors proposed to use mesoporous silica particles as a tool for the controlled release of molecules and loaded the mesoporous particles with cholestane. As mentioned earlier, gates were closed through photo-irradiation ($\lambda$ > 310 nm) but irradiation at 250 nm triggered cleavage of the cyclobutane moiety and consequently allowed the released of the loaded molecules from the particles. The system allowed thus a controlled released under irradiation.

Other molecules have been used as capping agent for the production of "smart gates" system. Disulfide bonds for example have been employed as capping agent because of it can act as a gate. Fujiwara and coworkers used this strategy to prepare functionalized mesoporous silica particles able to control a catalytic reaction: the dimerization reaction of α-methylstyrene (AMS), Figure 32.[127] The authors loaded first the silica particles with aluminium acetylacetonate which was reported to be a catalyst of AMS dimerization. The second step consisted in the reaction of 6-hydroxy-2-naphthyldisulfide with 3-(triethoxysilyl)propyl isocyanate. The product of this reaction was grafted on the aluminium-loaded mesoporous silica. The disilane-disulfide substituent was cleaved with reducing agents and reformed using iodine. With the control of the pores outlet, the authors demonstrated that the reaction occurred only inside of the pores where the catalytic aluminium species were present.
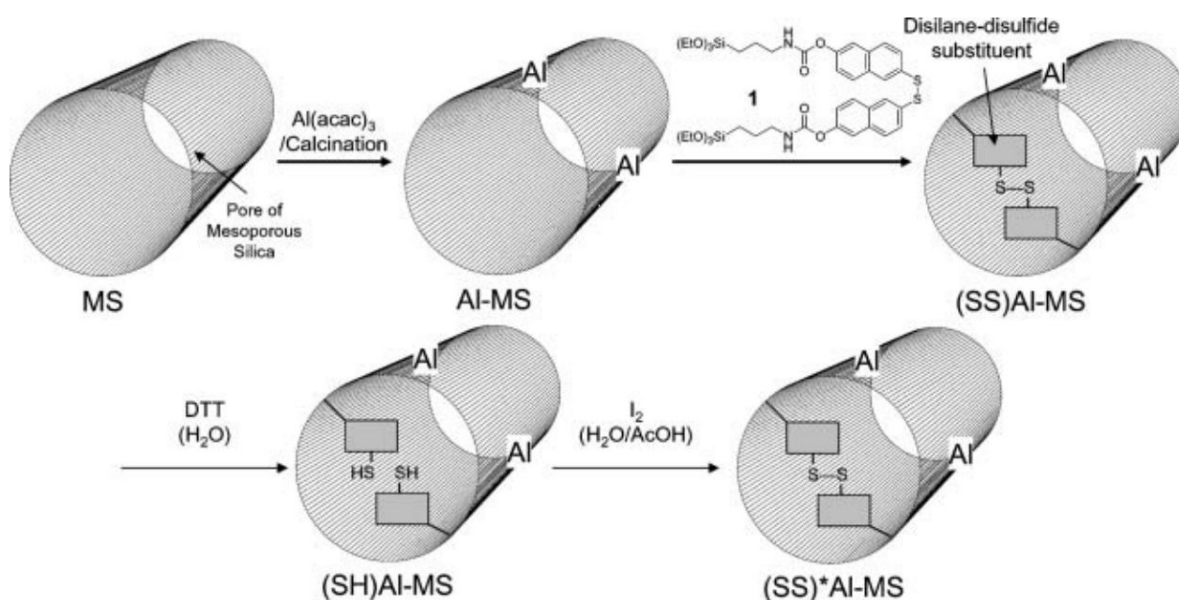


**Figure 32**. Scheme of mesoporous materials modified with a redox-responsive disulfide group. [Reproduced with permission from ref. 127. Copyright 2006. The Royal Society of Chemistry.]

More recently, several authors developed stimuli-responsive nanocontainers for the production of drug delivery system. Kim and coworkers functionalized the pore entrance of mesoporous particles with bulky CD molecules through a photocleavable *o*-nitroester bond, which upon irradiation at 350 nm, released a pre-loaded molecule.[128] Lin et al. produced mesoporous particles linked through an *o*-nitroester linker to gold nanoparticles. An anti-cancer drug (paclitaxel) was first loaded into the mesoporous particles and after functionalization with the gold nanoparticles, the mesoporous particles were administered to liver and fibroblast cells. After endocytosis of the drug-loaded nanocontainers, no cytotoxicity was shown for several

days which demonstrated an efficient control of the gate. After irradiation the cleavage of the *o*-nitroester linker caused the opening of the gates and resulted in the release of the paclitaxel, resulting in cell death. On the contrary, the exposition to irradiation of cells that have not been exposed to the drug loaded mesoporous particles did not lead to cell death, neither the cells that have been exposed to drug-free mesoporous particles.[129] Other methods have also been employed for the control of the gates implying ultrasound irradiation,[130] redox reaction,[131] pH, [132] or enzymatic trigger.[133] These stimuli-responsive nanocontainers may be used for imaging, therapeutic, biosensing or targeted delivery applications.

# Chapter 2

# Objectives of the Research

S ince the advent of supramolecular chemistry, chemists have devoted strong effort in molecular engineering and supramolecular design to produce novel nanostructures in order to respond to new needs.

CDPs have been the subject of a significant number of applications as sorbent materials. They have been intensively studied for their ability to bind molecules such as naphthenic acids, cinnamaldehyde or aniline and have been also used to trap organic compounds for remediation purposes. Other CDPs were produced for the capture of metals in water. A number of CDPs have been developed to extract compounds from different media but very few were designed to target specific compounds from complex matrices. On the other side, OMW represents a threat for our environment as its high organic content is toxic for the fauna and flora. The composition of OMW represents also an important source of value-added molecules. Several phenolic compounds with antioxidant properties could be recovered from this matrix. The use of CDPs can then represent an alternative for the treatment of these OMW. This 2-in-1 process would allow the recycling of toxic OMW and value-added molecules would also be extracted. The challenge lies in the complexity of the matrix and in the design of the CDP to target one or several specific compounds from the high content of organic compounds.

At the frontier of materials science and supramolecular chemistry, the hierarchical assembly and the accurate molecular design of organic building blocks of π-conjugated chromophores, from molecules to well-defined solid-state 1D supramolecular nanostructure is considered as a topic of great importance. In terms of molecular engineering, the interest of chemists for such molecules is due to the rigid and planar geometry of π-conjugated molecules and their adjustable substituents. These features provide π-conjugated chromophores geometrical predisposition to form well-defined 1D structures, which are driven by the synergistic contribution of π–π stacking and other non-covalent interactions, such as hydrogen bonds, electrostatic and hydrophobic interactions. The versatility of functionalization of these 1D structures bestow scientists with promising advanced soft materials with opportunities in several fields as nanoelectronics, photovoltaics, photocatalysis, or sensors. Among π-conjugated systems, pyrene derivative, have been selected to produce 1D nanostructures. As other chromophore, pyrene derivative could be designed in a bottom-up approach to possess the information within the building block that would lead to the formation of 1D nanostructure. The pyrene derivative would be designed so as it would form intermolecular π-π stacking

interactions and hydrogen bonds and would feature a reactive functional group to be able to integrate further chemical group on the nanostructure.

Water contamination by oil spill is a major global problem and several approaches for the degradation of oil spills are available but stay fairly limited in efficiency. Among them, biostimulation has emerged as one of the most promising treatment for oil spill.

Biostimulation consists in the assistance of bacteria in the degradation of hydrocarbons contained in oil spills. As several drawbacks are associated to biostimulation methods as nutrient dilution and the non-specific release, we propose in the present thesis an alternative way to overcome dilution related issues and to degrade hydrocarbons through the stimulation of the microbial growth to increase the rate and efficiency of hydrocarbons degradation. The system would be able then to target specifically the oil phase and avoid any dilution of the needed nutrients into the sea, which should lead to a higher performance of the bacteria.

In conclusion three main problems are addressed. First, the phytotoxicity of polyphenolic compounds in non-treated OMW. Secondly, the challenging design of novel nanostructure for the potential application in optoelectronic. Thirdly, the lack of specificity and efficiency of biostimulation methods. Through this thesis we aim thus to design novel nanostructures to address environmental issues through the design of CD-based polymeric materials. We aim to use molecular engineering for the formation of self-assembled nanostructures and to design smart-nanocarriers able to deliver nutrients specifically to oil-degrading bacteria.

# Chapter 3

# Results and Discussions

## 1. Specific recovery of phenolic compounds

Herein, the use of CDPs for the extraction of specific phenolic compounds to address environmental issues concerning OMW will be discussed in details.

### 1.1 Olive oil mill wastewater

Difficulties to recover valuable chemicals from waste steams lie on the complexity of designing sorption materials specific to a molecular target and able to operate in complex matrices. Nonetheless, supramolecular materials thanks to their efficient molecular recognition properties, may find a wealth of new applications for the selective removal of valuable target from industrial streams. Among different possible applications, the use of CDPs to extract phenolic compounds from OMW represents a great alternative to conventional methods as membrane processes and liquid-liquid extraction.[134] Indeed, the large amount of OMW produced by the olive oil industry represents more than 30 million $m^3$ per year,[135] a large number that hides a huge threat for the environment. These wastewaters contain high loads of phenolic compounds known to possess phytotoxic activities.[136] The disposal of these wastewaters without any treatment into the environment represents a risk for the flora and consequently for the fauna as well. Beyond this hazard, phenolic compounds are also natural antioxidants which properties can be exploited for several applications as food and cosmetic formulations or for therapeutic applications.[134] In this respect, the extraction of such molecules serves two different purposes: wastewater decontamination and the recovery of value-added molecules. None of the technologies to recover phenolic compounds have really stepped out of the crowd to become the standard procedure. There is then a real opportunity to find alternative and efficient ways to valorise phenolic compounds from OMW. CDPs as sorbent material could be a promising tool for the recovery of phenolic compounds as it can be tuned to presents particular features and interactions that permit to target specific phenolic compounds.

### 1.2 CDP synthesis

We developed in our group synthetic methods that allow producing and testing molecular recognition properties of CDPs.[76, 78] The high throughput method allowed testing a large number of different CDP formulations. We demonstrated that the selective molecular recognition properties of CDPs could be optimized by tuning the size of the CD macrocycle and

by the selection of additional monomers used for their synthesis.[137] Based on this approach we produced six different CD-based polyurethanes to be used for the specific extraction of phenolic compounds from OMW. For the production of these CDPs, different monomers and cross linkers were used, Figure 33.
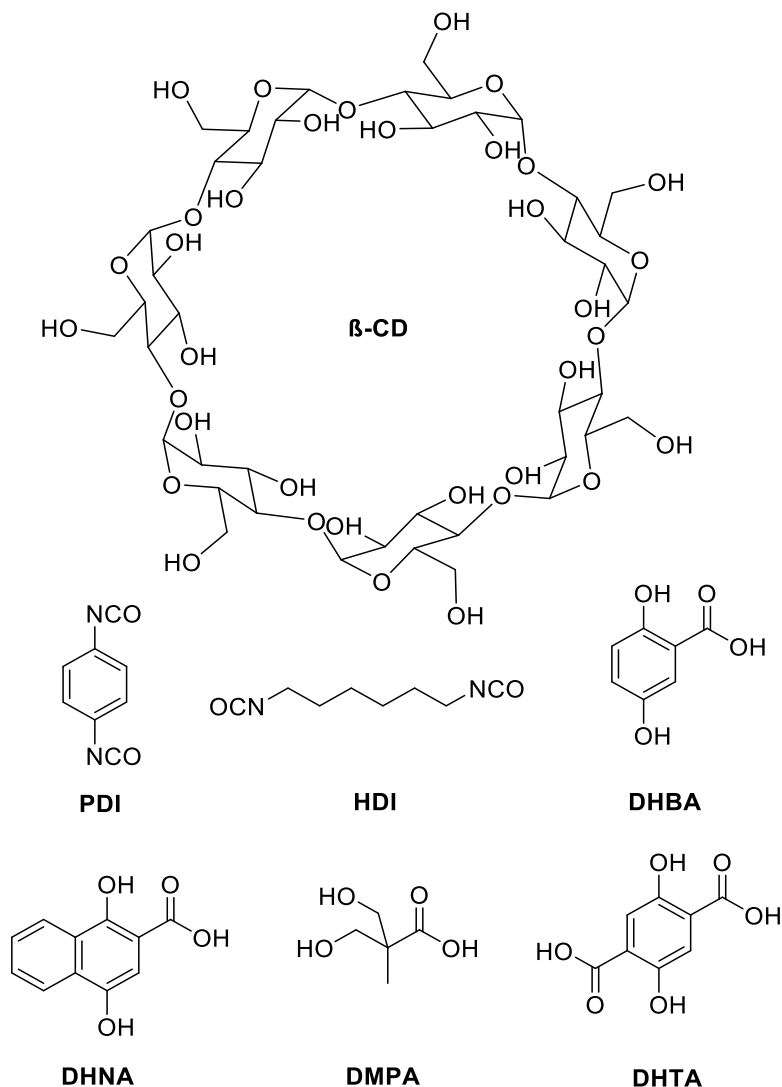


**Figure 33.** Chemical structures of β-CD and the monomers used to produce CDPs: 1,4-phenylene diisocyanate (PDI), hexamethylene diisocyanate (HDI), and cross linkers: dihydroxybenzoic acid (DHBA), 1,4-dihydroxy-2-naphthoic acid (DHNA), 2,2-Bis(hydroxymethyl)propionic acid (DMPA) and 2,5-dihydroxyterephtalic acid (DHTA).

In addition of β-CD, two monomers were used: 1,4-phenylene diisocyanate (PDI) and hexamethylene diisocyanate (HDI). PDI monomers contain an aromatic ring and are susceptible to interact with the phenolic compounds through π-π stacking. HDI monomers are made of an aliphatic chain that is expected to give more flexibility to the polymeric system but does not interact through π-π interactions with the phenolic compounds. Four cross-linkers were used: dihydroxybenzoic acid (DHBA), 1,4-dihydroxy-2-naphthoic acid (DHNA), 2,2-Bis(hydroxymethyl)propionic acid (DMPA) and 2,5-dihydroxyterephtalic acid (DHTA). DHBA and

DHTA both contain an aromatic ring, DHBA has also a carboxylic acid group and DHTA two carboxylic groups in positions 2 and 5. These two cross-linkers are expected to interact with the phenolic compounds through π-π stacking as PDI monomer. DHNA is made of two aromatic rings, and has been selected to assess the role of aromatic rings in the complexation with phenolic compounds. DMPA is the only cross linker with no aromatic ring but one carboxylic acid function that should gave hint on the potential role of hydrogen interactions and possible charge effect but also indirectly on the role of aromatic ring. Hydroxyl groups present on CD and cross-linkers are reactive groups that are potentially reacting with the urethane functions. The composition and the quantities used for each polymerization are given in Table 3. The reaction mechanism along with the scheme of the final structure of CDPs is given in Figure 34.

**Table 3.** Polymers produced and their composition.

| Polymers | Monomers | Quantity (mmol) | Mass m (g) |
|---|---|---|---|
| **CDP 71** | PDI | 48 | 7.69 |
| **CDP 74** | HDI | 48 | 8.07 |
| **CDP 76** | PDI | 48 | 7.69 |
| | DHBA | 6 | 0.93 |
| **CDP 78** | PDI | 48 | 7.69 |
| | DHNA | 6 | 1.23 |
| **CDP 87** | HDI | 48 | 8.07 |
| | DMPA | 6 | 0.80 |
| **CDP 89** | HDI | 48 | 8.07 |
| | DHTA | 6 | 1.19 |

Dibutyltin dilaurate (DBTDL) was used as catalyst for the synthesis of CDPs. The reaction occurs through an exchange/insertion mechanism and is divided into three steps.[138] The first one consists in the associative exchange of the alcohol with the carboxylic group of the tin compound. The second step is the coordination of the isocyanate followed by the insertion of the isocyanate into the Sn-O bond and the third step involves the associative exchange of the newly formed intermediate by another alcohol. A higher reactivity of primary alcohol functions and a higher steric hindrance of the secondary alcohol functions would lead to a kinetic regioselectivity but would not prevent the reaction to happen also on the secondary rim. It is worth to mention that the partial regioselectivity on the primary rim would give even less steric

hindrance on the secondary rim and facilitates the complexation of the phenolic compounds when entering CD molecules through the wider (secondary) rim of CDs.
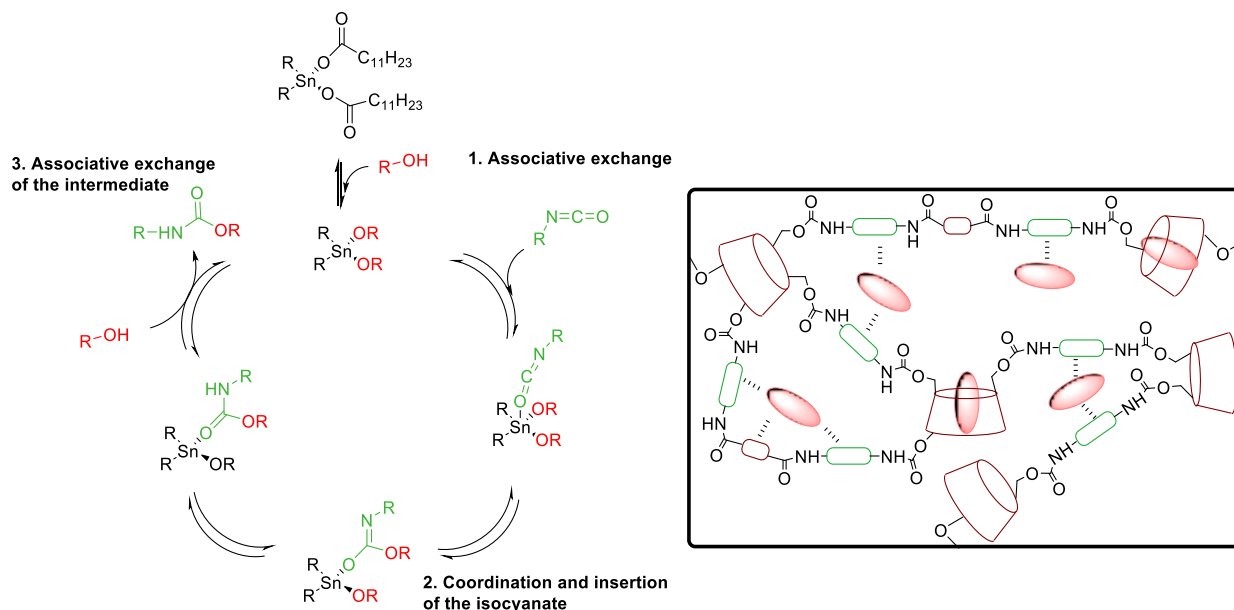


**Figure 34.** Possible reaction mechanism for the CD-based polyurethane formation and the schematic structure of CDPs with the possible interactions with polyphenolic compounds. CD (red truncated cone), monomers (green rectangle), cross-linkers (red rectangle) phenolic compounds (red ellipsoid).

To assess the polymerization efficiency, Fourier transform infra-red (FTIR) spectroscopy analyses were carried out on the CDPs, Figure 35. The appearance of the main polyurethane stretching vibration bands: $\nu$ (N-H) 3290 cm$^{-1}$, $\nu$ (C=O) 1660 cm$^{-1}$, $\nu$ (C-N) 1520 cm$^{-1}$, 1220 cm$^{-1}$, $\nu$ (C-O-C) 1040 cm$^{-1}$ and the absence of the isocyanate stretching band of the starting reactive $\nu$ (N=C=O) 2270 cm$^{-1}$ confirmed the effective polymerization process.
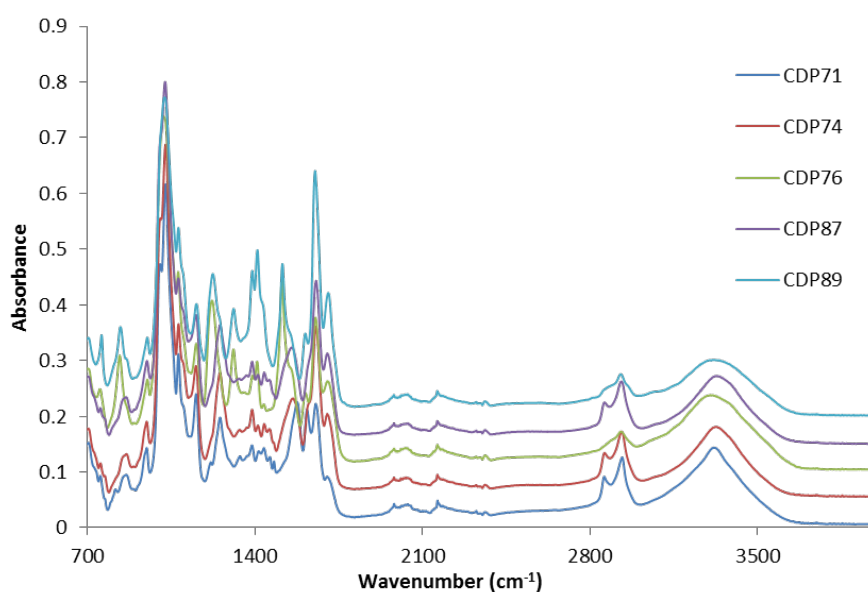


**Figure 35.** Stacked FTIR spectra of the produced CDPs.

**1.3 Cyclodextrin-based polymer doped with magnetic nanoparticles**

In order to increase the surface ratio of the CDPs and thus increase their efficiency to extract phenolic compounds but also to allow the recovery and the recycling of the polymer with an alternative method (other than the bed reactor method exposed in the following sections), magnetic particles of CDPs were produced using magnetic iron (II, III) oxide ($Fe_3O_4$) particles. These magnetic nanoparticles (MNPs) can be recycled through the use of magnetic field recovery system. The strategy implies the pre-functionalization of the $Fe_3O_4$ nanoparticles with 3-aminopropyltriethoxysilane (APTES) as depicted in Figure 36. APTES is first hydrolysed then the polycondensation occurs and forms at the surface of the MNPs an "amino layer". After addition of CDs and monomers, the monomers isocyanate groups undergo a nucleophilic attack from the amino groups covering the surface of the MNPs to yield a polymeric layer.
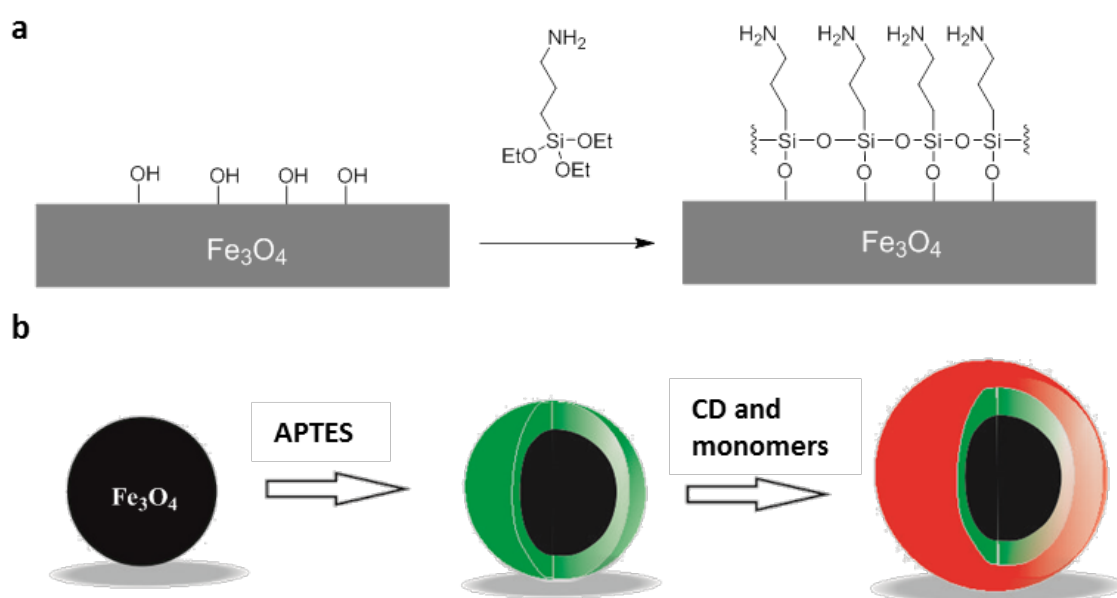


**Figure 36.** Schematic representation of the procedure to produce CDP MNPs. **a)** Chemical reaction between hydroxyl groups present on the surface of iron oxide particles and APTES. **b)** Synthetic pathway to produce CD-based polymeric. In green the amino layer and in red the CD-based polymeric layer.

The surface functionalization of MNPs was confirmed by ζ-potential measurements, Figure 37. The partial positive charges brought by the amino groups led to an increase of the ζ-potential from -5.2 mV to 14 mV. The iron oxide-doped CDPs produced were investigated by scanning electron microscopy (SEM). Among the four compositions tested only one polymerization successfully led to CDP spherical magnetic particles ranging from 100 nm to 1 μm (CDP 89). FTIR spectroscopic analyses also confirmed the effective polymerization around the magnetic particles with the appearance of the characteristic peaks of the

polyurethane at v (N-H) 3290 cm$^{-1}$, v (C=O) 1660 cm$^{-1}$, v (C-N) 1520 cm$^{-1}$, 1220 cm$^{-1}$ and v (C-O-C) 1040 cm$^{-1}$. The recovery of the final CDPs was achieved by simply approaching a magnet to the flask and separating the magnetic particles from the solution. This may be a potential straightforward method to recover the magnetic polymer to recycle it.
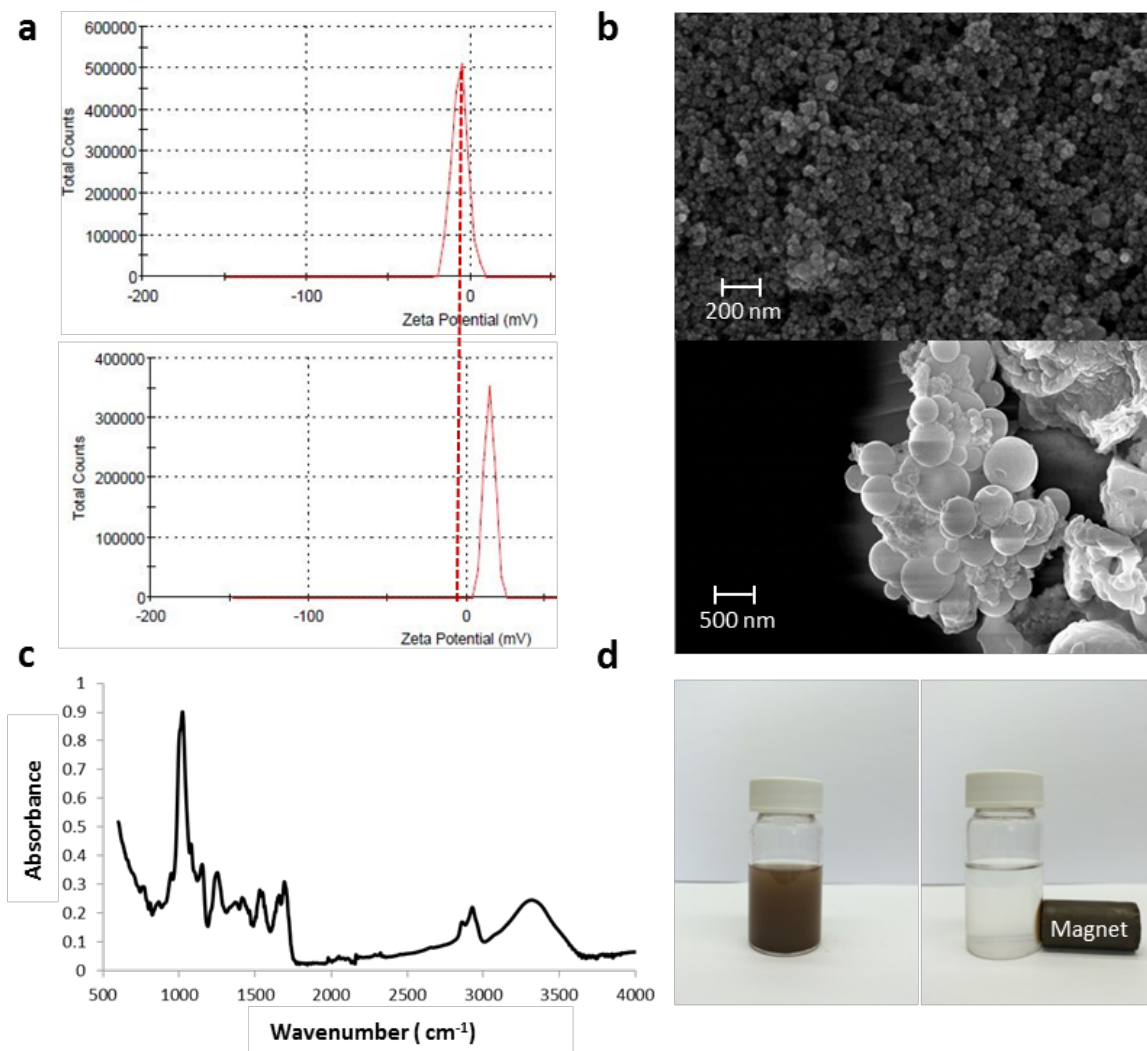


**Figure 37. a**) ζ-potential measurements of iron oxide particles before (up) and after (bottom) APTES functionalization. **b**) SEM micrographs of iron oxide nanoparticles (up) and CDP magnetic particles (bottom). **c**) FTIR spectrum of CDP 89. **d**) Photographs of iron oxide-doped CDP dispersed in water and their response to a magnetic field.

### 1.4 Recovery of selected polyphenols

The adsorption properties of the CDPs produced were tested for selected phenolic compounds commonly found in OMW, namely syringic acid, *p*-coumaric acid, TY and caffeic acid. In this study, four different water-insoluble polymers were tested (CDP 71, 74, 76 and CDP 89). Each polymer was prepared with a different monomer composition in order to evaluate their binding efficiency towards the four selected phenolic compounds. The chemical structures of the

selected phenolic compounds are shown in Figure 38. Binding assays were performed in water for each phenolic compound, Figure 39.
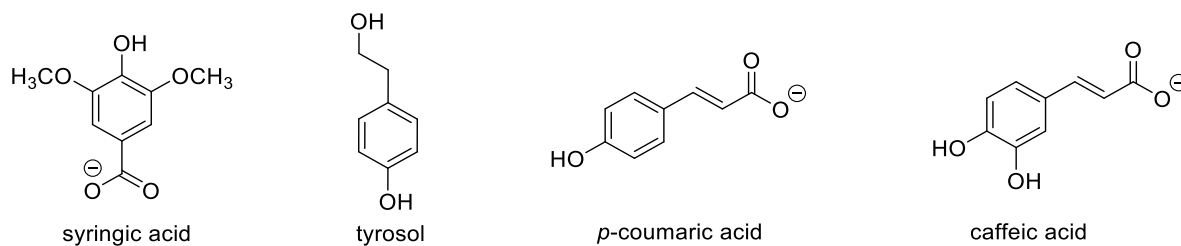


**Figure 38.** Chemical structures of the selected phenolic compounds at pH 6.
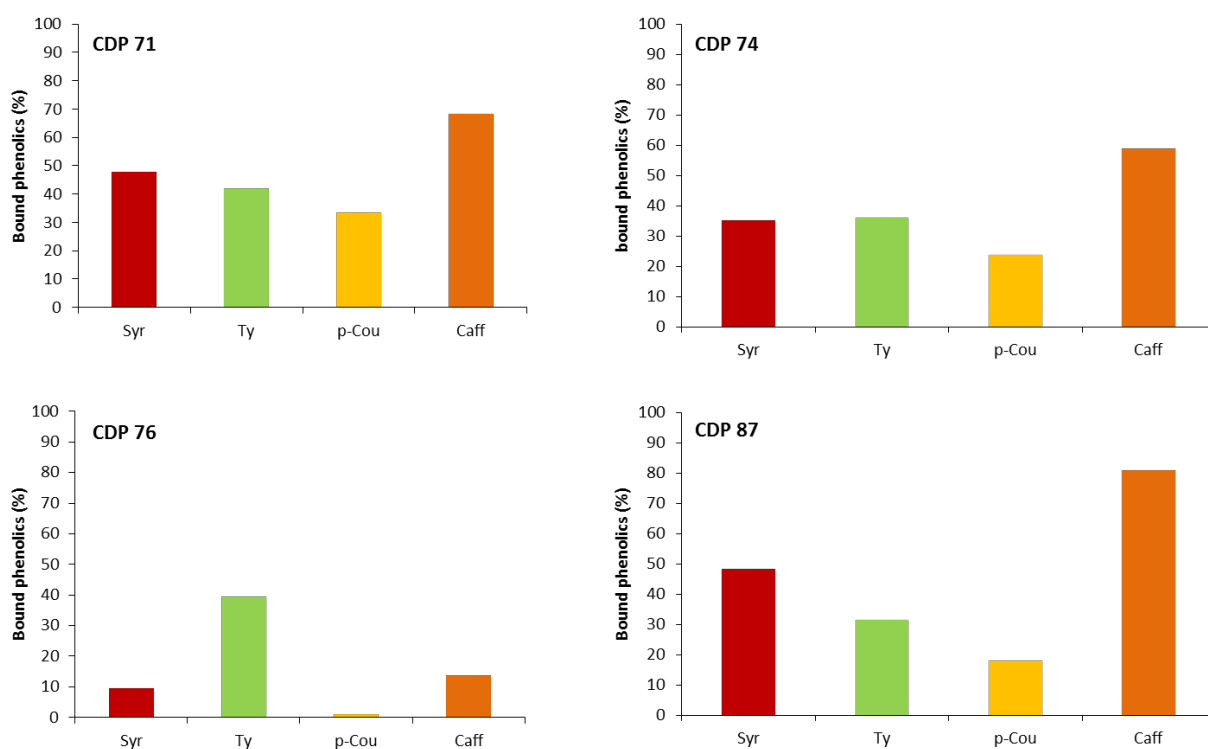


**Figure 39.** Percentage of adsorbed syringic acid (Syr), tyrosol (TY), p-coumaric acid (p-Cou) and caffeic acid (Caff) onto CDP 71, 74, 76 and CDP 87. Data are presented normalized with the initial phenolic concentration.

CDP 71 exhibited a higher binding affinity than CDP 74 for the four phenolic compounds with 48%, 41%, 32% and 68% of bound syringic acid, TY, p-coumaric acid and caffeic acid respectively for CDP 71. Absorption of phenolic compounds by CDP 74 reached 35%, 36%, 22% and 57% for syringic acid, TY, p-coumaric acid and caffeic acid respectively. The higher affinity of CDP 71 for the phenolic compounds may lie in the presence of aromatic groups in CDP 71 (absent in CDP 74), that induces π-π interactions with the phenolic compounds. CDP 76, because of the additional use of the DHBA cross-linker, was the least efficient of those polymers to adsorb phenolic compounds. In that case, electrostatic repulsion occurring between the negatively charged carboxylic groups of the phenolic compounds and the cross-linker DHBA may be the

reason for the decrease of binding efficiency. At the pH of the phenolic solution (pH 6), 100 % of the carboxylic acids of DHBA monomers (pKa 2.93) were deprotonated. The phenolic compounds syringic acid, *p*-coumaric acid and caffeic acid have respectively the following pKa: 3.86, 4.64, and 4.37.[139-141] The deprotonated state of these phenolic compounds may lead to electrostatic repulsions with the negatively charged polymer. Oppositely, the chemical structure of TY does not contain carboxylic function or negative charges; it was therefore not affected by the presence of other carboxylic functions within the polymer and remains well adsorb by all the CDPs. CDP 87 was produced with DMPA cross-linker, although it bears a carboxylic group (pKa 4.64) its pKa is higher than DHBA (pKa 2.93) used for CDP 76. Same consequence is observed for CDP 87 produced with DMPA monomers and CDP 76 produced with DHBA monomers. A higher binding percentage was observed for CDP 87 than for CDP 76 because of the negative charges exhibited by DHBA monomers.

Electrostatic interactions have thus an effect on the absorption process and play also, alongside π-π interactions, an important role on the affinity of CDPs for phenolic compounds. Moreover, CDP 71 exhibited the best profile for the adsorption of phenolic compounds. In the next section we will focus on the adsorption of phenolic compound from a complex matrix: OMW.

## 1.5 Recovery of phenolic compounds from olive oil mill wastewater

The polymers were dispersed in a solution of OMW for 2h at 25°C. Suspensions were then centrifuged and supernatants recovered and analysed by high performance-liquid chromatography (HPLC). The chromatogram of the corresponding supernatants and binding efficiencies of each polymer are shown in Figure 40.
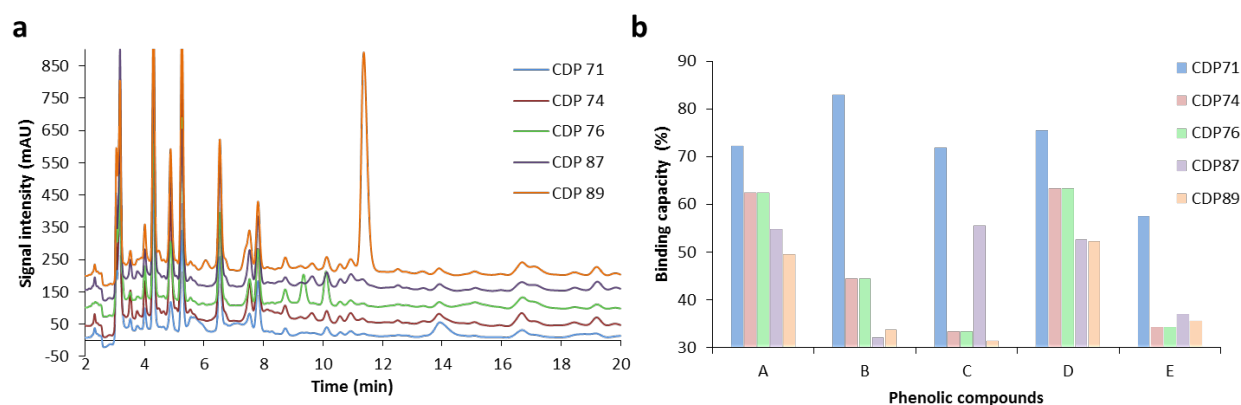


**Figure 40. a**) Stacked HPLC-DAD chromatograms of the supernatant after incubation of OMW samples with CDP 71, 74, 76, 87 and 89. (λ = 230 nm; injection vol.: 50 μL) **b**) Binding capacity of CDP 71, 74, 76, 87 and 89 for the selected phenolic compounds.

Each CDP revealed different affinities towards the phenolic compounds. The five major peaks at 4.3, 4.8, 5.3, 6.5 and 7.8 minutes elution time corresponding to the main phenolic compounds present in OMW were named respectively A, B, C, D and E for clarity.

Integration and comparison of the peaks before and after adsorption allowed evaluating the binding capacity of the CDPs. Among the CDPs tested, CDP 71 showed a binding profile with a high adsorption capacity where more than 70% of the labelled phenolic compounds were bound to the polymer with a maximum of 83% for compound B.

Both binding profiles of CDP 74 and CDP 76 showed adsorption of more than 60% for A and D. CDP 87 showed higher binding capacity for compounds A, C and D but a very low binding efficiency for B and E. The less effective polymer, CDP 89, bound efficiently compounds A (50%) and D (52%) only. This is probably due to its hydrophobic character and the difficulty to obtain a homogenous dispersion in water.

In order to improve the specific recovery of phenolic compounds, desorption of these organic compounds was evaluated through the use of a CDP-packed column and desorption was performed with organic and non-organic solvents: ethanol, methanol, ethyl acetate, water, acidic (pH 2) and basic (pH 12) aqueous solutions, and methanol/water mixture. Relevant results were obtained with a mixture water/methanol on CDP 71, Figure 41. The CDP packed column was prepared by packing the desired CDP into the column and then loading it with OMW sample previously filtrated. Desorption was carried out with the selected solvents. The ratio of methanol/water was gradually increased over the different fractions collected.
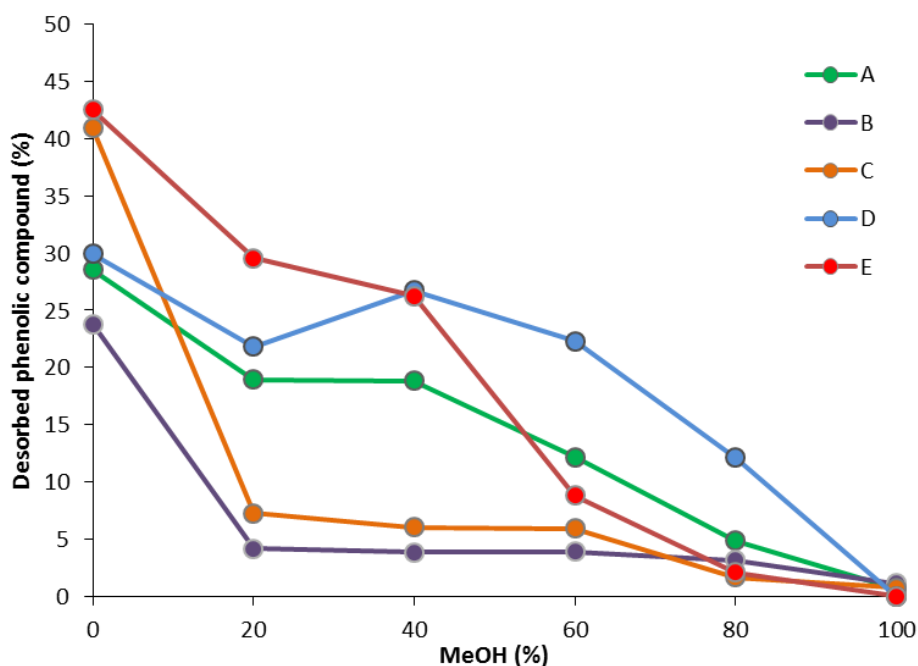
**Figure 41.** Desorption of phenolic compounds from CDP 71 with increasing proportions of methanol in a methanol/water mixture.

40% of compounds C and E, 30% of compounds A and D, and 25% of compound B were desorbed with 100% water for the first fraction. For the second fraction, the desorption percentage decreased for each compounds. This decrease was expected because the concentration of phenolic compounds contained into the CDP is decreasing over the fractions. However, an increase for compound D for the third fraction, precisely for a ratio 40/60 methanol/water, was observed. From these results, it appears that an enhanced selective desorption of compound D can be achieved using methanol/water mixture. We thus carried out the desorption of CDP packed column using methanol/water (60/40) over eight fractions, which were analysed by HPLC, Figure 42.
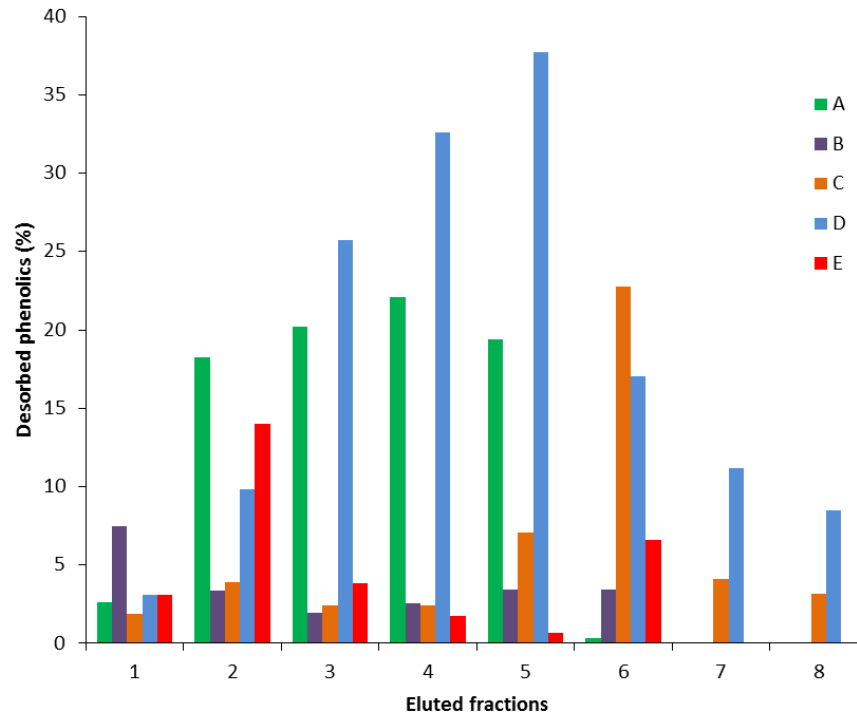
**Figure 42.** Percentage of the desorbed phenolic compounds from CDP 71 over the fractions with a mixture water/methanol 60/40.

The concentration of desorbed phenolic compounds is increasing until the fifth fraction where compound D represents about 40% of the overall fraction, and almost 60% for compound A and D together. Compound E is quickly desorbed and reaches its maximum for the second fraction while compound C is only eluted after a certain time at the sixth fraction. An enrichment ratio was calculated using the following formula:

$$E_{ratio} = \frac{(A_{(P)}/A_{(total)})_f}{(A_{(P)}/A_{(total)})_i}$$

With $E_{ratio}$ the enrichment ratio;

$A_{(P)}$ the area for the targeted phenolic compounds;

$A_{(total)}$ the area for the total phenolic compounds;

$i$ represents the initial values before adsorption and desorption from the CDP;

and $f$ represents the final values after desorption from the CDP.

The enrichment ratio is shown for each phenolic compound in Figure 43.
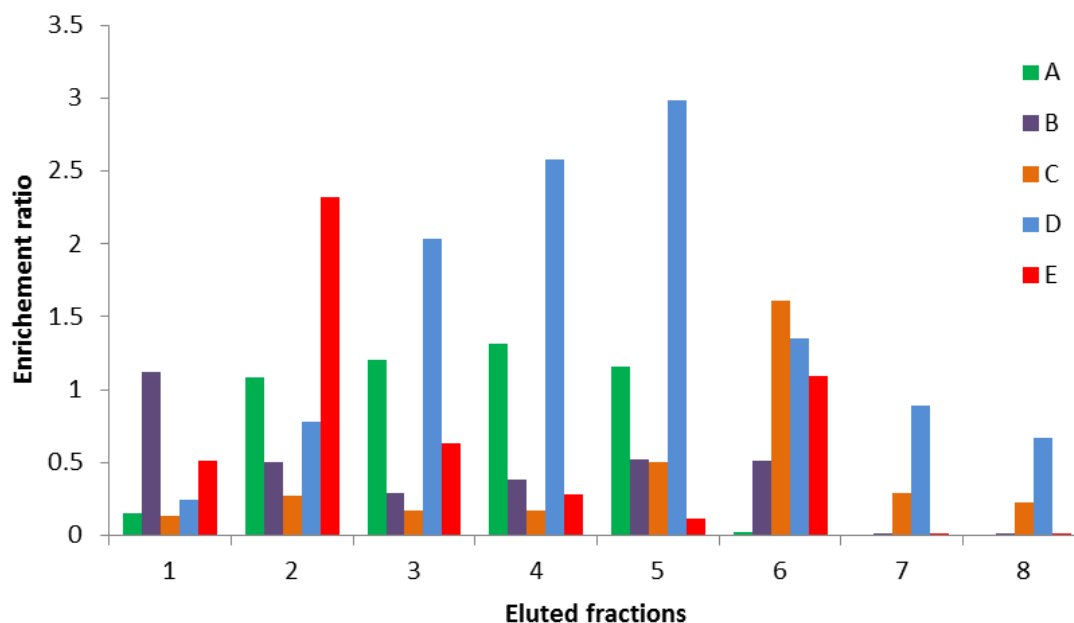
**Figure 43.** Enrichment ratio of the studied phenolic compounds.

The highest concentration of compound D was recovered in fraction 5 and its concentration was 3 times higher than in the original fraction. This result allowed us to confirm the selective desorption of compound D compared to the other phenolic compounds. Compound E was also recovered with a high enrichment ratio of 2.5 in fraction 2.

The chromatograms before adsorption and after desorption (fraction 5) of phenolic compounds from OMW are presented in Figure 44. Compounds A and D were isolated as major compounds. Additional ion trap mass spectroscopy analyses were carried out on compound D that was recovered in an effective manner. The results allowed identifying TY, a major phenolic component of olive oil known for its antioxidant properties.[142] Also compound A was identified by matching of retention time with the standard compound HT.
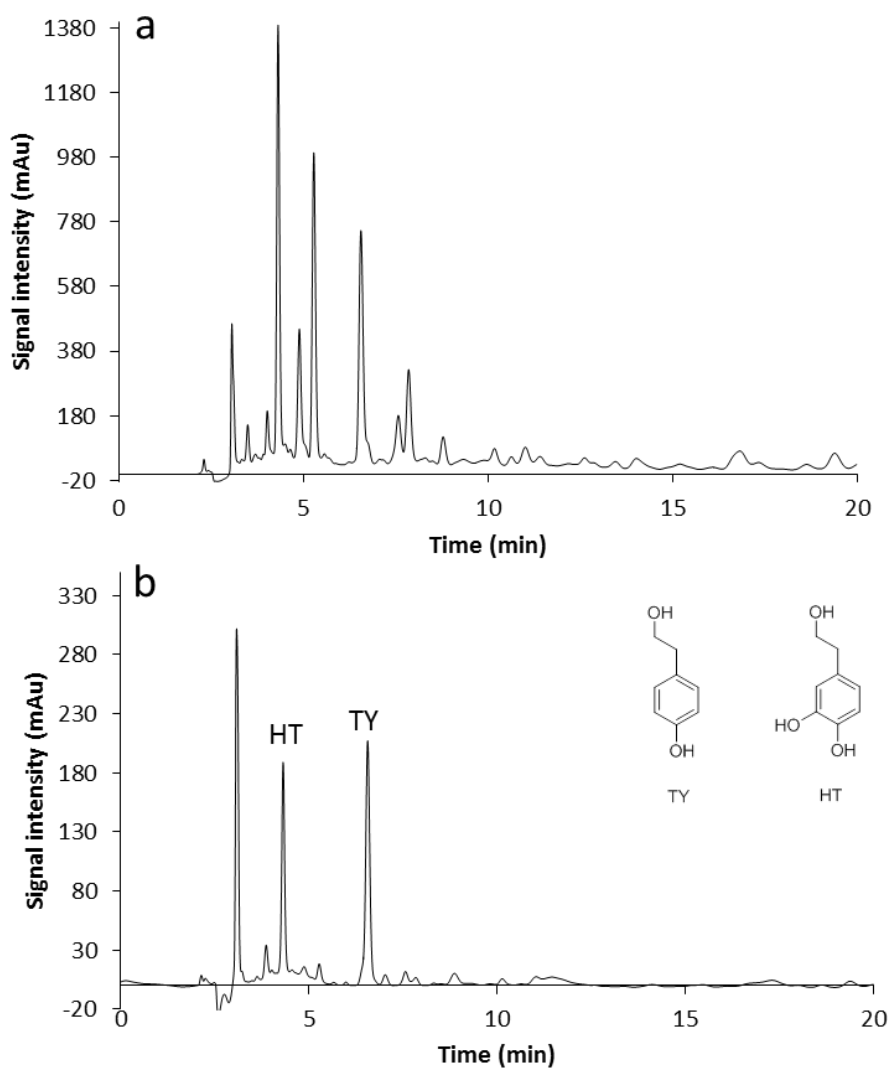
**Figure 44.** HPLC-DAD chromatograms before adsorption **a**) and after desorption **b**) from CDP 71. HT and TY were isolated.

## 1.6 Adsorption models

In order to determine the adsorption process of TY and HT onto CDPs, several adsorption models were studied. The results suggested that the adsorption of TY and HT onto CDPs were best described with the Freundlich model that defines a multilayer adsorption process, Figure 45 and Figure 46.
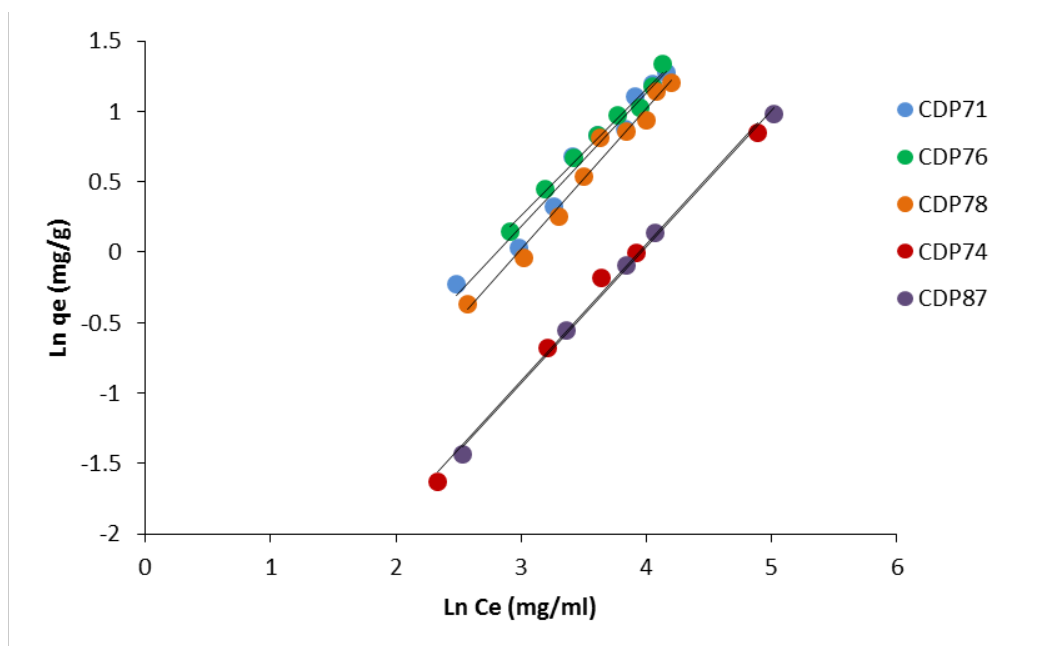
**Figure 45**. Freundlich adsorption isotherm of TY onto CDP 71, 74, 76, 78 and CDP 87 at 25°C. qe (mg/g) represents the amount of phenolic compounds adsorbed per amount of CDP and Ce (mg/L) represents the concentration of phenolic compounds in solution at equilibrium.

In Figure 45, linear Freundlich isotherms are presented. The affinity of the CDPs for TY was expected to depend only on the presence of π-π interactions. The isotherms confirmed the higher adsorption capacity of CDP bearing aromatic groups (CDP 71, 76 and 78) for TY. The adsorption parameters indicated that CDP 71 was the best CDP to adsorb TY despite the use of DHNA monomers for CDP 78, Table 4

**Table 4.** Adsorption parameters of TY onto CDP. $K_F$ represent the Freundlich constant related to adsorption capacity and 1/n is a dimensionless parameter related to intensity of adsorption that varies between 0 and 1 for a favourable sorption process.

| CDP | 71 | 74 | 76 | 78 | 87 |
|---|---|---|---|---|---|
| $R^2$ | 0.972 | 0.993 | 0.9867 | 0.979 | 0.991 |
| $K_F$ | 0.069 | 0.022 | 0.086 | 0.059 | 0.012 |
| 1/n | 0.952 | 0.968 | 0.902 | 1.001 | 1.032 |

The Freundlich constant $K_F$ was the lowest for CDP 87 and the highest $K_F$ values was obtained for CDP 76 and CDP 71. CDP 71 presents also the best 1/n value for a favourable sorption process. On the contrary CDP 78 and 87 showed 1/n values higher than 1 for the adsorption. These values confirmed us that the CDP 71 remains the best CDP for the adsorption of TY.

HT differs from TH by a unique hydroxyl group on the aromatic ring. Therefore it was assumed that CDP 74 and CDP 87 would exhibit the similar binding capacity for HT than for TY. It was thus decided to perform the assay with the following polymers: CDP 71, 76 and CDP 78, Figure 46. Freundlich parameters were extracted from the plot and are presented in Table 5. CDP 78 exhibits a very low $R^2$ and the $K_F$ is extremely low to be interpreted with the Freundlich model but CDP 71 exhibits the best $K_F$ and $1/n$ values for the adsorption of HT. Again, CDP 71 remains the best polymer to adsorb HT.
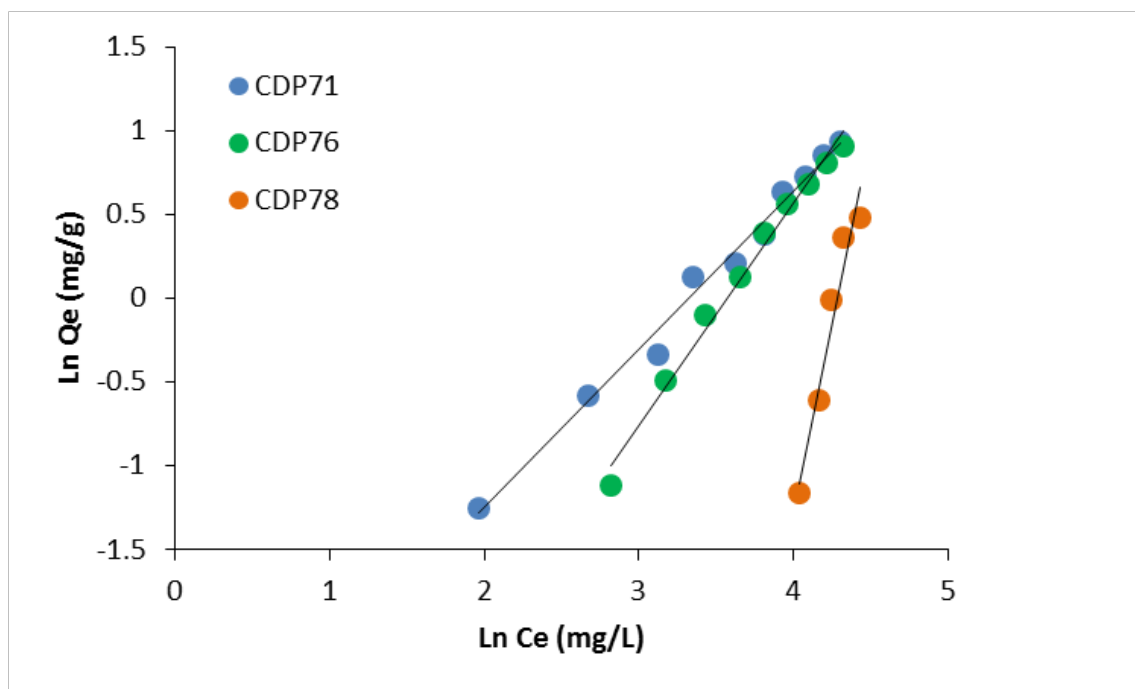


**Figure 46.** Freundlich adsorption isotherm of HT onto CDP 71, 76 and CDP 78 at 25°C.

**Table 5.** Adsorption parameter of HT onto CDP.

| CDP | 71 | 76 | 78 |
|---|---|---|---|
| $R^2$ | 0.988 | 0.988 | 0.952 |
| $K_F$ | 0.043 | 0.008 | $3.38 \times 10^{-9}$ |
| $1/n$ | 0.938 | 1.325 | 4.552 |

## 1.7 Adsorption kinetics

Adsorption kinetic of the two compounds TY and HT were obtained by following the adsorption kinetic procedure described in the experimental part. The adsorption kinetic allowed us to perform the next experiments with the correct time set. The amount of TY and HT in the liquid

was determined by HPLC and the amount of TY and HT adsorbed in the CDP was calculated from the following equation and the adsorption kinetics are shown in    Figure **47**.

$$Q = \frac{(C_{Lo} - C_{Li}) \times Vol}{W}$$

With,

$Q$ the mass of total phenols per gram of CDP

$C_{Lo}$ the initial concentration of total phenols in the liquid phase

$C_{Li}$ the total phenolic compounds concentration in the sample

$Vol$ is the total volume of the liquid phase

$W$ is the mass of CDP
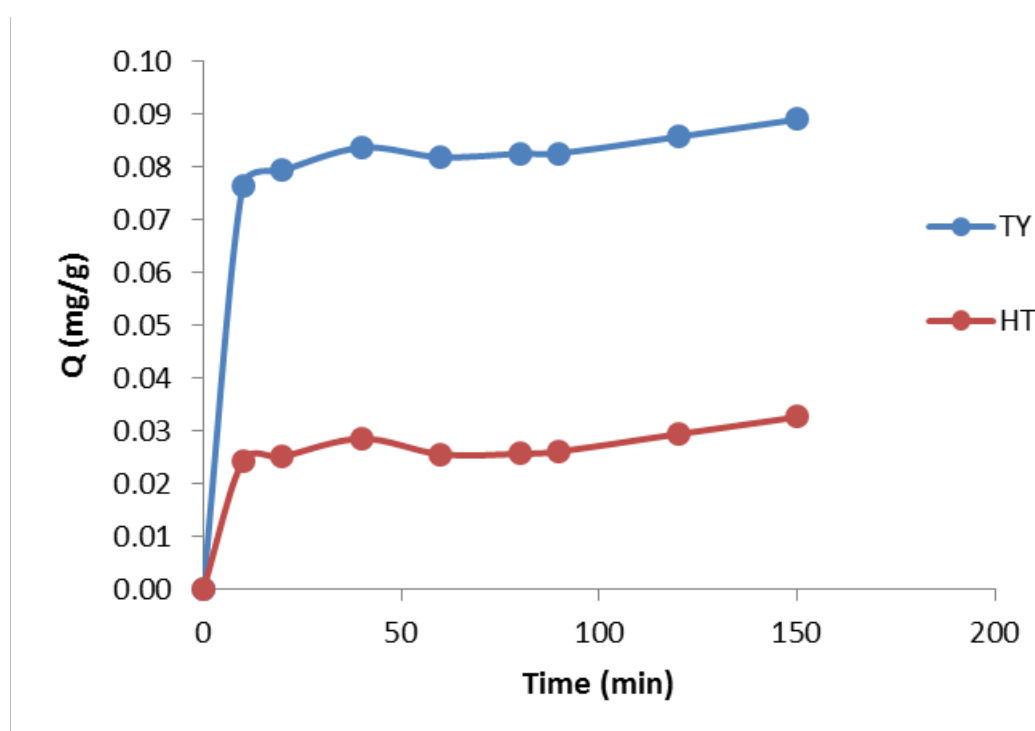


**Figure 47**. Adsorption kinetic for TY and HT.

The high adsorption rate between 0 and 10 minutes corresponds to the phase where the CDP has all his sites unoccupied until it reaches a plateau after 10 minutes where the majority of the sites are occupied and cause the adsorption rate to decrease. The concentration slightly increases and reaches a maximum at 150 min. The maximum time of experiment was therefore set to 150 min.

### 1.8 Scale-up on pilot plant

In order to perform the specific extraction of the phenolic compounds at a larger scale and assess if the method could be viable for industrial purpose a pilot plant has been built, Figure 48. A process flow diagram of the pilot plant is shown in Figure 81 (Annex). The pilot plant was equipped with reactors filled with the CDP. A scale up of CDP 71 to several kilograms was achieved. Several issues concerning the scale up of the synthesis of CDP 71 were addressed as the toxicity of dimethylformamide and its high boiling point, the long reaction time and the large amount of solvent needed to wash the polymer. The procedure is described in the experimental part and the conditions of optimization are shown in Table 9 (Annex). In order to keep the same adsorption efficiency towards the phenolic compounds, 4,4'-methylene diphenyl diisocyanate (MDI) was selected as monomer and β-CD was replaced by methylated β-CD (Me-β-CD) to perform the reaction in acetone as Me-β-CD possesses a higher solubility than β-CD in acetone and do not alter the binding performance of the polymer, Figure 49. The presence of two aromatic rings on the monomer linked through a methylene bridge gives the possibility to interact through π-π interactions but also endow the polymer with more flexibility than with the PDI.



**Figure 48**. Pilot plant for the recovery of phenolic compounds, (left: overview of the pilot plant; right: two reactors containing the CDP).
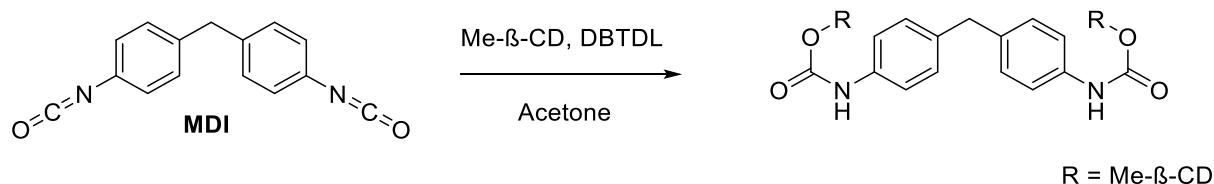


**Figure 49**. Reaction scheme for the production of CDP 100.

To assess if the polymer was well packed inside the reactor, a fluidynamic test was performed, Figure 50. A saline solution (0.01 M) used as tracer was passed through the reactor at a liquid velocity of 0.87 cm/min and the conductivity at the outlet was recorded.
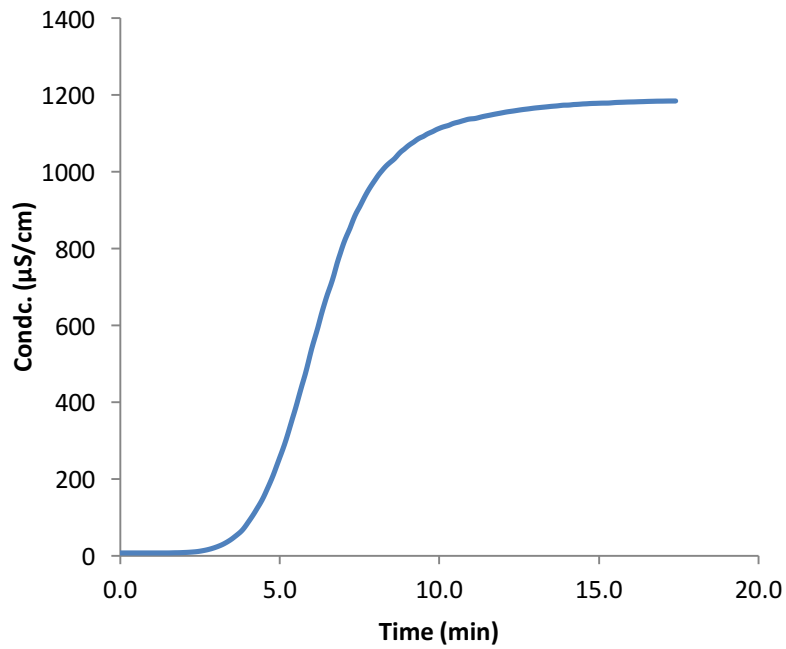


**Figure 50**. Sigmoidal conductivity curve of the tracer obtained for the CDP packed bed reactor.

The uniformity of the sigmoid describing the cumulative residence time distribution curve indicated a high quality and a high stability of the polymer packing.

Breakthrough tests were realised to assess the adsorption process using the chemical processing system, Figure 51. To avoid a significant pressure increase in the adsorption column and eventually the complete clogging of the inlet section, OMW were pre-treated to remove solid as described in the experimental part.
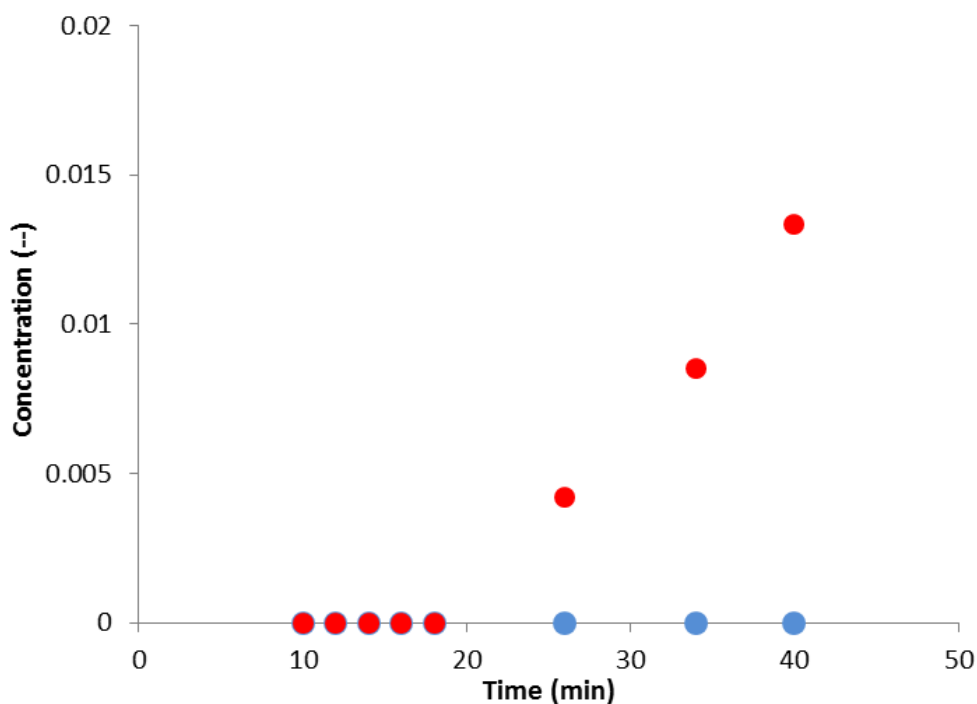
**Figure 51**. Breakthrough of TY (●) and HT(●) in CDP 100.

The results showed a high adsorption of TY as no amount of the phenolic compound is detected at the outlet of the pilot plant after 45 minutes. On the contrary, HT with a lower affinity for the CDP is detected after 25 minutes. These results also confirmed the results previously found with the isotherms showing the higher adsorption of TY by the CDP.

A procedure was then established to assess the desorbing process on the pilot plant. OMW were first fed to the pilot plant and run for 2h with a flow rate of 1.5 kg/L to saturate the CDP. Then the adsorbed phenolic compounds were desorbed with methanol and the fractions were recovered at the outlet of the pilot plant and analysed by HPLC. The concentrations recovered in the different fractions of TY and HT are reported in Figure 52.
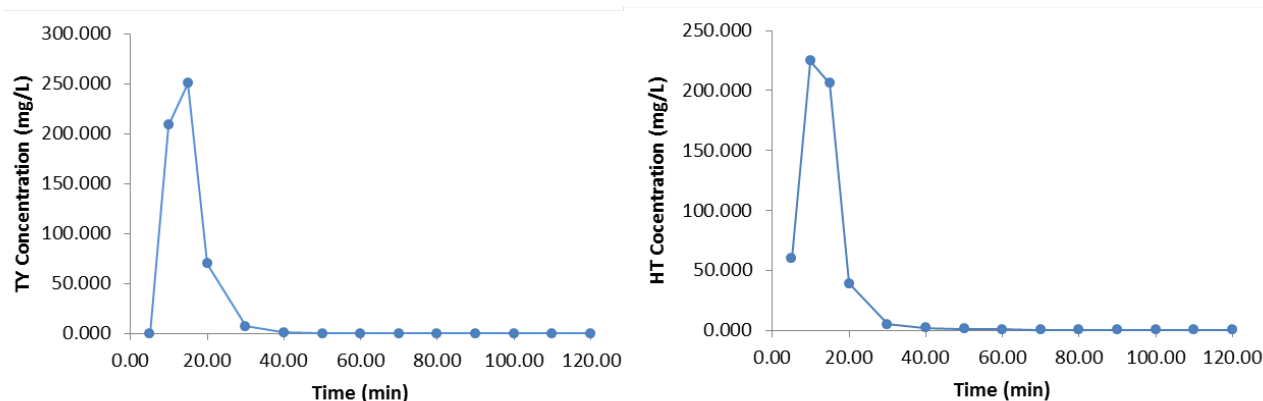


**Figure 52**. Evolution of desorbed TY and HT over time.

TY and HT were entirely desorbed from the CDP after 40 minutes. The highest concentration of TY was found at 15 minutes and at 10 minute for HT. An increase to 45.5% of TY and to 37.4% of HT was achieved for these fractions.

Experiments were performed and evaluated through HPLC to increase the purity of the phenolic compounds in the desorbed fractions by using different solvents of desorption. The desorption was carried out with a gradient of acidified water, acetonitrile (ACN) and methanol. The procedure is detailed in Table 10 (Annex).

The fractions with the highest concentration of TY and HT were recovered at 63 min with 75% acidified water and 15% of ACN. The richest fraction of TY collected at 90 min using a mixture of 40% acidified water and 60% methanol gave the richest fraction of TY (61%). Chromatograms of these two latter fractions are presented Figure 53. In the raw OMW, TY and HT account only for 14.1% and 2.1% respectively which represent an enrichment by 4 times for TY and by 2 times for HT.
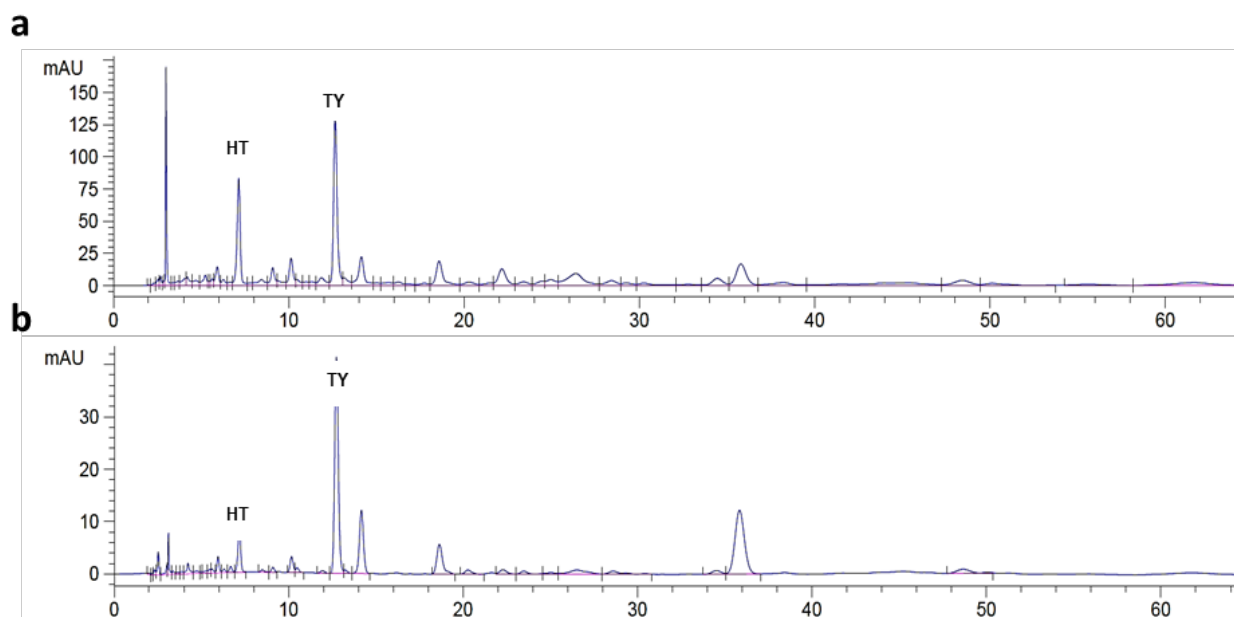


**Figure 53**. **a**) Desorption Fraction at 63 min (75% Acidified Water and 25% ACN). **b**) Desorption Fraction at 90 min (40% Acidified water and 60% MeOH).

## 1.9 Chemical oxygen demand analyses

COD analyses were performed to assess the amount of organic compounds in raw OMW and in the desorbed fractions. Gallic acid was used as reference for the polyphenols COD calculation. Fractions that were supposed to be non-relevant for the extraction of value-added phenolic

compounds were analysed, the average values is reported in Table 6. The results clearly indicated a decrease of COD between the non-treated OMW and the treated one. The total amount of organic compounds was reduced by 5 times in the OMW after the adsorption/desorption process. The COD coming from other organic compounds (sugar, lignin, protein) was also reduced by 5 times.

**Table 6.** COD level for raw OMW and for desorbed fraction from CDP.

| Sample | Total COD (g/L) | COD from phenolic compounds (g/L) | COD from other organic compounds (g/L) |
|---|---|---|---|
| **Raw OMW** | 22.0 | 1.39 | 20.61 |
| **Desorbed sample from CDP** | 4.67 | 0.18 | 4.49 |

## 1.10 Conclusion

Synthesis of 6 non-water soluble CDPs was carried out using different composition of monomers and cross-linkers. Each monomer or cross-linker was carefully chosen to assess how they will affect the binding capacity of the CDP.

Four selected phenolic compounds were tested and the different binding profiles allowed us to point out the central role of π-π and electrostatic interactions. CDP 71, produced with PDI monomer was demonstrated to bind significantly the targeted phenolic compounds and was shown to be the best CDP for the selective recovery of TY and HT from OMW.

CDPs were also produced as magnetic nanoparticles polymer through the amine-functionalization of iron oxide nanoparticles confirmed by ζ-potential measurement. This method allowed the recovery of the CDP with a simple magnet and also offers an alternative way to recycle CDPs.

Several organic solvents and mixtures were screened for the recovery of phenolic compounds from CDP. The mixture of methanol/water with a ratio 40:60 was the best to desorb effectively the CDP. It was chosen as solvent of choice for the recovery of TY and HT.

Adsorption models were studied and the linear Freundlich isotherm model matched the type of adsorption and provided the highest regression coefficient compare to other models and allowed us to confirm the heterogeneous adsorption process of TY and HT onto the polymer.

The adsorption kinetic was determined by calculation after HPLC analyses of the liquid phase and allowed us to assess the time of adsorption for TY and HT.

In order to perform the adsorption and the extraction of TY and HT at higher scale and to assess if the recovery of these two phenolic compounds could be achievable at higher scale a pilot plant was built. Equipped with two reactors, the latter was loaded with the produced CDP. The synthesis of CDP 71 was optimized for industrial scale using a solvent of low toxicity and reducing quantities of solvents and catalyst.

The good packing of the CDP in the reactor was assessed through fluidynamic test where a saline solution was passed through the reactor and conductivity was measured at the outlet. The sigmoidal curve confirmed the good quality of the packed bed reactor.

Breakthrough experiments were carried out on the pilot plant and adsorption profiles confirmed the higher adsorption of TY over HT. A method was developed with the pilot plant and a protocol established to extract the targeted phenolic compounds. The pilot plant reactor offered a good adsorption performance and the use of a solvent gradient for desorption appeared to be an efficient method for increasing TY and HT purity in the recovered fractions. TY content was raised to 61% after recovery when it was only 14.1% in the OMW sample.

Level of total COD in the recovered wastewaters was also reduced by 5 times, with a strong reduction of phytotoxic content making them relevant for irrigation purposes.

## 2. Hierarchical self-assembly formation of pyrene derivative into nanorods

In this section, will be discussed the supramolecular hierarchical self-assembly of a pyrene derivative into nanorods. We produced nanorods in a bottom-up approach in which a pyrene derivative was designed to display characteristic structural features.[143] The hierarchical self-assembly was realized in the absence of template and led to stable and well defined nanorods. Photoluminescence, X-ray diffraction studies and structural characterizations were carried out.

### 2.1 Design of the pyrene derivative

One of the remaining challenges of supramolecular chemistry is the design of large self-assembled and functional materials at the nanoscale, with accurate 3D control over the positioning of the constitutive building blocks.[144-146] The ambition to accurately predict the resulting assembly has driven scientists to design building blocks with chemical groups or entities with predictive interactions or behaviour in different environments. With the same approach, a new pyrene derivative, **1,** was designed so as to possess the following features: i) ability to form intermolecular π-π stacking interactions, ii) complementary H-bond donor and acceptor group (i.e. amide) that provides additional control over the self-assembly process, and iii) presence of bulky chemical functions (triethoxysilyl) that may be further exploited to functionalize the resulting self-assembled nanostructures, Figure 54.
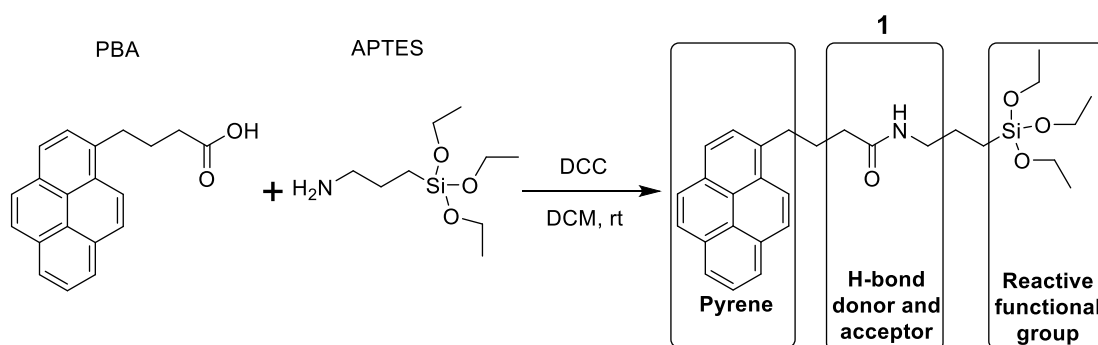


**Figure 54**. Schematic of the reaction.

Aromatic groups and pyrene moieties are found in numerous 1D nanomaterials and play a role in the stability of the material. In our case, the pyrene derivative **1** was made from an essential core: pyrene butyric acid (PBA). Synthesis of **1** was carried out by activating PBA with N,N'-dicyclohexylcarbodiimide (DCC) first and further reacted with APTES in dichloromethane at 25°C. **1** was characterized by ^{1}H and ^{13}C NMR, FT-IR, ESI-Mass spectrometry and elemental analysis, Figure 82, 83, 84 and 85 (Annex).

### 2.2 Photoluminescence

Taking advantage of the characteristic chromogenic properties of **1**, UV-Vis absorption spectroscopy was used to assess the self-assembly process. When the spectrum of **1** was recorded in ethanol, the analysis revealed well-resolved vibronic bands in the 250-370 nm range with four main peaks at 264, 274, 326 and 340 nm, Figure 55. The ratio of the peak intensities obtained in ethanol of the vibronic bands at 326 and 340 nm, $I_{326/I340}$, was found to be 1.33.
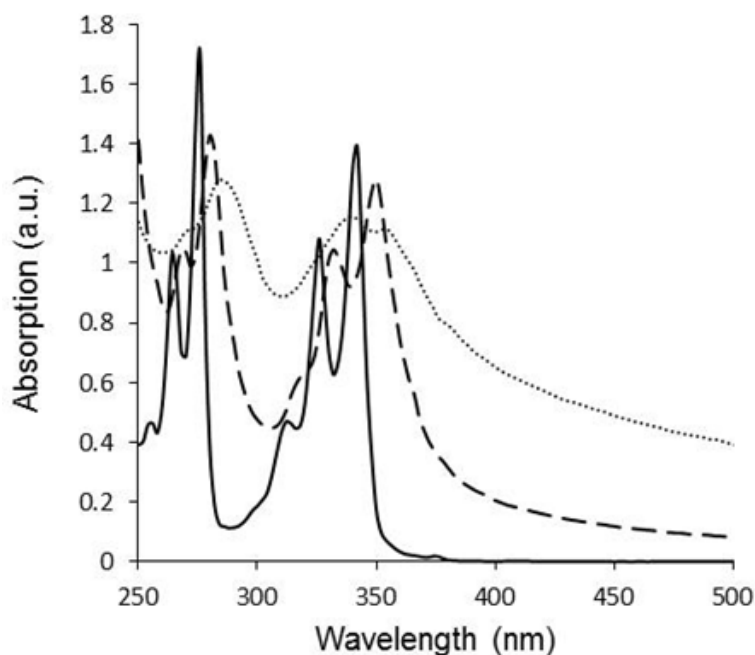


**Figure 55**. UV/Vis spectra of **1** (0.1 mM) in ethanol (solid line), in water (ethanol 10 vol. %) (dashed line) and in water (ethanol 10 vol. %) after ultrasonication (dotted line).

Solution of **1** in ethanol was poured into pure water to obtain a final ratio of water:ethanol 90:10. After the addition of ethanol into water the vibronic bands underwent a bathochromic shift. Indeed the bands at 264, 274, 326 and 340 nm were red-shifted to 268, 280, 332 and 350 nm, respectively. In addition, a significant decrease of the peak-to-valley ratio for all the bands was also observed. These observations are an evidence of the self-assembly process of 1 in aqueous medium, Table 11(Annex).[105, 147]

In order to favour the assembly process of supramolecular structures through non-covalent interactions, aqueous solution of **1** was subjected to ultrasonic treatment. As a result, the vibronic bands at 264, 274, 326 and 340 nm were red-shifted to 272, 284, 340 and 354 nm respectively. A stronger bathochromic shift than the one obtained without ultrasonic treatment was observed. Moreover, the ratio of intensities $I_{326/I340}$ was found to decrease significantly

from 1.33 to 0.96. From these observations, the spectroscopic changes suggested that the pyrene derivative monomers had self-assembled into supramolecular structures with an offset stacking arrangement specific to J-type aggregates.[105, 113, 147-148] A sharp red-shifted band is typically expected for J-type aggregates, but several examples of broad absorption band, as observed in the present case, have been reported.[113]

The fluorescence properties of **1** were investigated to gain further insights into the assembly process in ethanol at 0.2, 0.4, 1, 2, 5 and 10 mM, Figure 56. Upon increasing concentration of **1**, the intensity of the monomer peak measured at 378 nm decreased with concomitant appearance of a new peak at 480 nm, this can be safely attributed to excimer formation.[149-151] A significant change of the fluorescence maximum wavelength emission at low and high concentration of **1** could be observed. After ultrasonic treatment in aqueous medium, the fluorescence maximum wavelength changed to 412 nm, which corresponded to neither monomer nor excimer emission. This change is likely due to the formation of a self-assembled structure with a higher degree of structural order.
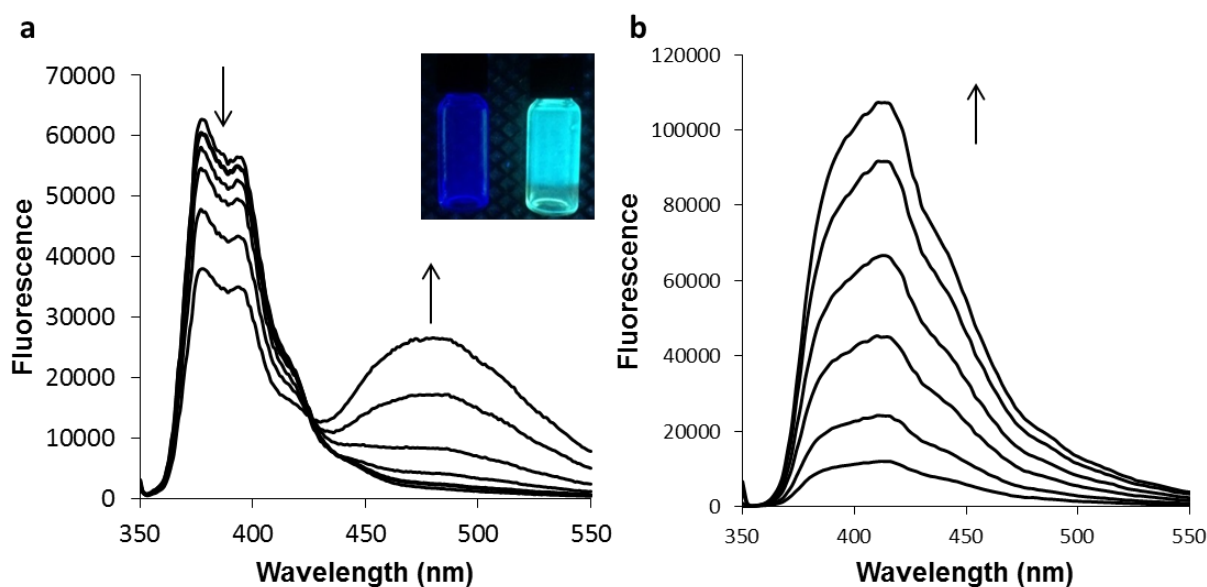


**Figure 56**. **a**) Fluorescence spectra of **1** ($\lambda$exc = 326 nm) in ethanol. Inset: photo of solutions of **1** in ethanol at low concentration (left) and at high concentration (right) under UV light ($\lambda$exc = 366 nm). **b**) Fluorescence spectra of **1** ($\lambda$exc = 326 nm) in aqueous medium (ethanol vol. 10%) after ultrasonication at 0.2, 0.4, 1, 2, 5 and 10 mM.

### 2.3 Dynamic light scattering measurement

In order to evaluate the aggregation formation dynamic light scattering (DLS) experiment were carried out. Pyrene derivative **1** was solubilised in ethanol and poured into water; the mixture was then subjected to sonication. Several concentrations were tested in aqueous medium

directly after sonication or several days later. DLS provided further evidence for the formation of aggregates of **1**, revealing stable colloidal objects with an average hydrodynamic diameter of 580 nm at 25°C, Figure 57.
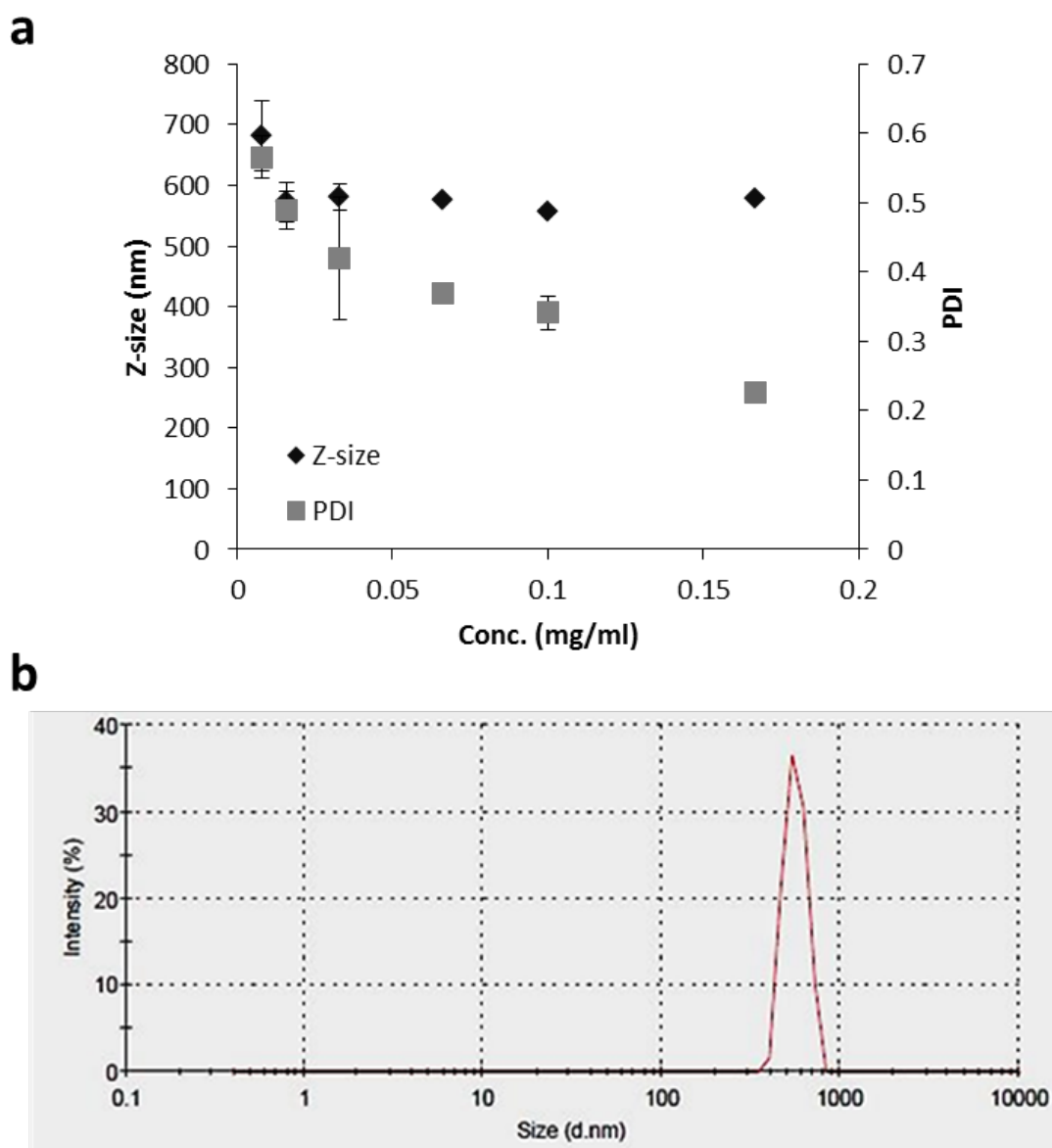


**Figure 57**. **a**) Plot of the hydrodynamic size and polydispersity index of the colloidal suspension of **1** over concentration. **b**) DLS chromatogram of the colloidal suspension of **1** (Conc. 0.1 mg/mL).

## 2.4 Electron microscopy characterization

The samples analysed by DLS were then further studied by field-emission scanning electron microscopy (FE-SEM). The supramolecular assembly in aqueous medium under stirring formed without any ultrasonication treatment provided a fibre-like structure, Figure 58 **a**) and **b**). After ultrasonication treatment, well-defined linear rods with a diameter ranging from 150 nm to 500 nm and a length ranging from 1 to 3 μm were produced, Figure 58 **c**) and **d**). In order to ensure

reproducibility the procedure was reproduced more than 50 times and always provided the same nanorod shape. The supramolecular structures were stable for several months at 25°C, but higher temperatures (>40°C) promoted the disassembly of the supramolecular structures. Further investigations with FE-SEM allowed for the identification of smaller nanorods at the extremity of the self-assembled rods. The size of these nanorods ranged from 15 to 35 nm, Figure 58 **e**) and **f**).

Transmission electron microscopy (TEM) investigations were carried out and confirmed a high density to electrons of the entire structure, ruling out the possibility of a tube-like structure with an empty core, Figure 59. In order to verify the integrity of **1** following self-assembly, we carried out FTIR and $^1$H NMR analyses, Figure 60 and Annex. Our results strongly suggested that **1** did not remarkably undergo any side reaction or hydrolysis and that the overall structure was the outcome of non-covalent interactions.
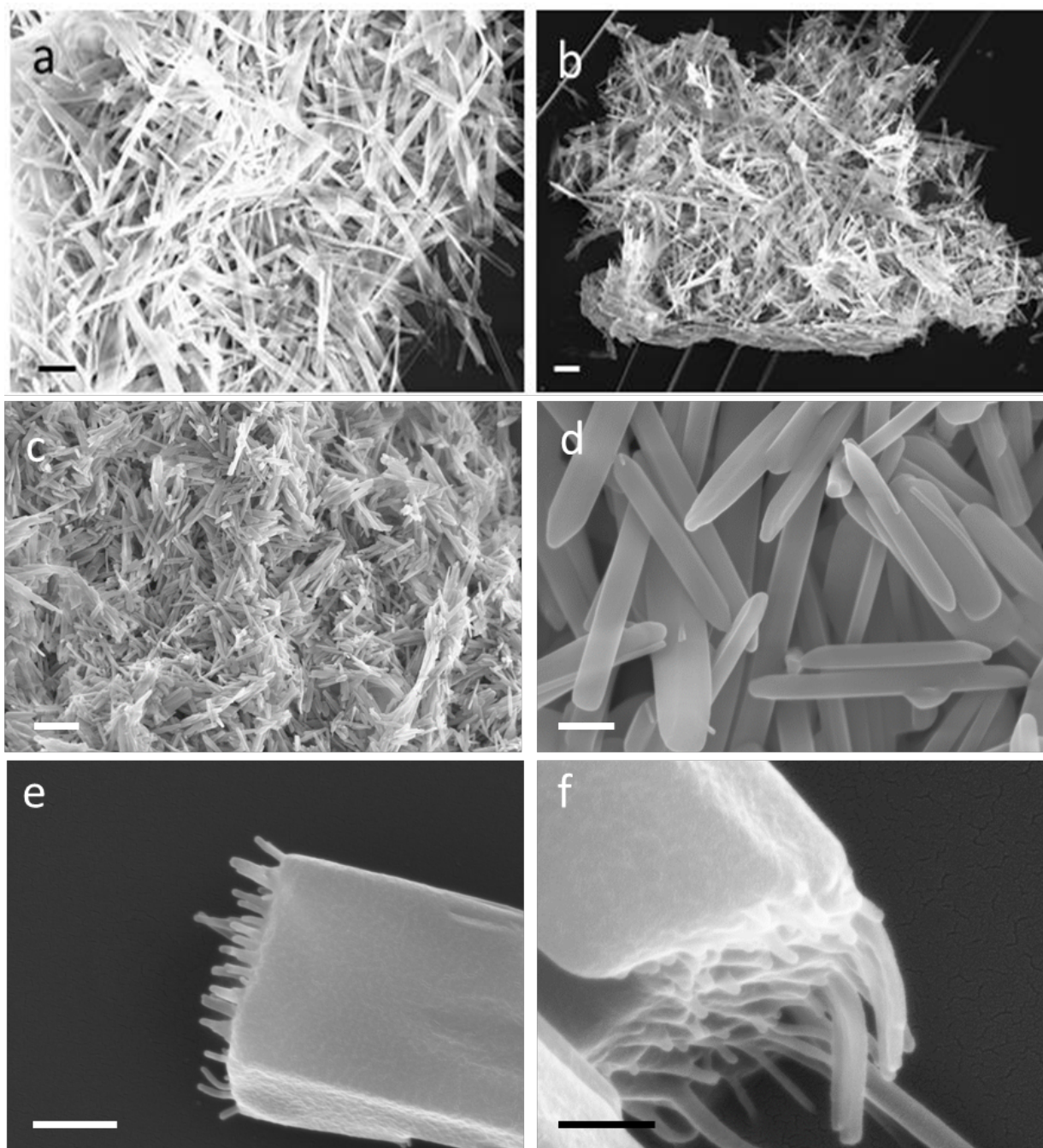
**Figure 58**. FE-SEM micrographs of self-assembled supramolecular nanorods of pyrene derivative **1**. **a**) and **b**) without ultrasonication treatment; **c**) to **f**) with ultrasonic treatment. (Scale:  **a**) 2 μm; **b**) 400 nm; **c**) 4 μm; **d**) and **e**) 400 nm; **f**) 200 nm.)
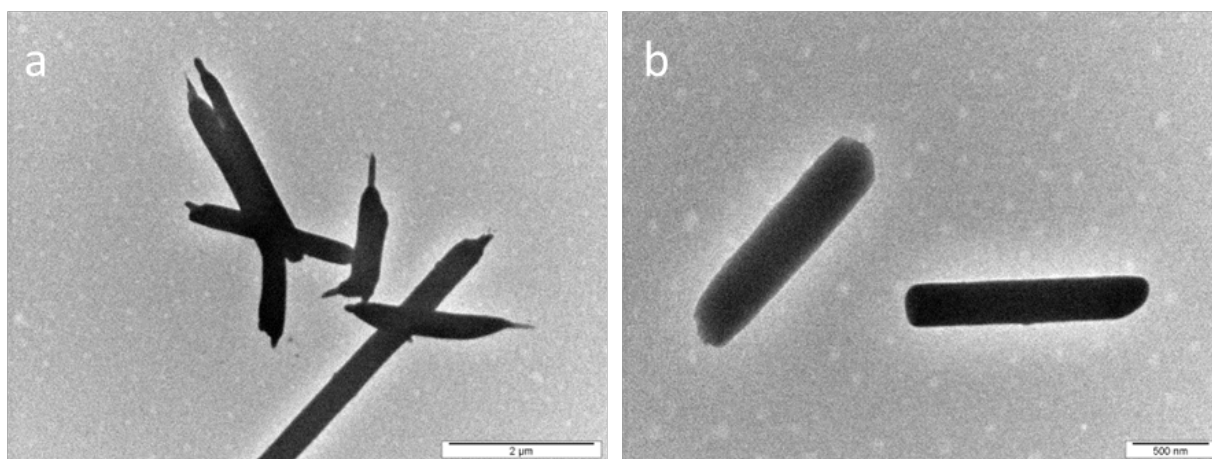
**Figure 59**. TEM micrographs of self-assembled supramolecular nanorods of pyrene derivative **1**. (Scale bars represent **a**) 2 µm and **b**) 500 nm.)
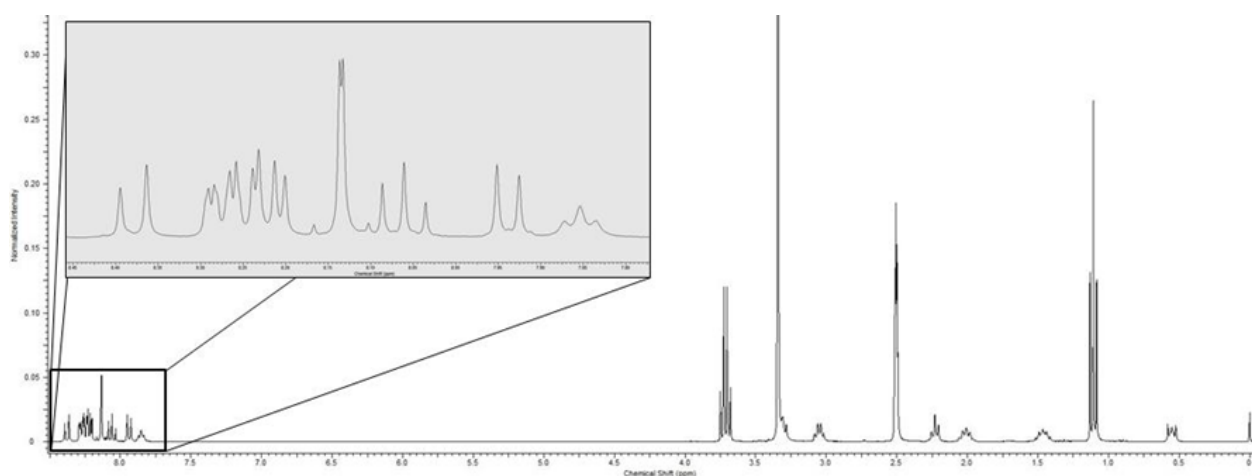


**Figure 60**. $^{1}$H NMR of **1**-based assemblies solubilized in deuterated dimethyl sulfoxide.

## 2.5 X-ray measurement

Single crystal X-ray crystallography was employed. Slow diffusion of an ethanol solution of **1** into water over a period of *ca.* 10 days afforded large needle-shaped single crystals that were suitable for diffraction studies. The crystals were found to be in a monoclinic cell and structure solution was performed in the space group Pc. The asymmetric unit comprised four molecules of **1**, all of which showed disorder that was modeled at partial occupancy accordingly.

As J-aggregates, the examination of the extended structure showed that the molecules are arranged in an offset stack fashion where pyrene moieties are stacked one above each other with a specific angle. Measurement of the distance separating two neighboring pyrene derivatives units gave a length of 3.5 Å, whilst the angle between the pyrene planes was *ca.* 48°; the latter is below the limit of 54.7° that states the difference between J-type ($\theta < 54.7°$) and H-type aggregates ($\theta > 54.7°$).[113, 152]

The structure also exhibits H-bonding between neighboring donors (N-H) and acceptors (C=O), with average N•••O and NH•••O distances of 2.8 and 1.9 Å respectively. Comparison of Figure 61 **a**) and **c**) further stresses the isolation of stacks within the extended structure; owing to the arrangement of both the directing H-bonded spacers and the triethoxysilyl groups. These observations allowed us to confirm the successful molecular design of the pyrene derivative in crystals.
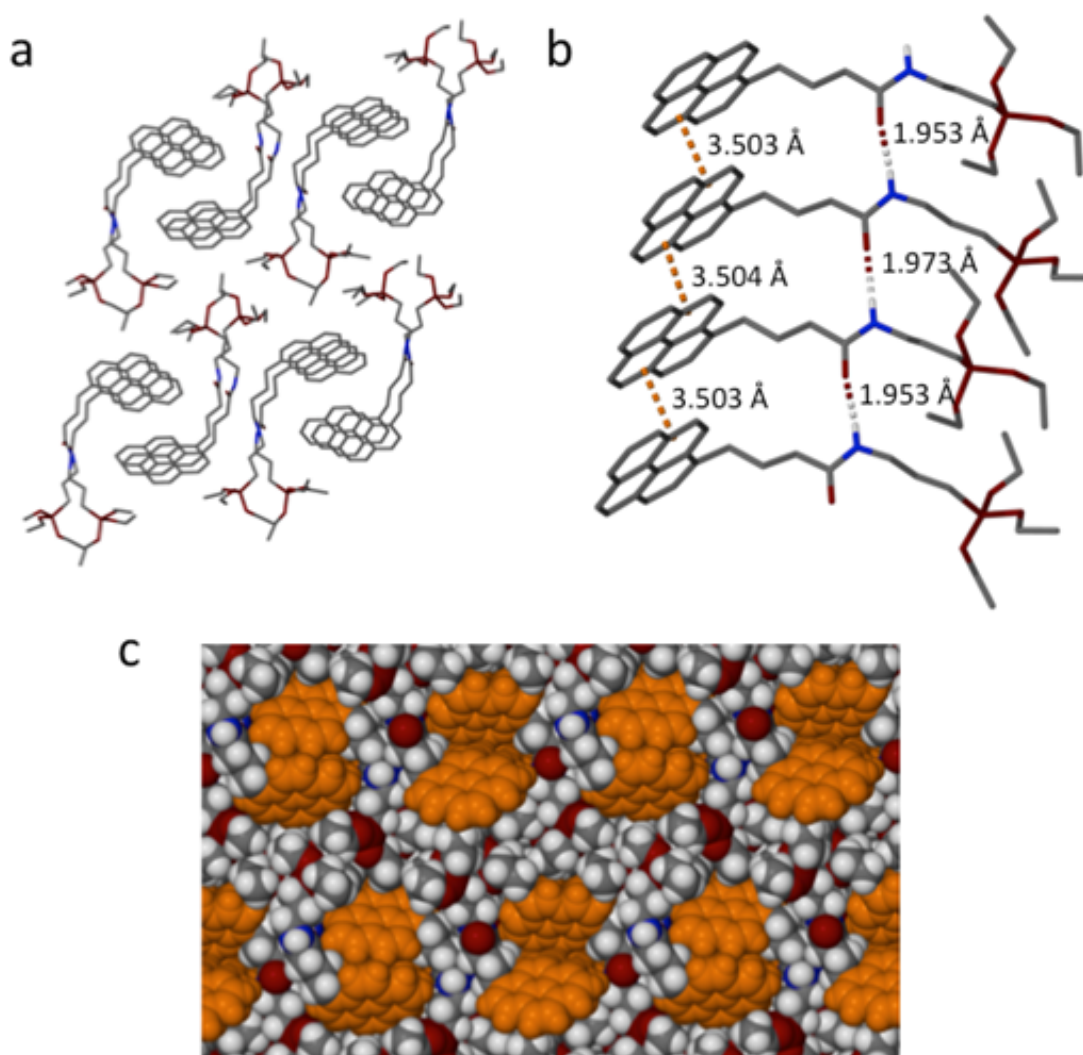


**Figure 61**. Views of the single crystal X-ray structure of **1**. **a**) Stick representation of the extended structure showing pyrene stacks. **b**) Example of H-bonding and π-stacking interactions found between neighboring molecules of **1**. **c**) Space filling representation of the extended structure. H atoms in **a**) and **b**) (except for those involved in H-bonding) are omitted for clarity.

### 2.6 X-ray powder diffraction measurement

The supramolecular rods were also analysed by powder X-ray diffraction in order to determine the bulk sample structure by comparison with the X-ray powder diffraction pattern of the crystals. Relative good agreement between the simulated powder pattern from crystal X-ray

and the powder pattern of nanorods was obtained, Figure 62. Background signal for the nanorods is coming from remaining bulk material in the sample. This result undoubtedly demonstrated the similarity of the molecular packing of **1** in the self-assembled nanorods and in the crystal state.
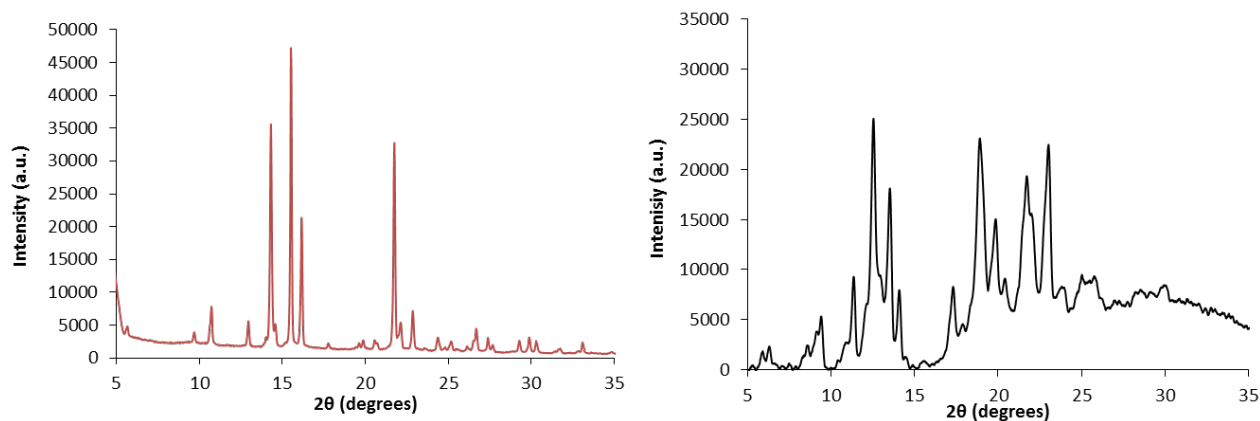


**Figure 62**. X-ray powder diffraction spectra of crystals (red) and nanorods (black) of **1.**

## 2.7 UV-initiated color change

Upon exposure to sunlight over several weeks, crystals of **1** were found to change from colorless to brown (**1***). No differences in the crystal morphology could be observed. Due to poor diffraction of crystals **1*** structural study could not be complete but it was possible to obtain a data set of limited quality from which some major connectivities could be established. Structure solution was performed in *Pc*, as for **1**, and crystals of **1*** were found to be in a monoclinic system. The unit cell parameters of **1*** match very closely those of **1** (Annex), providing further evidence that the crystals of **1** and **1*** are isostructural. The asymmetric unit in **1*** comprises four molecules and these are arranged in stacks as expected, but a high degree of disorder is observed in the structure; this is the likely reason for such a marked drop-off in diffraction upon moving from **1** to **1***, and is evidenced by the presence of significant diffuse electron density. As a result of poor diffraction / disorder in the structure, the best $R_1$ that could be achieved was ~ 21%. In subsequent experiments freshly formed crystals of **1** could be rapidly transformed to **1*** upon exposure to UV irradiation at 365 nm for 3h, Figure 63.
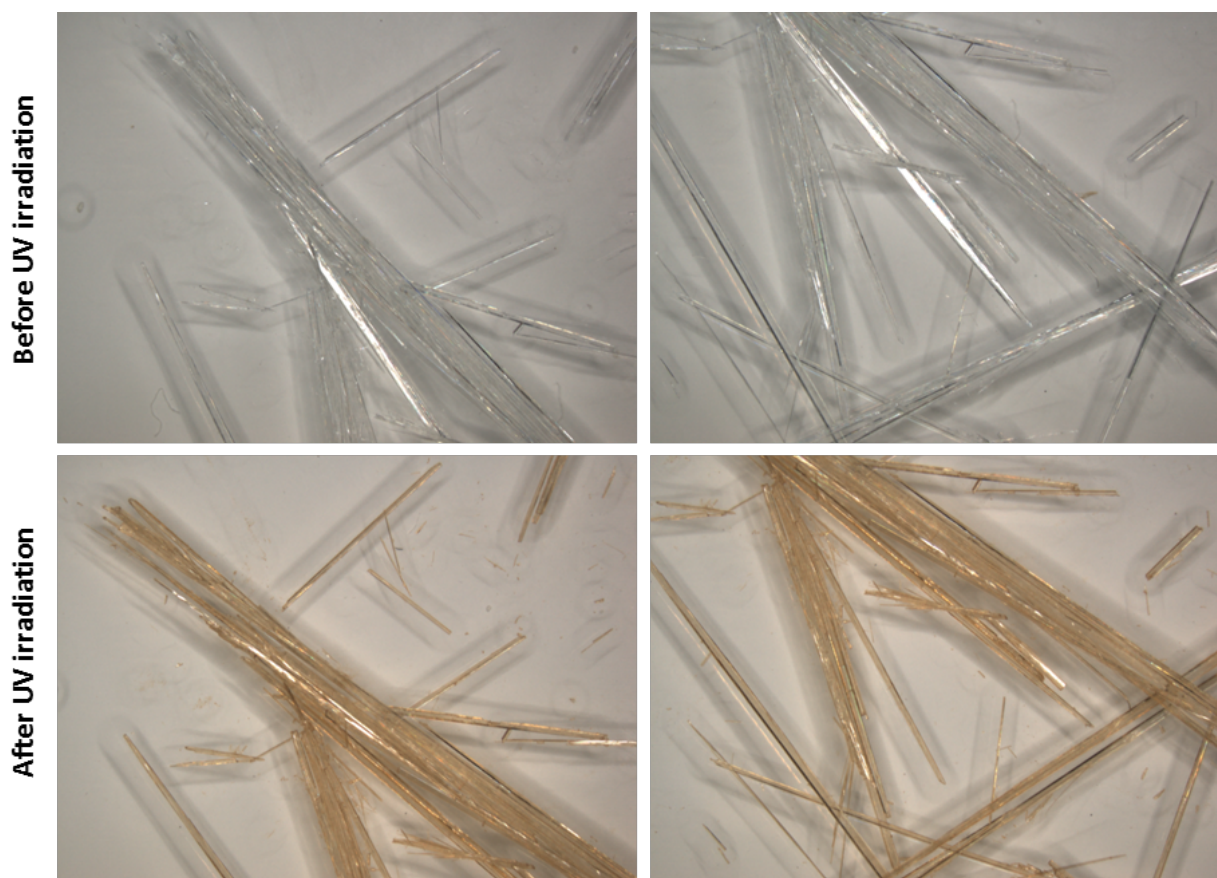
**Figure 63**. Optical micrographs of crystals of **1** before and after UV$_{365}$ irradiation for 3h. (Magnification x7)

With such a marked light-induced color change occurring, computational studies were carried out to gain insight into this solid-state process. Density functional theory (DFT): ωB97XD/aug-cc-pVDZ, and time-dependent DFT: CAM-B3LYP/aug-cc-pVDZ, were used to model the ground and excited states of two interacting pyrene pairs of **1** minus the silyl ether groups (2 x 2 stack of 4 molecules) respectively. The ground state optimal structure is that of a J-aggregate with a structure agreeing well with the experimental one. The TD (time dependent)-DFT shows a large density of states between 280-330 nm, with a significant degree of charge transfer up/down the pyrene stacks. The position of the bright states in TD-DFT agrees reasonably with the observed absorption spectra, Figure 64. Due to computational overhead geometry, optimization in the excited states was performed with smaller 6-31G* basis augmented with a diffuse set of functions on the carbons. Exploratory calculations revealed that states responsible for the CT band optimise to a similar J-aggregate but with a closing of the tilt angle between dimer pairs. Displacements were not fully optimised, but the key geometrical relaxation coordinate is indicated to be a change in the pyrene dimer angle.

As stated above, the poor quality of diffraction data precludes the possibility to quantify parameters such as π-stacking/hydrogen bonding distances, angles between pyrene moieties and other structural features. Although this is the case, dissolution of orange crystals of **1\*** afforded a colorless solution and $^1$H NMR analysis confirmed that no change happened to the molecules of **1**. All of this is suggestive that there is movement of the pyrene moieties within the stacks and that this is the origin of the drastic change in color upon irradiation.
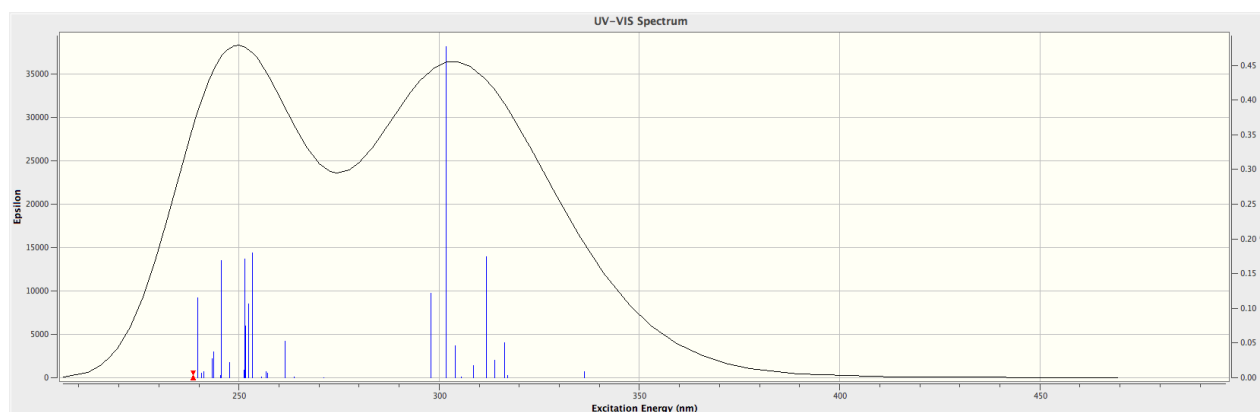


**Figure 64**. UV-vis simulated spectrum of **1**.

### 2.8 Silica layer growth

To endow the nanorods with the possibility to be functionalized *à façon*, a silica layer was grown on the surface of the nanorods. Through the polycondensation of the bulky triethoxysilyl groups with APTES and tetraethoxysilane (TEOS) in 2-(*N*-morpholino)ethanesulfonic acid buffer (pH 6) and using Triton X-100 as surfactant in some cases to obtain a suitable dispersion of the nanorods in solution. The polycondensation was followed by FE-SEM analysis and allowed to confirm the effective silica layer growth on the nanorods, Figure 65. The conditions for each micrograph are described in Table 7 and permitted to select the best conditions to perfom an effective polycondensation reaction and grow a homogenous silica layer on the nanorods.

**Table 7**. Conditions and results of the different reaction for the optimization of the silica layer growth.

| Experiment [a] | TEOS (uL) | APTES (uL) | Triton X-100 | MES buffer | Time | SEM Fig. S8 | Results |
|---|---|---|---|---|---|---|---|
| 1 | 6 | 3 | - | - | 18h | - | HE.L*, A* |
| 2 | 12 | 6 | - | - | 18h | - | HO.L*, SPs*, A |
| 3 | 18 | 9 | - | - | 18h | a | HE.L, SPs, A |
| 4 | 8 | 4 | - | - | 24h | c | HE.L, A |
| 5 | 12 | 4 | - | - | 24h | - | HO.L, A |
| 6 | 8 | 4 | 3 mL (0.2%) | - | 24h | b | HE.L, SPs |
| 7 | 12 | 4 | 3 mL (0.2%) | - | 24h | d | HE.L, SPs |
| 8 | 12 | 4 | 1.2 mL (0.1%) | - | 24h | e | HE.L, SPs |
| 9 | 12 | 4 | 100 µL (0.1%) | 15 mM pH 6 | 24h | - | A |
| 10 | 12 | 4 | - | 15 mM pH 6 | 50h | - | HO.L, A |
| 11 | 12 | 4 | 10 µL (0.1%) | 15 mM pH 6 | 50h | f, g, h, i | HO.L |

[a] *For a final volume of 12 mL with 1 mg/ml concentration of nanorods.*

*\* HE.L: heterogeneous layer, HO.L: homogeneous layer, SPs: spherical particles, A: aggregates*
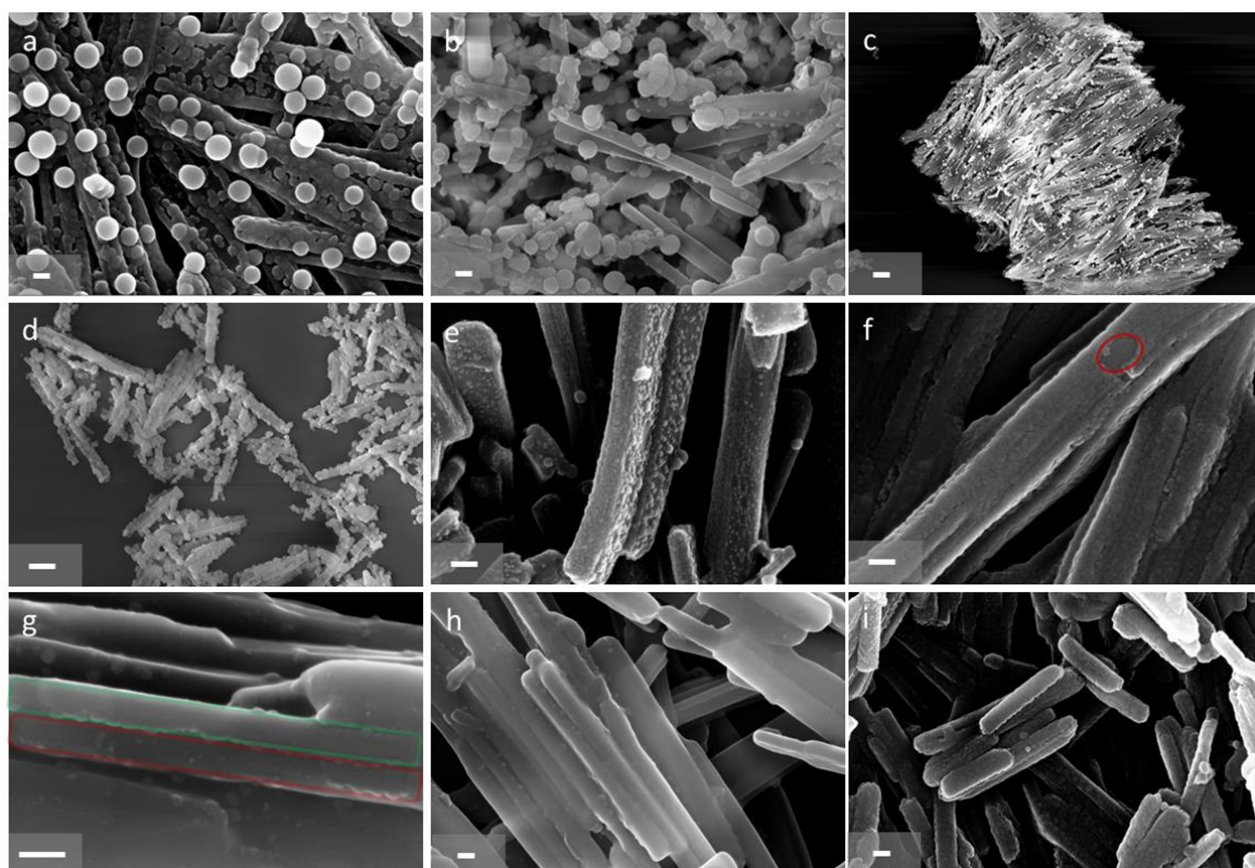


**Figure 65**. FE-SEM micrographs of the nanorods after silica layer growth for different conditions.
(Scale bar represents 200 nm for **a**), **b**), **e**), **f**), **g**), **h**) and **i**), and represents 2 µm for **c** and **d**.) In micrograph **f**) the red circle indicates a surface exposed and not covered by the silica layer, darker and more uniform than the silica layer. In micrograph **g**), the green rectangle indicates where the silica layer is present and the red rectangle where it is absent, a clear separation is observable between these two parts.

Those clear differences observed allowed to confirm the effective silica layer growth around the nanorods.

## 2.9 Conclusion

We successfully achieved the synthesis of a pyrene derivative and developed a strategy to produce hierarchical self-assembled nanorods following a template-free approach. The self-assembly process is demonstrated to first occur through the self-assembly, via π-π stacking, of the molecular building block into excimers. When transferred to water, hydrogen bonds and π-π stacking act synergistically to form the aggregates. Hydrophobic effects (due mainly to the pyrene moiety) likely assist the construction of the nanorods. Ultrasonication favour the self-assembly of these nanorods into bundles to form the observed supramolecular structures, Figure 66. Single crystal X-ray crystallography provided insight into the packing behaviour of **1**, whilst powder X-ray diffraction confirmed the persistence of this arrangement within the nanorods.
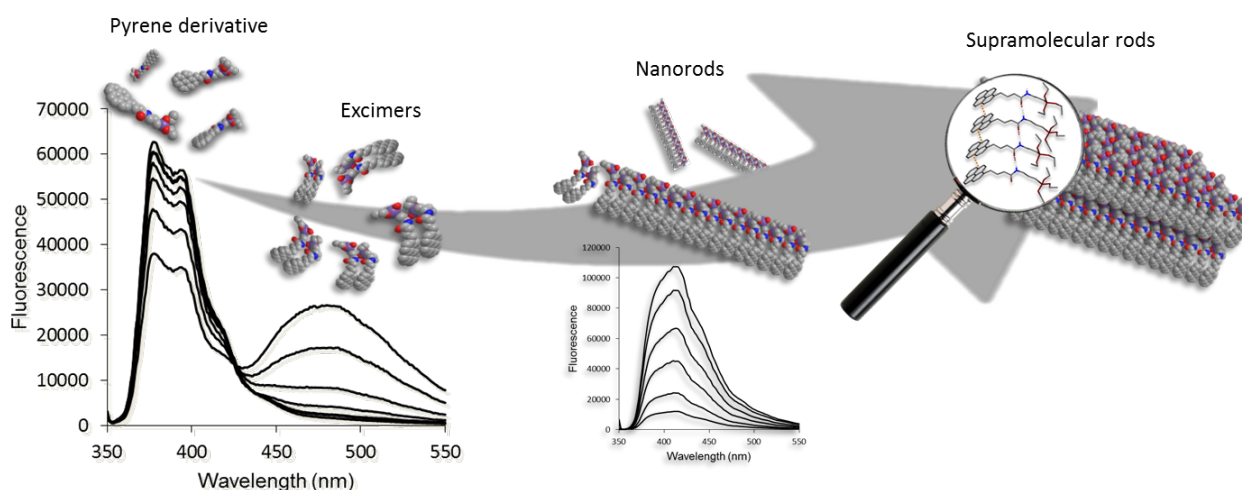


**Figure 66**. Schematic representation of the self-assembly process of **1** in aqueous medium with the corresponding spectra.

A silica layer was successfully grown on the surface of the nanorods. A surface modification made possible by the presence of the triethoxysilyl groups. This silica layer enlarges the possibilities of functionalization of the supramolecular assemblies and the opportunities of application.

## 3. Mesoporous silica particles for water remediation

This section will cover the production process of the so-called "Smart Gate Particles". Templated synthesis of the mesoporous particles, surface functionalization and their application in bioremediation in case of contamination by oil spill will also be detailed in this section.

### 3.1 Oil spill and bioremediation

Nowadays, hydrocarbons and oil still cover most of our energy needs. The world oil demand reached 85.6 million barrels per day in 2008.[1] In parallel, incidents arising from the huge trading of hydrocarbons are also significant and affect considerably marine environment causing the destruction of marine species and flora. Several natural and chemical approaches for the degradation of oil spills are available as photooxidation, evaporation, biodegradation and the use of dispersants or demulsifiers. Among them, bioremediation has emerged as one of the most promising treatment for oil spills, it is divided between two branches: biostimulation and bioaugmentation.

Bacteria degrading oil are ubiquitously present in marine environments. However, the concentration of necessary nutrients (*i.e.* nitrogen and phosphorus) to sustain an efficient biodegradation of hydrocarbons in marine environment is not sufficient. Biostimulation, which consists in the addition of nutrients to adjust the metabolic needs of hydrocarbon-degrading bacteria, is a promising alternative of the aforementioned methods as it provides a good balance of their nutritional needs. Oil-degrading bacteria feed on hydrocarbons to multiply themselves but also needs nitrogen for nucleic acid and protein production as well as phosphorus for nucleic acid, adenosine triphosphate (ATP) and protein production. Bioaugmentation which consists in the addition of hydrocarbon-degrading bacteria represent also an alternative method but it is still limited by the amount of available nutrients. The main drawback of the biostimulation approach is the quick dilution of nutrients resulting in low degradation efficiency. To overcome this issue, one strategy would consists to design a system that target the oil droplet directly.[153] Despite efforts to produce such system their efficiency remains fairly limited.

### 3.2 Synthesis of Smart Gate Particles

The design of the mesoporous material is based on three criteria, Figure 67.

1.      Appropriate nutrients loading for the bacteria

2.      Targeting petrol/oil phase and organic solvents (lipophilic particles)

3.      Localised release of the nutrients at the interface water/oil
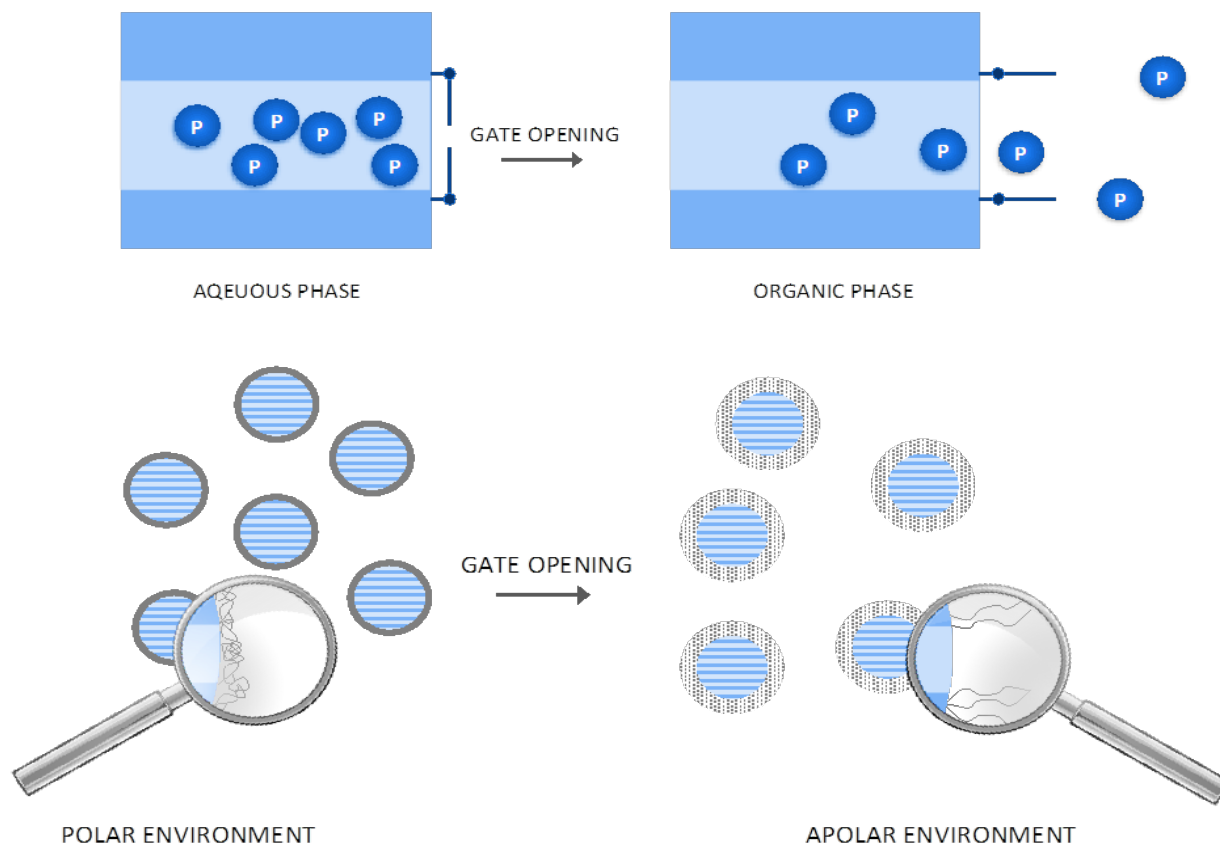


**Figure 67**. Action mechanism of the "Smart Gates Particles".

Mesoporous silica particles were synthesised following a procedure adapted from a published protocol.[154] The synthesis of mesoporous particles was carried out using cetyltrimethylammonium bromide (CTAB) as surfactant. The self-assembly of this cationic surfactant is a cooperative phenomenon driven mainly by hydrophobic interactions where the size and shape of the ionic micelles depend directly on the charges of the polar head of the surfactant and the length of its apolar chain. The micelle formation in water led to cylindrical micelles. Once TEOS is added, the hydrolysis of the molecules occurs and polycondensation starts around the CTAB micelles where attractive interactions occurs as detailed in Chapter 1, Figure 68.
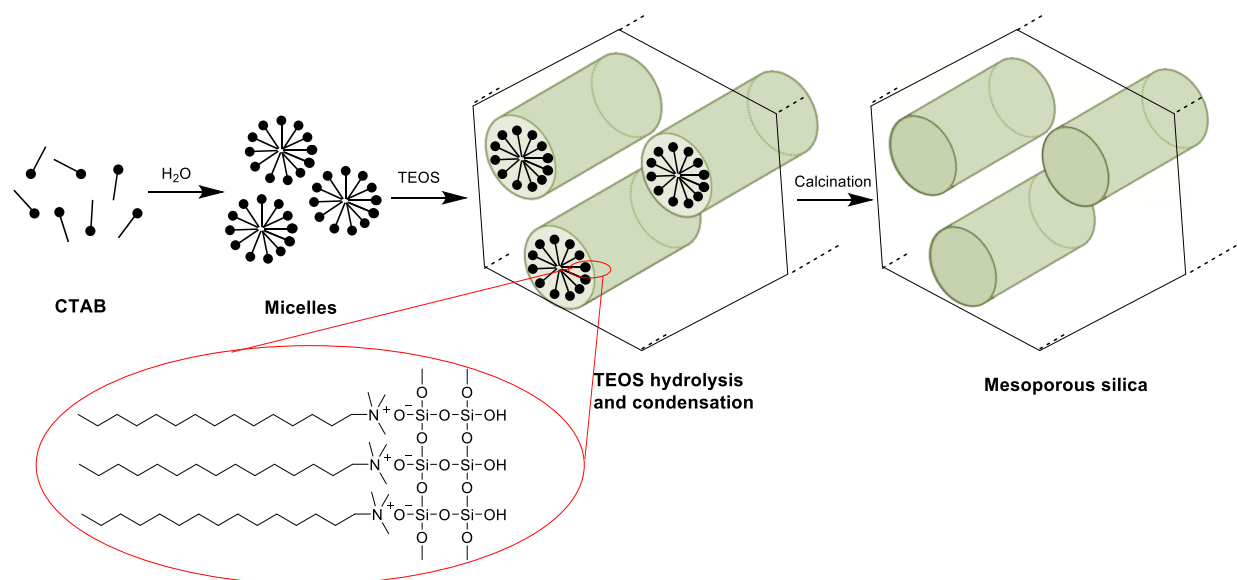
**Figure 68**. Schematic of mesoporous silica particles formation.

The polycondensation of TEOS yields monodisperse silica nanoparticles with a pore size of few angstroms. To obtain the mesoporous particles, the silica particles are calcined at 600°C to remove the organic and inner part of the silica particles. The mesoporous material allows the loading of the desired nutrients into the pores without the need of complex techniques.

The loading of the nutrients into the mesoporous particles was carried out using dipotassium phosphate as phosphorus (P) source and urea as nitrogen (N) source. The mesoporous particles were first dried under vacuum to remove water molecules from particles. Subsequently, solutions of urea or dipotassium phosphate were prepared and added directly to the mesoporous particles and stirred during 6 h to allow the nutrient loading into the particles, a significant increase in mass is observed after isolation of the particles (details available in the next section).

To endow the particles with hydrophobic properties and permit the particles to target specifically oil phase, functionalization of the surface of the particles was carried out using silane compounds. This step is a 2-in-1 process where not only the particles are functionalized and become hydrophobic but also where "smart gates" are created. Indeed, the pores are surrounded by alkyl chains that are, because of non-solvation, collapsing in aqueous phase and thus forming a hydrophobic barrier, preventing the release of the nutrients and their rapid dilution in aqueous medium. In an oil phase the opposite is expected to occur, the alkyl chains are solvated, the pores are not anymore closed and the nutrients can be released.

In order to fully close the pores the alkyl chains should be sufficiently long to obstruct the pores. Several hydrocarbons length has been considered from 16 carbon atoms with a length of 19.6 Å to 24 carbon atoms with a length of 28.6 Å. The functionalization of the loaded mesoporous particles with the nutrients was eventually carried out with octadecyltrichlorosilane (OTS) which bears 18 carbon atoms for a length of 21.2 Å. The pore size and characterization of the SGPs are detailed in the following section.

### 3.3 Surface characterization

The effective functionalization at the surface of the mesoporous particles was assessed by FTIR analysis, Figure 69. Characteristics peaks of the alkyl chain are present at 2854 cm$^{-1}$ and 2923 cm$^{-1}$ which are characteristic of C-H bonding (stretch).
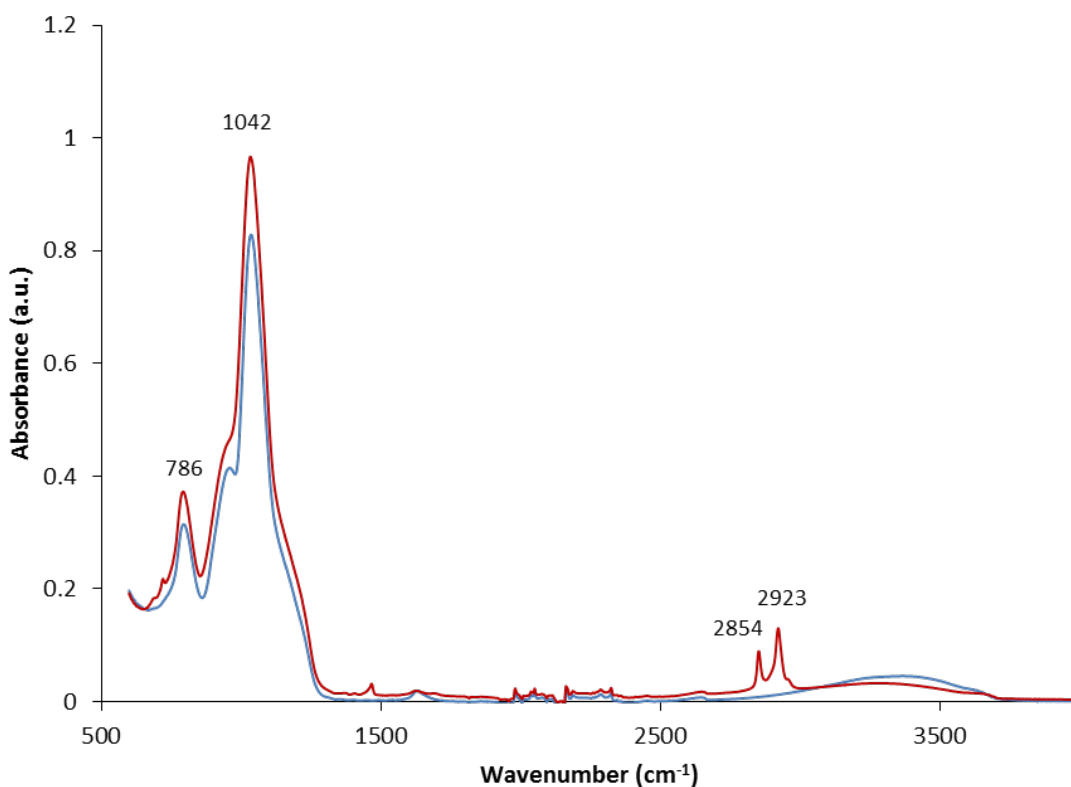


**Figure 69**. FTIR spectra of the mesoporous particles, (blue: before functionalization, red: after functionalization).

ζ-potential measurements also confirmed the effective silane functionalization at the surface of the particles, Figure 70. Measurement before surface functionalization afforded a negative ζ-potential of -46.4 mV with a standard deviation of 20 mV mainly due to the deprotonated hydroxyl groups localised at the surface while after functionalization a ζ-potential of 6.8 mV with a standard deviation of 6 mV was obtained. The reaction of OTS with the hydroxyl groups provided neutral alkane instead of charged oxygen at the surface of the particles and caused

the increase of the ζ-potential as expected. A visual evidence of the effective functionalization of the mesoporous particles is provided, Figure 71. For the same mixture water/heptane the mesoporous particles are well dispersed in water while the SGPs are localised in heptane at the interface water/heptane (because of their density they precipitate at the interface), no particles are present in water. Their hydrophobic surfaces prevent them to be solvated in water but are well dispersed in heptane. This is a clear evidence of the hydrophobicity of the SGPs.
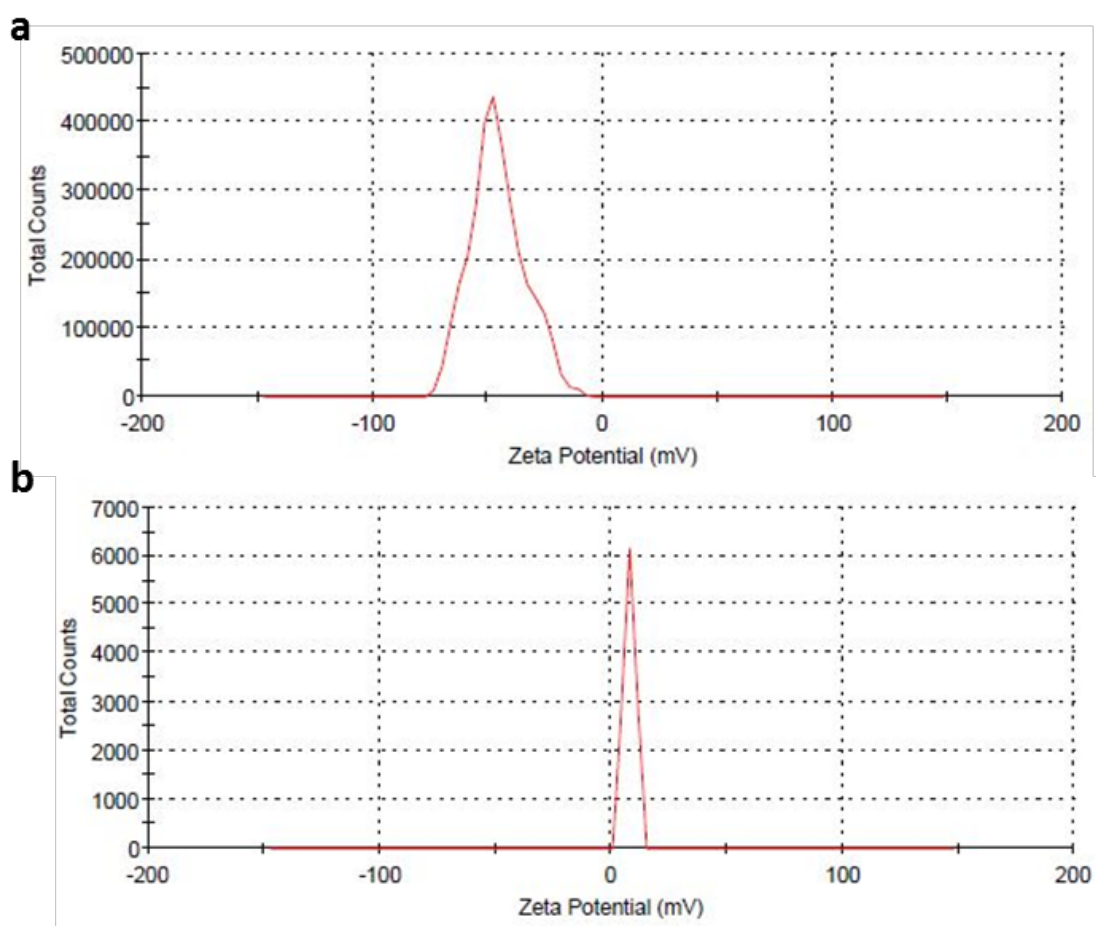


**Figure 70**. ζ-potential distribution of particles **a**) before and **b**) after functionalization of silica particles.
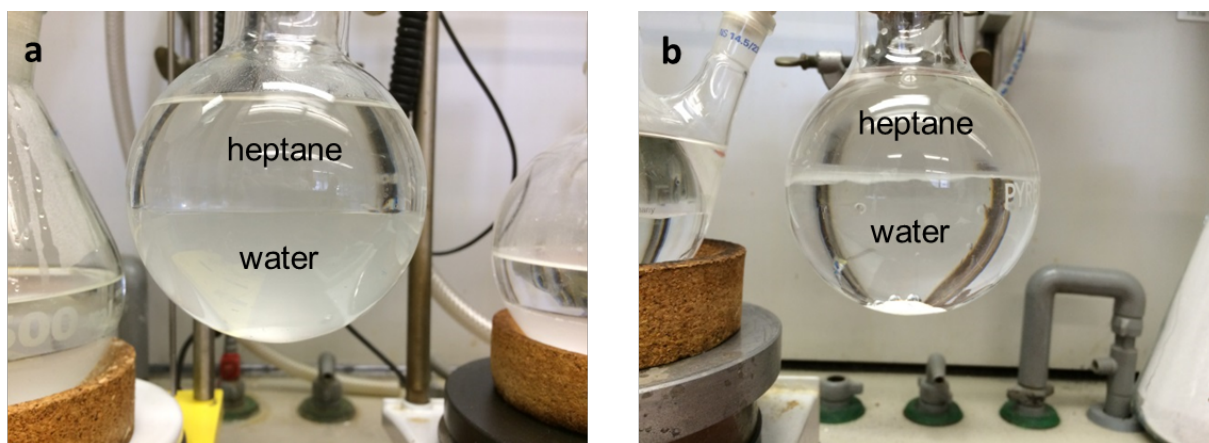


**Figure 71**. **a**) Mesoporous silica particles and **b**) SGPs dispersed in water/heptane mixture.

### 3.4 Electron microscopy characterization

Characterization of the mesoporous particles was also carried out by means of electron microscopy. SEM analysis revealed particles with size ranging from 100 nm to 400 nm, Figure 72. No significant structural differences at the surface of the particles could be observed between non-functionalized and functionalized particles.
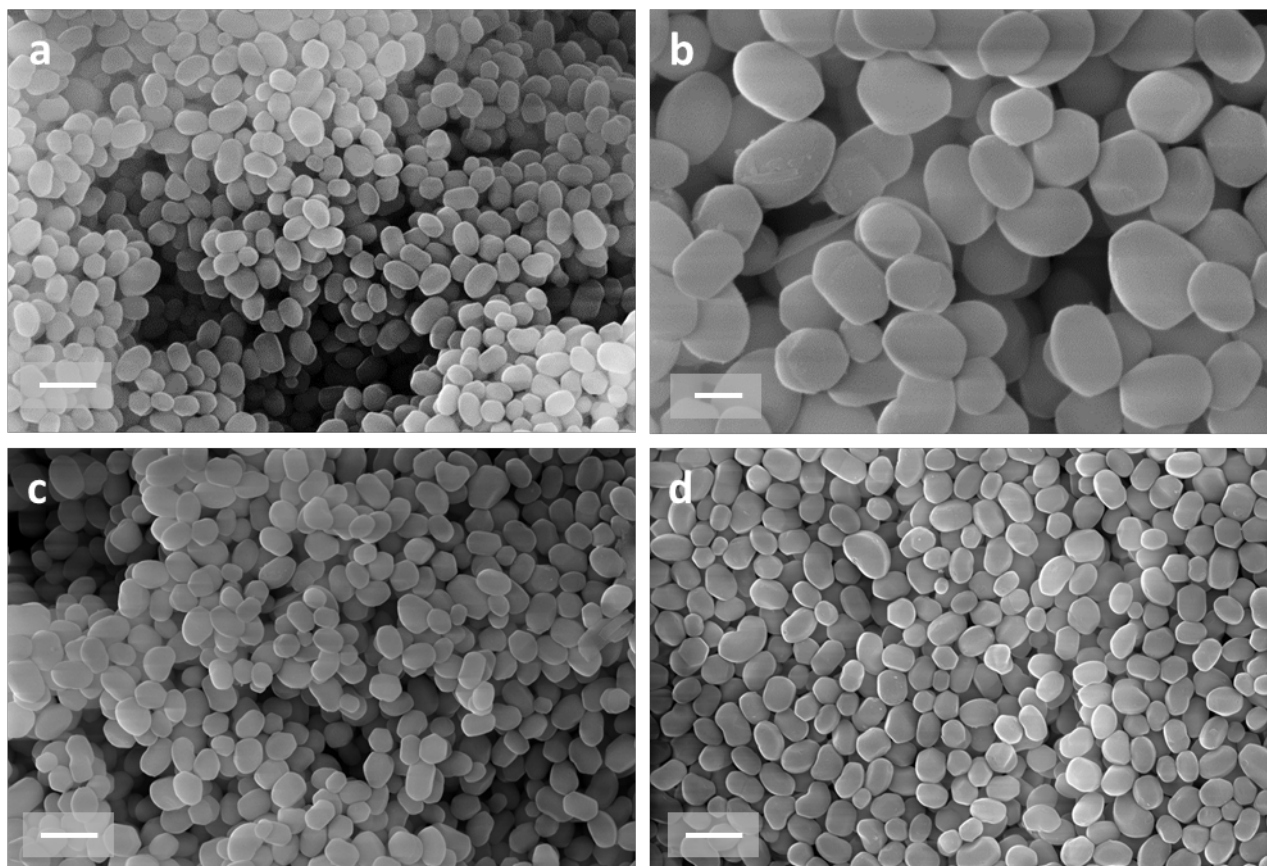


**Figure 72**. SEM micrographs of non-functionalized mesoporous particles. (Scale: **a**) 1 μm **b**) 200 nm **c**) and **d**) 1 μm.)

In order to assess the porosity of the mesoporous particles TEM analysis was carried out on copper grid, Figure 73. The mesoporous structure was clearly evidenced and typical contrast between dark and bright lines was observed on the particles, characteristic of MCM-41 particles.
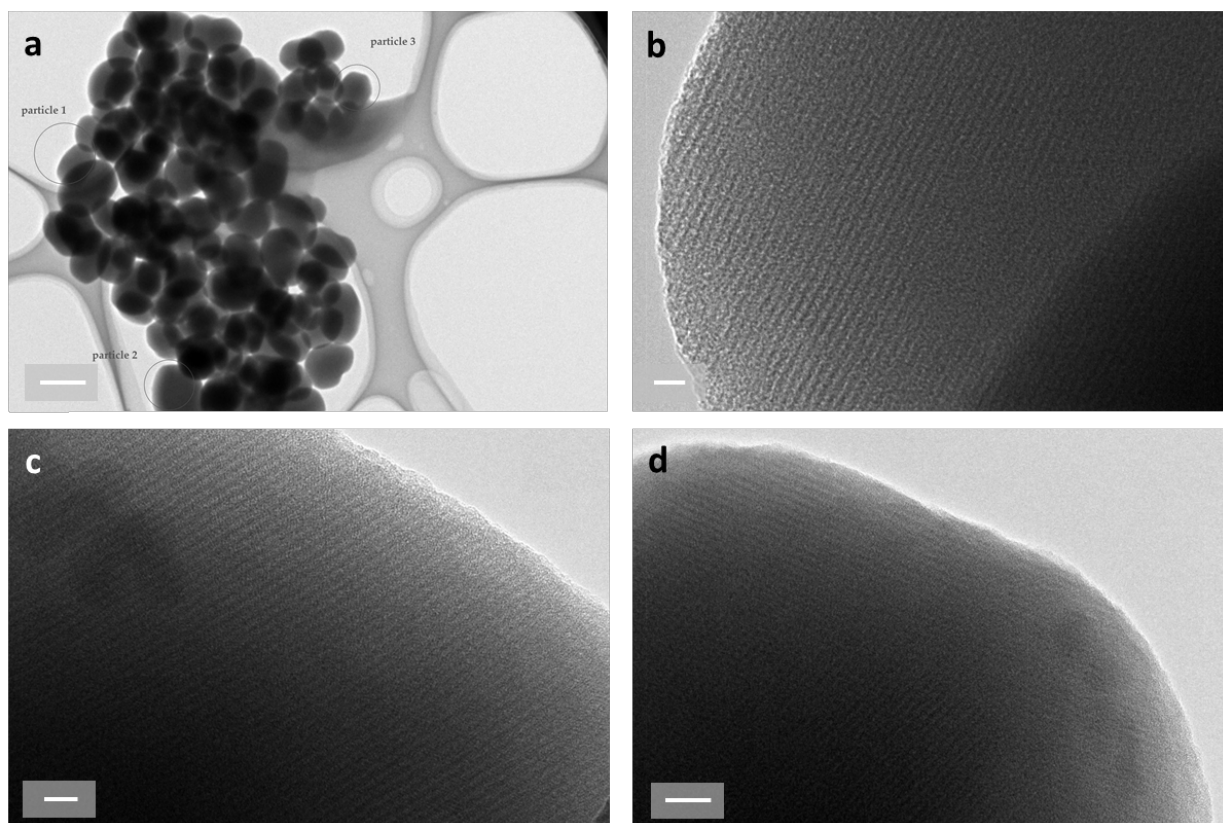
**Figure 73**. TEM micrographs of mesoporous particles (Scale: **a**) 0.5 µm **b**) and **c**) 10 nm **d**) 50 nm). Particle 1, 2 and 3 in picture **a**) correspond to picture **b**), **c**), and **d**), respectively.

### 3.5 Brunauer-Emmett-Teller measurement

Another method to obtain precise data on the porosity and pore volume of the particles is the Brunauer-Emmett-Teller (BET) method. BET measurement confirmed the high porosity of the silica particles after effective removal of the CTAB molecules by calcination. Mesoporous silica particles with surface area of 707.28 $m^2$/g ± 4.8144 m²/g, pore volume of 0.51 $cm^3$/g and pore size of 28.82 Å were obtained, these results were deduced from BET isotherm linear plot and are consistent with literature values, Figure 86 (Annex).[155-156]

The adsorption isotherm is obtained by measuring the amount of gas adsorbed over a range of relative pressures at a constant temperature. The type of adsorption isotherm obtained for the MCM-41 particles are typical of mesoporous materials for which the exposed surface is mainly localised inside the mesopores. Once the mesopores are filled, little or no adsorption occurs at the outer surface of the particles.

The set of characterization allowed us to confirm the effective synthesis of the mesoporous particles as well as their effective functionalization but provided also precise information on the porosity.

### 3.6 Nutrient's loading and release

The loading of the MCM-41 was carried out by suspending the mesoporous particles in solution of dipotassium phosphate or urea. In order to assess the effective loading into the particles different concentrations of dipotassium phosphate and urea were prepared for the loading, Table 8. The amount of MCM-41 and the volume of the solution were kept constant, the concentration of the dipotassium phosphate and urea was the only parameter changed over the experiments. After being stirred for 6h into the solutions, the particles were filtered and dried at 35°C under vacuum.

**Table 8**. Conditions for the loading of dipotassium phosphate and urea into mesoporous particles.

|  | A | B | C | D |
|---|---|---|---|---|
| **MCM-41 (g)** | 20 | 20 | 20 | 20 |
| **Dipotassium phosphate (g)** | 9 | 18 | 36 | 54 |
| **Urea (g)** | 6.5 | 13 | 26 | 39 |
| **Water (mL)** | 200 | 200 | 200 | 200 |

The difference between the initial mass of particles and the mass after incubation in the solution was reported as the mass loaded and plotted against the corresponding concentration, Figure 74. The corresponding percentages of loading (experimental mass loaded over maximum theoric loading mass calculated from BET data) are also reported.
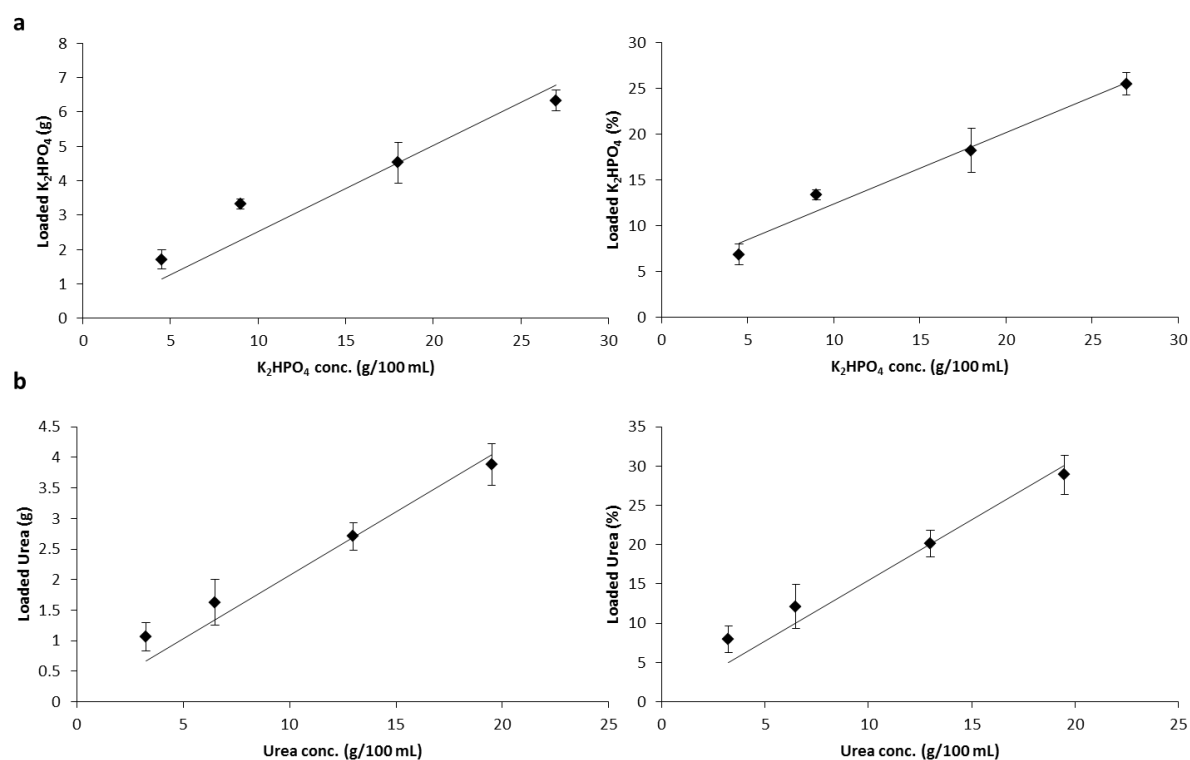


**Figure 74**. Plot of the loaded **a**) dipotassium phosphate and **b**)urea vs the concentration of the incubation solution.

As expected, increasing the concentration of the solution increased the loading into the particles. The coefficient of determination obtained for the dipotassium phosphate ($R^2$=0.8561) and for the urea ($R^2$=0.9439) allowed us to conclude on a linear trend of the nutrients loading into the mesoporous particles.

Kinetic studies of the release of the nutrients were performed to assess the rate of nutrients release into water under stirring and under sonication. Two experiments were carried out in parallel. In one experiment, SGPs were added to water under stirring for 5 h, and in another experiment SGPs were added to water and were subjected to ultra-sonication for 5 h, Figure 75. As observed, only 7% of the loaded phosphate was released after 5 h under stirring in water. This is a strong evidence of the efficacy of the SGPs that prevent the release of the phosphate in aqueous medium. For the second experiment under ultra-sonication, which represents extreme conditions compare to real sea environment, less 25 % of the loaded phosphate was released after 30 minutes. Around 80 % of the loaded phosphate was released after 5 h, the release rate decreased over the time probably because of the deeper location of the phosphate into the pores. Nonetheless, the phosphate in the particles is still not completely released after 5 h.
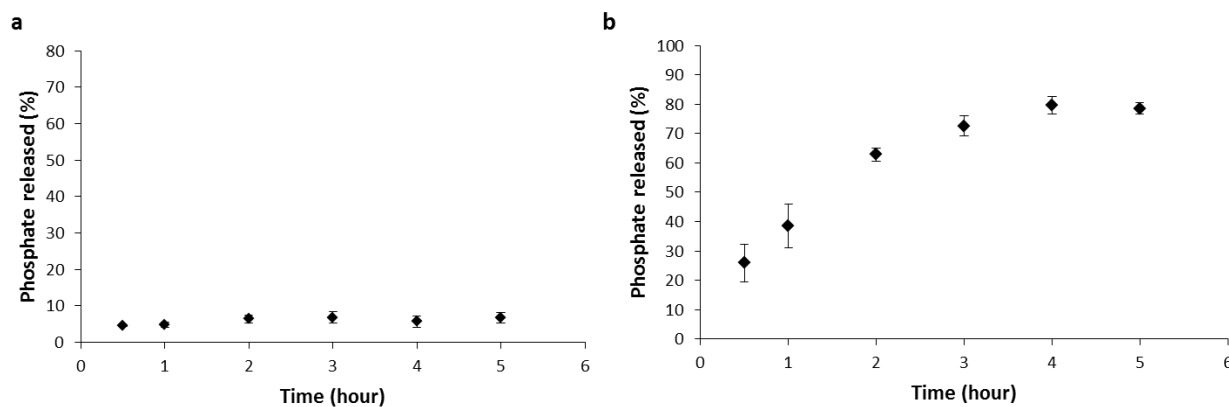
**Figure 75**. **a**) Kinetic release of dipotassium phosphate under stirring in water. **b**) Kinetic release of dipotassium phosphate under ultrasonication in water.

The SGPs were designed to allow a slow release of the nutrients for hydrocarbon-degrading microorganisms once in contact with oil phase. The slow release permits to prevent a dilution of the nutrients in water before consumption by the bacteria. To assess the difference of release rate between mesoporous particles (MCM-41) and SGPs, kinetic studies were performed in a mixture of water and heptane at two different stirring speeds, Figure 76.
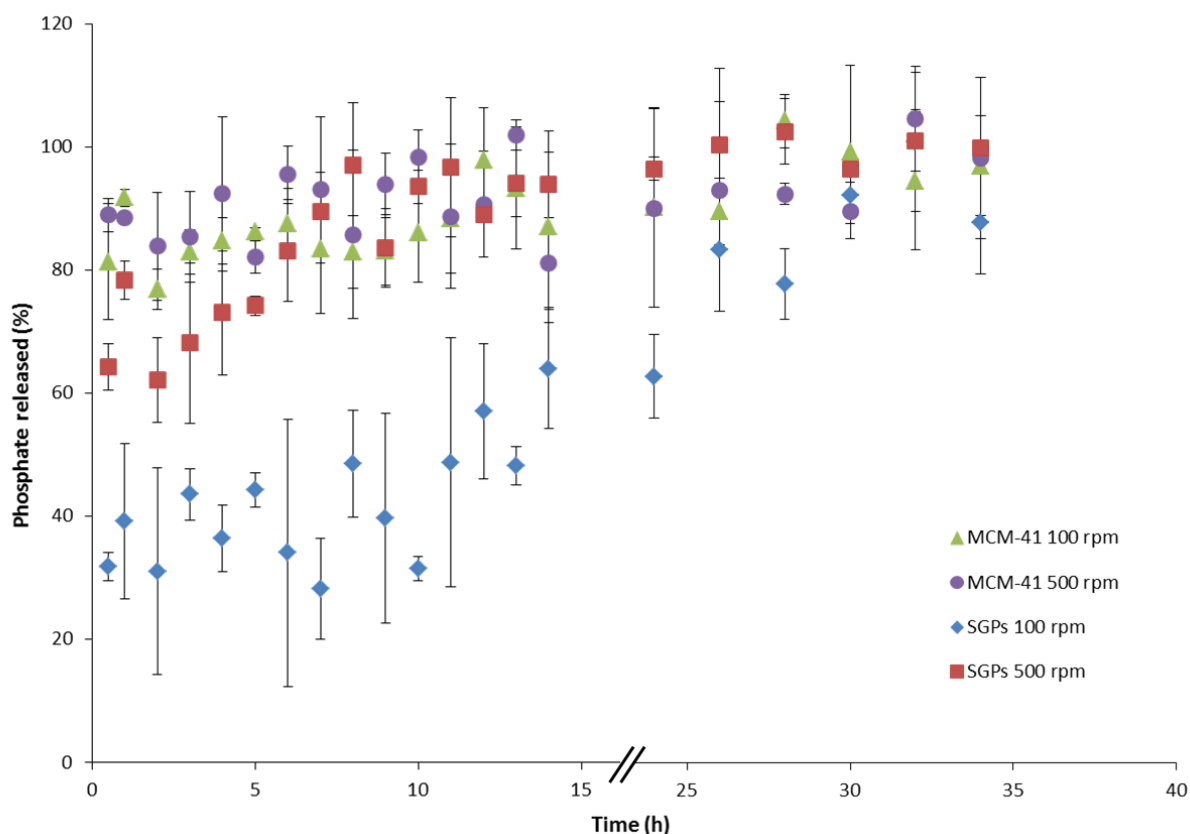
**Figure 76**. Kinetic release of phosphate of MCM-41 particles and SGPs at two stirring speeds in a mixture water/heptane.

A significant difference is noted between the MCM-41 particles and the SGPs. After only 30 min around 90 % of the loaded phosphate is dissolved in water by the MCM-41 particles. The pores were readily accessible and consequently the nutrients dissolved in water in the first minutes of the experiment independently from the speed stirring. Concerning the SGPs, the phosphate release reached maximum after 10h at 500 rpm and after 30h at 100 rpm. From these observations it was concluded that the release rate was directly correlated with the stirring speed. The higher the stirring speed the higher the surface area between heptane and water. At 500 rpm the mixture formed a pseudo-emulsion that allowed a higher extraction rate from heptane to water. To show that phosphate is diffusing through heptane before reaching the aqueous phase an experiment was set in which dipotassium phosphate has been added to heptane and left for 3h under stirring. The solution was then filtrated and extracted with water, a phosphate concentration of 0.95 µM was found in water. This was an evidence of the diffusion of phosphate through heptane and explained the higher rate observed at higher stirring speed.

### 3.7 Biostimulation

The performances of the SGPs for crude oil biodegradation were assessed using the oil degrading bacterium *Marinobacter hydrocarbonoclasticus* KS-ANU5. Experiments were carried out by the group of Prof. Corvini (FHNW). A *Marinobacter* strain was inoculated to artificial seawater containing crude oil for a final biomass of $5.3 \times 10^7$ CFU (colony forming unit)/mL. The effect between N and P released from the SGPs and the dissolved form of N and P (from urea and phosphate sources) on the oil degradation was compared. An additional biotic control (inoculated with *Marinobacter* strain) without addition of N and P was taken as reference.

For this study the degradation was monitored measuring the biomass over the time, Figure 77. For each time point, a sample was sacrificed and the hydrocarbons were extracted using liquid-liquid extraction with hexane.
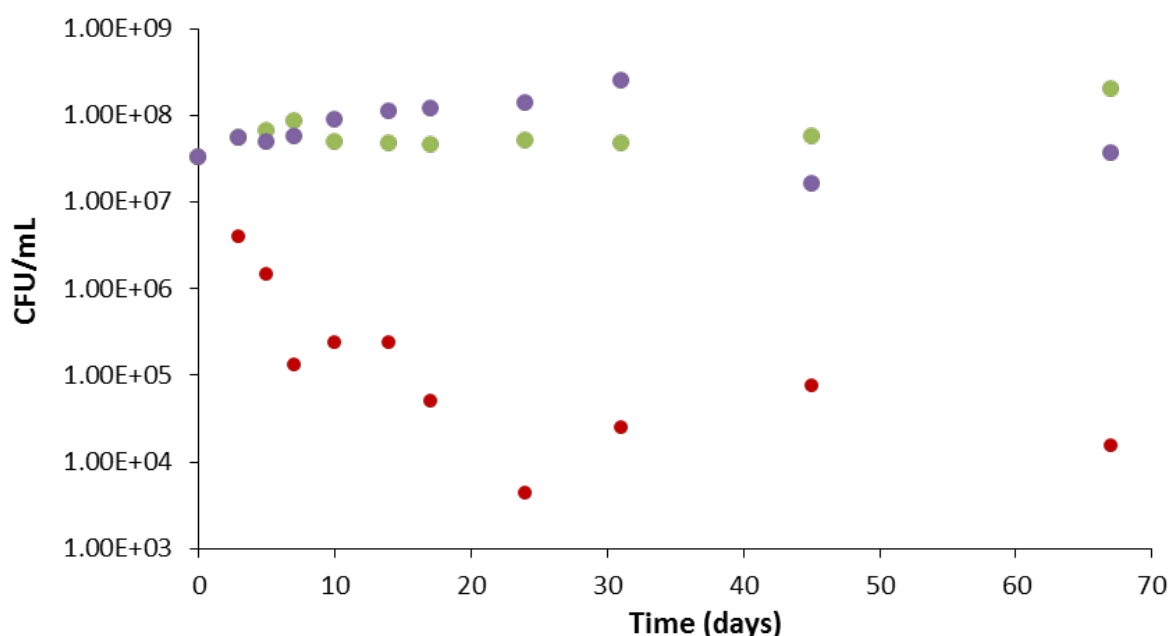


**Figure 77**. Microbial growth over time. N/P dissolved (●), SGPs (●), biotic control (●).

In this experiment, the addition of a direct source of N and P does not really correspond to an open sea environment as in open sea the N and P would be immediately diluted but this experiment served as a relevant reference for the assessment of SGPs effect. The amount of SGPs containing the N and P was calculated to match the quantity of N and P dissolved. In biotic conditions, an expected decrease of the microbial growth is observed; the absence of nutrients (N and P) cannot sustain a viable microbial growth. In the case of dissolved nutrients, which corresponds to the conditions where the nutrients are directly available for the bacteria, the microbial growth was higher than for the treatment with SGPs in a first stage. A slight decline in

the bacterial population incubated in the presence of dissolved nutrients is observed after 45 days, SGPs sustain the growth and degradation over a longer period of time than the dissolved N and P. This is a consequence of a more regulated system where the release is controlled by the presence of oil.

An alternative method was used to assess the performance of biostimulation by the SGPs in presence of crude oil or tetradecane, a hydrocarbon used as a basic model for crude oil degradation. The measurements were carried out in aerobic conditions and were based on the consumption of molecular oxygen by the *Marinobacter* bacteria. These latter consumed the oxygen during degradation of hydrocarbons. An OxiTop® system was used, which contains sodium hydroxide and a pressure sensor. The carbon dioxide produced during the mineralization of hydrocarbons was absorbed by the sodium hydroxide contained in the solution. The consumption of the oxygen by the microorganisms during the degradation of organic compounds caused a pressure drop in the headspace of the bottle. This change was detected and pressure measurement data were continuously recorded to be determined as BOD (biological oxygen demand). The BOD reflects the amount of oil components that was consumed by the *Marinobacter*.

Different conditions were tested to assess the effect of SGPs on the degradation of hydrocarbons, Figure 78. In abiotic conditions after 24 days, extremely low microbial growth was observed whatever the source of hydrocarbons, crude oil or tetradecane. In biotic conditions and in presence of hydrocarbons, a higher microbial growth was observed. The addition of nutrients as direct source (dissolved N and P) improved the microbial growth in the case of tetradecane and crude oil compared to the conditions where no additional source of N and P were available. The level of microbial growth in the case of SGPs as source of N and P surpassed all the conditions previously mentioned and reached the limit of 800 mg/L, suggesting that the use of SGPs was an effective method to increase the hydrocarbon degradation.
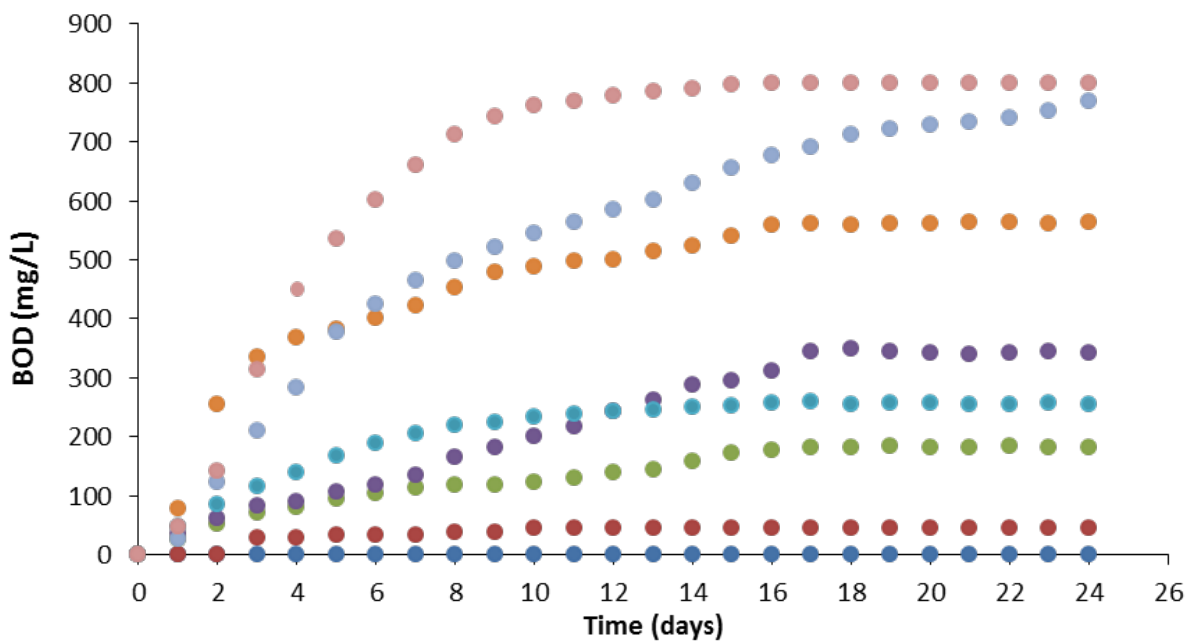
**Figure 78**. BOD evolution during hydrocarbon degradation. Tetradecane in abiotic conditions (●); crude oil in abiotic conditions (●); tetradecane in biotic conditions (●); crude oil in biotic conditions (●); dissolved N and P + tetradecane (●); dissolved N and P + crude oil (●); SGPs + tetradecane (●); SGPs + crude oil (●).

The biostimulation effect of SGPs was benchmarked with an existing commercial solution for biostimulation, namely S200. S200 is an oleophilic fertilizer, containing 7.9% N and 0.6% P. The solution is made of a microemulsion containing a saturated solution of urea in oleic acid as a carrier, an oleophilic phosphate ester (P source and surfactant). The experiment was carried out in artificial sea water, Figure 79.
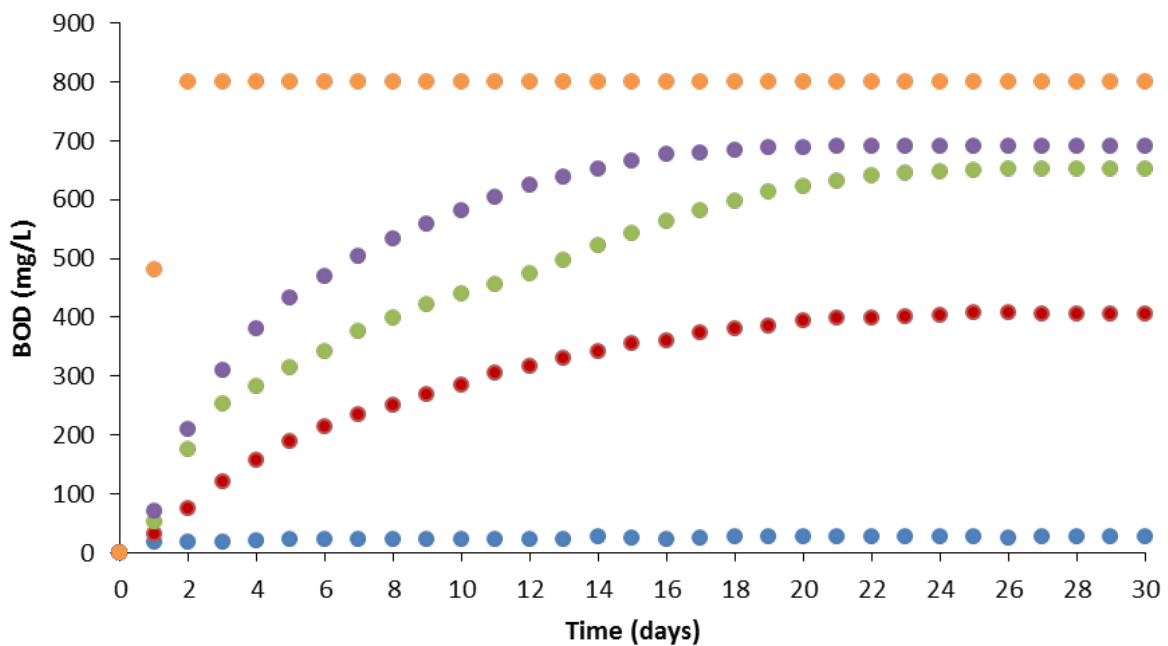


**Figure 79**. Biostimulation in the presence of oil-degrading bacteria measured in seawater. Crude oil + abiotic conditions (●); crude oil in biotic conditions (●); crude oil + N and P dissolved in biotic conditions(●); crude oil + SGPs in biotic condition (●) crude oil + S200 in biotic conditions (●).

From the results, it could be seen that as expected, in the absence of oil-degrading bacteria, no biodegradation occurred. The highest and fastest rate of biodegradation was observed with the addition of S200. However, these results could not be correlated with oil degradation as S200 contains high quantities of oleic acid, which is also degraded by the bacteria resulting in a fast increase of the BOD during the first two days of the experiment. This also prevented us from establishing a clear comparison between S200 and SGPs. In the case of SGPs, the degradation is sustained over a period of 18 days and the plateau is reached faster than with dissolved nutrients. It is worth to mention that the relevance of the dissolved nutrients experiment is also limited, as in real conditions the concentrations used would not be sustained for more than few minutes because of the dilution of the soluble nutrients in the open sea environment. To overcome these issues, we decided to perform experiments in real environmental conditions. Recent results obtained from the group of Prof. Corvini (FHNW) allowed us to assess the efficiency of SGPs.

### 3.8 From lab to open sea scale

The efficiency of SGPs was examined in an outdoor experimental system to assess the efficiency of SGPs in natural environment. The experiment was carried out in Aegean Sea (Greece). Booms were placed around a heavy oil leak to avoid dispersion of the oil during the treatment with the SGPs. Water was free to flow under the booms in order to take into account an eventual dilution of the dissolved nutrients in water as it would be the case in real conditions. The degradation was visually monitored during few days and pictures were taken after the first spreading of the SGPs and each day to check the evolution of the oil degradation, Figure 80.
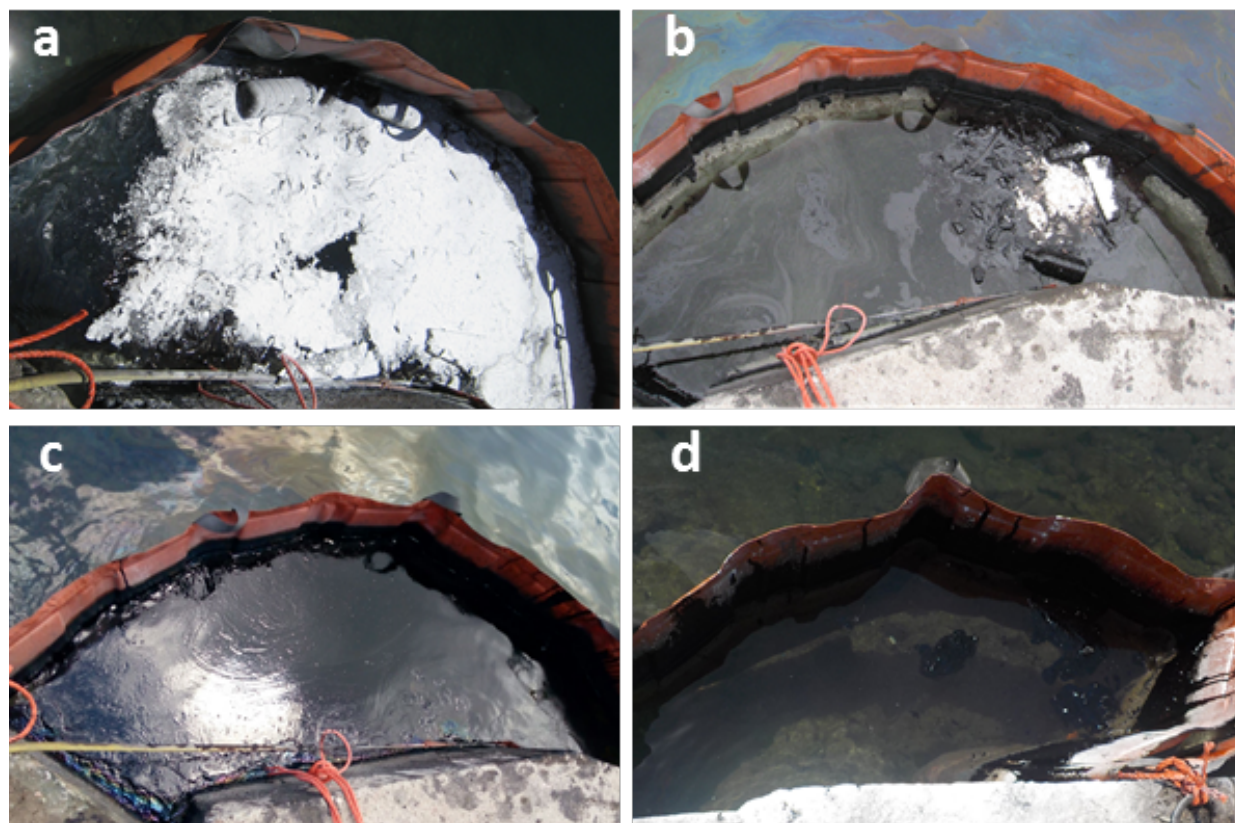
**Figure 80**. Pictures taken over time of the degradation of heavy oil in sea water (Aegean sea, Greece) restraint in small area with containment booms. **a**) day 1; **b**) day 2; **c**) day 3; **d**) day 4 after a second application.

The SGPs were spread directly on oil spill and no further forces were applied to the system than natural sea waves. The second day, the majority of the oil spill has been degraded. Few wastes were still covered by oil spill and SGPs. The third day, a thin layer of oil remains all over the surface contained in between the booms. SGPs were then applied a second time on this thin layer and the fourth day no oil was observed at the surface only small aggregates of oil spill were remaining under the suface of water.

### 3.9 Conclusion

We successfully synthesized SGPs with ordered mesopores that could act as nanocarriers and deliver specifically the nutrients to bacteria. The introduction of functional groups on the external surface of the material allowed to control the interactions of the particles with the environment. The design of such particles represents an alternative way to overcome the dilution or the non-targeted release of nutrients for bacteria in sea.

With such system the ratio between nutrients can be adjusted depending on the needs and the loading can also be changed as desired until a maximum loading.

It has been shown that the Smart Gates system was efficiently responding to environmental changes and that no further external trigger was needed to cause the opening and closing of the gates. The SGPs exhibited no premature release in aqueous media.

Experiment in a mixture water/oil, proved that we could achieve with the SGPs a slow release of the nutrients that would be more beneficial to a long hydrocarbon degradation process by the bacteria. After nutrients intake from the bacteria, the BOD increase evidenced an enhancement in the hydrocarbon degradation.

The use of SGPs have been tested in real conditions for oil leaking in sea water and demonstrated after few days an efficient degradation of oil and thus showed a great potential for the application of SGPs in biostimulation.

# Chapter 4

# Conclusions and Outlook

## 1. Cyclodextrin-based polymers

Through the present thesis we successfully demonstrated that CDPs could be tuned to act as a specific tool for the recovery of phenolic compounds from OMW. The central role of π-π interactions was pointed out but not only. Electrostatic interactions have been revealed to be of major importance in the adsorption capacity of the polymer. The monomers that enter into the composition of the polymeric material have thus to be carefully selected upon its potential electrostatic interactions with the targeted molecules. Adsorption experiments proved that we could produce CDPs that showed specificity towards TY and HT compounds. The desorption efficiency was also increased with the use of mixture of methanol/water (40:60). Characterization of adsorption rate was determined by means of HPLC analyses and the heterogeneous adsorption process of the CDP for TY and HT was confirmed by fitting the data to the Freundlich model.

In order to evaluate the performance at higher scale for possible applications at industrial scale the extraction of TY and HT was achieved on a pilot scale where the synthesis of the CDP was first optimized to reduce its environmental fingerprint. The high affinity of CDP for TY and HT was confirmed at kilogram scale with a TY content raised to 61% after recovery (14.1% in the OMW sample). COD level have been divided by 5 times in the recovered wastewaters, which make them relevant for irrigation purposes.

The finding reported in this manuscript goes beyond the recovery of phenolic compounds from OMW. Indeed, the possibility of controlling the interactions between the polymer and the compound of interest is one of the key achievements of this PhD thesis. By extension, it could be hypothesized that other molecules, including toxic or high value-added molecules, could be targeted through the proper design of CDP that would act as a high selective tool for the recovery and recycling of these molecules. Two approaches are envisioned: the screening of monomers to adapt the composition of the CDP depending on the affinity for the target molecule or a careful interpretation of the possible interactions between the CDP and the target prior the CDP synthesis.

## 2. Supramolecular self-assembled nanorods

The research work of this PhD thesis allowed the development of a new synthetic strategy for the design of supramolecular nanorods. We first achieved the synthesis of a pyrene derivative and developed a strategy to produce hierarchical self-assembled nanorods following a template-free approach. We described the nanomaterial that forms after molecular self-assembly with SEM and TEM analyses. In order to understand their internal structures UV-vis, FTIR, X-ray analyses were carried out and allowed us to conclude that the self-assembly process occurs via π-π stacking of the molecular building block. The bathochromic shift of the characteristic bands observed when transferred to aqueous medium and the decrease of the ratio of intensities allowed us to conclude on the formation of J-type aggregates. Single crystal X-ray crystallography provided detailed insights into the crystal packing of **1**, whilst powder X-ray diffraction confirmed the similar arrangement within the supramolecular nanorods. We confirmed that hydrogen bonds and π-π stacking act synergistically to form the final aggregate as it was intended. A surface modification was successfully achieved through the reaction of the triethoxysilyl groups to form a silica layer on the supramolecular nanostructures.

Pyrene derivative self-assembly is an effective method to create functional nanomaterials as optoelectronically relevant organic nanostructures. But one of the possible outlooks for such structures is the combination of the organic nanomaterials with biological components as enzyme. The potential that may come from bringing π-conjugated electronic function in combination with catalytic potential of proteins is poised to impact on biocatalytic applications. This approach originates from these PhD findings and is currently under investigation in the laboratory in which this doctoral research work was carried out.

## 3. Smart Gates Particles

The conception of nanomaterial able to release their content in a specific area or environment is of great importance in several domains such as in drug delivery. Herein, we demonstrated how SGPs could act as nanocarriers and deliver specifically nutrients to bacteria under environmental trigger. The design of such particles represents an alternative and ecological way to overcome the dilution or the non-targeted release of nutrients for bacteria in aqueous medium.

The system allows to select the nutrients; their quantity and the loading can also be achieved with more than two molecules. SGPs efficiency was assessed in sea water and demonstrated after few days an efficient degradation of oil and a promising potential for the application of SGPs in biostimulation. In addition, the simplicity, inexpensive and eco-friendly method of production makes SGPs even more attractive.

One of the goals will be to convert the acquired knowledge into technical application. In view of the complex nature of the topic, the number of research groups, companies, governmental organisations and private corporations involved; it is still difficult to predict whether or not this type of product might be substantial for industrial exploitation but definitely needs the attention of industrials and further thorough research.

# Chapter 5

# Experimental Methods

## 1. General

β-CD was purchased from CycloLab (Hungary). All other solvents (analytical grade) and other chemicals were obtained from Sigma-Aldrich and used without any further purification unless otherwise mentioned. Reactions were followed by thin-layer chromatography (TLC) carried out on Polygram® G/UV254 pre-coated polyester plates. Flash silica gel chromatography was performed over Macherey-Nagel® silica C60 (40-63µm). Nanopure water was produced with a Millipore Synergy purification system (resistivity ≥ 18 MΩ cm). Elma® S30H Elmasonic bath sonicator was used. FTIR spectra were measured in attenuated total reflection (ATR) mode using a single reflection diamond ATR device (Golden Gate) and a Varian 670-IR spectrometer, spectra were recorded between 500 and 4000 cm-1. Elemental analyses were performed on a Leco® CHN-900 microanalyser (C-, H- and N-detection) and are reported in mass per cent. NMR spectra were recorded on a Bruker® 400 MHz spectrometer and are reported as chemical shift in parts per million (ppm). All coupling constants (J) are reported in hertz (Hz). The abbreviations s (singlet), d (doublet), dd (doublet of doublet), t (triplet), q (quartet) and m (multiplet) are used to describe multiplicities. Mass spectra (m/z) were recorded on a Finnigan® thermoquest LCQ Deca instrument using positive electrospray ionization (ESI). Melting point was measured using a Büchi® 530 apparatus and measurements were carried out in triplicate to ensure the reproducibility of the result.

## 2. Microscopic characterization (SEM, TEM)

FE-SEM micrographs were acquired using a Zeiss SUPRA® 40VP field-emission scanning electron microscope, 5 µL of each sample were spread on freshly cleaved mica sheets, dried under ambient conditions and sputter-coated with a gold-platinum alloy for 30 seconds at 15 mA (SC7620 Sputter coater). Micrographs were acquired using the InLens mode with an accelerating voltage of 10 kV. Transmission electron microscope measurements were performed on a Zeiss EM900 microscope equipped with an Olympus Megaview III CCD camera. 10 µL of suspension of supramolecular structures was dropped on the copper grid and left to dry in air before characterization.

### 3. UV-visible absorbance and fluorescence measurements

Absorbance and fluorescence intensity were measured using a Biotek Synergy™ H1 hybrid multi-mode microplate reader. All measurements were performed at 25°C. Absorbance characterization was performed using Greiner Bio-one 96 well UV-Star microplates and spectra were recorded between 250 and 500 nm. Spectrum of pyrene derivative **1** in ethanol was recorded following these procedures. For the spectrum recorded in ethanol, pyrene derivative **1** was solubilized in ethanol (concentration 0.1 mM) and an aliquot of 200 µL was then analysed. For the spectrum in water (ethanol 10 vol. %) of **1**, pyrene derivative **1** was first solubilized in ethanol. The latter solution was then added to water to reach a concentration of 0.1 mM and a final ratio vol. water/ethanol 90:10. The suspension was stirred at 600 rpm for 1 h before measurement.  For the spectrum in water (ethanol 10 vol. %) under ultrasonication, pyrene derivative **1** was first solubilized in ethanol, and the latter solution was then added to water while under ultrasonication (concentration: 0.1 mM, ratio vol. water/ethanol 90:10). The suspension was subjected to ultrasonic treatment for 1h before measurement. Fluorescence characterization was performed using Greiner Bio-one 96 well black microplates, samples were excited at 366 nm and spectra were recorded between 350 and 550 nm. Fluorescence spectra were first obtained by solubilizing pyrene derivative **1** in ethanol and concentrations of 0.2, 0.4, 1, 2, 5 and 10 mM were prepared. For the spectra obtained after ultrasonication pyrene derivative **1** was solubilized in ethanol and was added to water under ultrasonication (ratio vol. water/ethanol 90:10). Different solutions of pyrene derivative **1** in ethanol were prepared to obtain the following concentrations: 0.2, 0.4, 1, 2, 5 and 10 mM. The suspension was subjected to ultrasonic treatment for 1h before measurement.

### 4. Dynamic light scattering and Zeta-potential measurements

Dynamic light scattering measurements were carried out by means of a Malvern® Zetasizer nano-ZS instrument on suspensions of the produced nanorods in water (ethanol 10 vol. %) at different concentrations (0.008, 0.016, 0.033, 0.066, 0.1 and 0.167 mg/mL) using ZN0112 low volume disposable sizing cells. Measurements were carried out in triplicate to ensure reproducibility of the results. ζ-potential measurements were carried out by means of  a Malvern® Zetasizer nano-ZS instrument with Malvern® DTS 1070 cells after equilibration for 2 minutes at 25°C.

## 5. HPLC analyses and nanoflow LC-MS measurements

An Agilent HPLC 1100 system was used with a reversed-phase column Zorbax® SB-C18 (4.6 x 250 mm, 5 µm) for HPLC analyses. The mobile phase consisted in solvent A ($H_2O$: $CH_3CN$: TFA, 95:4.9:0.1, v:v:v) and solvent B ($H_2O$:$CH_3CN$:TFA, 4.9:95:0.1, v:v:v). An isocratic gradient was applied and flow rate kept constant (1.0 mL min$^{-1}$). The HPLC-UV detector was set to 230 nm and 280 nm. Ion trap mass spectrometry analyses were performed on an Agilent 1260 liquid chromatography setup coupled to an Agilent 6320 ion trap spectrometer via a nano-ESI interface, using $H_2O$/ACN as eluent both solvent containing 0.1% TFA.

## 6. Adsorption kinetic procedure

CDP (30 g) were added to OMW (1L) and stirred for 3h at 140 rpm. During the first hour, an aliquot of 2 mL was sampled from the mixture every 10 min and filtrated to remove any solid particles. For the second hour an aliquot of 2 mL was sampled every 20 min from the mixture and filtrated to remove any solid particles. The third hour, an aliquot of 2 mL was sampled from the mixture every 30 min and filtrated to remove any solid particles. The samples were then analysed by HPLC.

## 7. X-ray crystallography

Data were collected at 100(2) K by shutterless scans using a Bruker® D8 diffractometer equipped with a PHOTON 100 detector and operating with a silicon 111 monochromator and synchrotron radiation of wavelength 0.77490 Å. Diffraction data on the air-stable dried nanorods were collected using a Bruker® D8 Advance powder diffractometer, operating with Ge-monochromated Cu Kalpha1 radiation (wavelength = 1.5406 Å) and a Bruker® LYNXEYE linear detector. Data were collected over the angular range 5- 50 degrees in two theta.

## 8. Chemical oxygen demand measurements

COD measurements were carried out using the Aqualytic® COD Vario kit (range 0-1500 mg/L). 2 mL of the samples were added to the tubes containing potassium permanganate in an acidic medium. The tubes were then incubated at 150°C for 2 h. Once the tubes were cooled down to room temperature, the absorbance was measured ($\lambda$ = 610 nm). Calibration curve was prepared using 5 different concentrations of glucose.

## 9. Synthesis of CDPs

DBTDL (1 mL) was added to 160 mL of DMF extemporaneously dried over molecular sieves and degassed with nitrogen. Subsequently, the appropriate amount of monomers was added (Table 1). After 120 min of reaction under stirring at 65°C, 200 mL of a solution of β-CD (12 mmol, 13.61 g) and 1 mL of DBTDL in DMF were added and allowed to react at 75°C for 3 h. The mixture was then poured in 100 mL of acetone to yield a white precipitate that was washed with acetone (3 x 200 mL), water (3 x 200 mL) and ethanol (3 x 200 mL) to remove unreacted DBTDL, monomers, and β-CD. Finally, the CDP produced was dried under vacuum at 60°C for 24 h prior to use. In Table 3 and Figure 33 are given the quantities used for each polymerization reaction and the chemical structures of β-CD and the selected monomers.

## 10. Synthesis of magnetic CDPs

Monomer (1 eq), cross-linker (0.5 eq), dibutyltindilaurate (cat.) and MNPs (400 mg) were mixed in DMF (50 mL). After 90 min of reaction at 65 °C under stirring, a CD solution (2.4 g, 2.1 mmol, 1 eq) in DMF (30 mL) was added and reacted at 75 °C for 2h. The produced MNPs coated with CDPs were washed with acetone (3 x 2 mL), water (2 x 1 mL), and acetone (1 x 1mL) to remove unreacted DBTDL, HDI and CD. Magnetic particles were isolated by magnetic separation. Finally, the MNPs were dried under vacuum at 60 °C for 24 h.

## 11. Binding assay of selected and OMW phenolic compounds

The polymer was added to 1.5 mL aqueous solution of the selected phenolic compounds (phenolic compounds:CDP, 1:150, w:w). The suspension was maintained at 25°C for 2 h and subsequently centrifuged at 8,050 $g$ for 10 min. The supernatant was then collected to measure the absorbance at 270 nm for syringic acid and HT, at 290 nm for $p$-coumaric acid and at 320 nm for caffeic acid.

For the phenolic compound from OMW, a fraction of 1 mL of phenolic compounds solution extracted from OMW (2 mg mL$^{-1}$) was incubated with the CDP (100 mg) for 2 h at 25°C. Consequently, the mixture was centrifuged at 8,050 $g$ for 10 min and the supernatant was recovered and analysed by HPLC. The adsorption and desorption of phenolic compounds from CDPs was performed also using a packed CDP column built using a classical chromatographic column filled with CDP. The sample of OMW was deposited on the CDP column and the OMW

sample was eluted through the column using several solvents as ethanol, methanol, ethyl acetate, water, and methanol/water to desorb the phenolic compounds from the CDP. The different fractions recovered were then analysed by HPLC-DAD.

## 12. Scale up of CDP

Me-β-CD (580 g) was added in a 2.5 L reactor containing acetone (1.2 L). In a 2 L flask, MDI (756 g) was added to acetone (540 mL). Both flasks were stirred at 500 rpm and heated at 40°C for 30 min. Catalyst DBTDL (1 mL) was added to the Me-β-CD suspension and it was stirred for an additional 10 min. Then, the mixture was cooled down to room temperature and the MDI suspension was added dropwise to the Me-β-CD suspension under strong stirring. A white polymer (1.33 kg) was obtained. The CDP was washed with acetone, water and ethanol to remove residual DBTDL, monomers and β-CD. The polymer was dried under vacuum overnight at 60°C for 24h and grinded prior to use.

## 13. Synthesis of PySi

Dichloromethane was dried over $CaH_2$ and distilled for 4 h. PBA (17.34 mmol, 5 g) was dissolved in freshly dried DCM (700 mL) in a round bottom flask under a nitrogen atmosphere at 0°C. DCC (17.34 mmol, 3.6 mg) was then added and the mixture was stirred for 15 min before APTES (17.34 mmol, 4.1 mL) was added. The suspension was then stirred for 30 min at 0°C before the reaction mixtures was allowed to warm up at 25°C and stirred for additional 24h. The reaction mixture was then cooled at 0°C for 2h and the resulting precipitate (DCU) was eliminated by filtration. The mixture was placed at 0°C overnight and was then filtrated. The purification was achieved by flash chromatography using ethyl acetate/cyclohexane mixture (3/7) as eluent, yielding a yellowish powder (2.12 g, 25% yield). $[M+Na]^+$= 514.1. Elemental analysis calcd (%) for C29H37NO4Si: C 70.84, H 7.59, N 2.85; found: C 70.71, H 7.55, N 2.94. Mp: 91°C, TLC ethyl acetate/cyclohexane (6:4) Rf = 0.38.

$^1$H NMR and $^{13}$C NMR spectra are presented in Annex.

1H NMR (($CD_3$)$_2$SO, 400MHz): δ = 8.38 (d, J=9.4 Hz, 1H), 8.25-8.30 (m, 2H), 8.22 (dd, J=8.5, 3.4 Hz, 2H), 8.13 (d, J=2.0 Hz, 2H), 8.03-8.09 (m, 1H), 7.94 (d, J=7.9 Hz, 1H), 7.85 (s, 1H), 3.72 (q, J=6.9 Hz, 3H), 3.25-3.37 (m, 2H), 3.00-3.10 (m, 1H), 2.17-2.28 (m, 1H), 1.96-2.08 (m, 1H), 1.41-1.52 (m, 1H), 1.06-1.15 (m, 5H), 0.50-0.59  (m, 1H) ppm.

$^{13}$C NMR ((CD$_3$)$_2$SO, 400MHz): δ = 171.64 (CO), 136.54 (Ar C), 130.85 (Ar C), 130.39 (Ar C), 129.26 (Ar C), 128.11 (Ar C), 127.43 (Ar C), 127.40 (Ar C), 127.14 (Ar C), 126.45 (Ar C), 126.07 (Ar C), 124.87 (2 x Ar C), 124.71 (Ar C), 124.21 (Ar C), 124.12 (Ar C), 123.43 (CH$_2$), 57.63 (3 x CH$_2$), 41.24 (CH$_2$), 35.03 (CH$_2$), 32.23 (CH$_2$), 27.62 (CH$_2$), 22.79 (CH$_2$), 18.13 (3 x CH$_3$), 7.37 (Si-CH$_2$) ppm.

## 14. Self-assembly procedure

1 mL solution of pyrene derivative **1** in ethanol (5 mg/ml) was prepared and was then added to 9 mL water in a 20 mL glass vial. The suspension was subjected to an ultrasonic treatment for 1h. The suspension was then recovered and centrifuged for 3 min at 20,000 g. The supernatant was removed and the resulting white solid was dried under vacuum at 20°C.

## 15. Silica layer growth on PySi nanorods

Nanorods were suspended in 12 mL (0.25 mg/mL) of a 2-(N-morpholino)ethanesulfonic acid (MES) buffer (15 mM) and triton X-100 (10 μL, 0.1%) was added. The suspension was subjected to sonication for 10 min. The suspension was left to stir at 400 rpm for 30 min at 20°C (pH 6). Tetraethoxysilane (12 μL) was added and the suspension was stirred for 2h. (3-aminopropyl) triethoxysilane (4 μL) was added and the mixture was stirred at 400 rpm at 10°C for 50h. The nanorods were centrifuged at 20,000 x $g$ for 3 min and the supernatant was removed. The solid was suspended in 1 mL nanopure water and centrifuged again. This last step was repeated one more time before the solid was dried under vacuum at 20°C.

## 16. OMW pre-treatment

OMW were first centrifuged at 2000 x $g$ for 30 min using a Thermoscientific SC16R centrifuge. The liquid was then filtrated through 25 μm and 11 μm GE Healthcare Life Science Waltham filters at 1.67 cm/min superficial velocity. For TY and HT adsorption experiment, OMW were centrifuged at 2000 x $g$ for 20 min and filtrated then on 11 μm Healthcare Life Science Waltham filters at 2.5 cm/min superficial velocity.

## 17. Pilot plant

Pilot plant was made of stainless steel (tanks and pipes). It combined a storage tank (25L) for the OMW, a feed tank (2L), two solvent tanks (2L), one for the rinsing solvents and one for the elution solvents. The feed, rinsing and elution tanks were equipped with an EGE MFP 075 GA-LM030 filling level meters to insure minimum level of solvent in the tanks and pipes. The system also included two reactors (13.0 cm x 6.0 cm) connected in series that could be used separately, one tank (15L) to recover the rinsing solvents, two elution tanks (5L) to recover the desorbed solvents, two reclaim tanks (5L) and a collecting tank (30L) for the dephenolized OMW. The mass flow was monitored by two Bronkhorst mini CORI-Flow mass meter. One situated between the feed tank and the reactors and another one between the elution tanks and the reactors. OMW were pre-filtrated on Whatman filter paper to get rid of the biggest solid particles and a Wolftechnik F-10 cartridge filter (5 µm) was installed between the storage and feed tank to insure minimum solid particles in the pipes.

The pilot plant was equipped with two auto sampling systems, one for collecting the adsorption samples, and the second for the desorption samples. Up to 46 different fractions could be collected in a row on each auto sampling system. The software allowed among other options to control the mass flow, time of adsorption and desorption, the temperature with WIKA TR-30 temperature sensors and to monitor the pressure after the feed, rinsing and elution tanks with WIKA A-10 pressure sensors. The use of the different pipes was controlled using Gemü 0322, 0324 and 0326 magnetic valves and HOKE R6000 overflow valves that were controlled through the software. All liquids contained in the feed, eluent and rinsing tanks were fed to the system using a magnetic-diaphragm metering Prominent Delta pump, a Bram hose pumps and a Verder motor VEM pump respectively. The complete adsorption system and program software to control the pilot plant were made by SIMA-Tec GmbH (Schwalmtal, Germany).

## 18. Production of Smart Gates particles

Mesoporous particles (50 g) were dried in an oven at 80°C under vacuum for 12 h before adding them to a round bottom flask (500 mL), a magnet bar was added and the flask was put under vacuum and left for 3h. A saturated solution of urea and a saturated solution of potassium dibasic phosphate were prepared at room temperature. The saturated solution of urea (or potassium dibasic phosphate) was added to the flask (400 mL for 20 g) and left to stir overnight. The particles were filtrated and dried at under vacuum at rt for 12 h. The particles loaded with

urea (or potassium dibasic phosphate) were then suspended in toluene (10 g of particles in 100 mL) in a round bottom flask. A solution of OTS (3 mL) was then added to the suspension. The mixture was stirred for 20 h at room temperature. The particles were filtrated and washed with heptane and dried at 30°C under vacuum.

## 19. Synthesis of mesoporous particles MCM-41

A solution of CTAB (2.0 g), 7.0 mL of $NaOH_{aq}$ (2.0 M, 7.0 mL) and $H_2O$ (480 g) was prepared (pH=12.3) and heated at 80 °C for 30 min To this clear solution, TEOS (10.0 mL) was added rapidly via dropwise injection and solution was stirred at 80°C for 2h. The white solid was isolated by hot filtration, washed with copious amount of water and methanol, and dried under vacuum at 70°C. The surfactant was then removed by calcination overnight at 600°C.

## 20. Phosphate colorimetric assay

A MAK030 colorimetric phosphate assay kit from Sigma was used. To obtain the standard curve phosphate standard solution S0 (10 uL, 10 mM) was diluted in 990 µL of water, to prepare 1 mL of standard solution SS (0.1 mM). 0, 10, 20, 30, 40 and 50 µL of the SS solution was added into a 96 well plate, generating 0, 1, 2, 3, 4 and 5 nmol/well samples. Water was added to each sample to bring the volume to 200 µL. Then 30 µL of the phosphate reagent was added to each well and mixed for few seconds. The plate was covered and protected from light. Then the well plate was incubated for 30 min at 300 rpm and at 30°C. Absorbance was measured at 650 nm.

Assay reaction was performed as follow. Samples of 100 to 200 µL were recovered and added to wells. The volume was brought to 200 µL with water and phosphate reagent (30 µL) was added to the sample. The well plate was covered, protected from light and incubated for 30 min at rt. Absorbance was measured at 650 nm.

## 21. Urea colorimetric assay

Assay reaction was performed as follow. Samples of 100 µL were recovered from the supernatant and added to a 2 mL Eppendorf tube. Water (900 µL) was added to obtain 1 mL sample. Then sequentially diacethylmonoxime (50 µL), thiosemicarbazide (8 µL) and $Fe_2(SO_4)_3$ (8 µL) and $H_2SO_4$ (667 µL) were added. The mixture was heated to 85°C for 30 min and then cooled down by immersing the Eppendorf tubes in water for 10 min. Samples of 200 µL were added to the well plate and absorbance was measured at 520 nm.

# Chapter 6

# Annex

# 1. Specific recovery of phenolic compounds
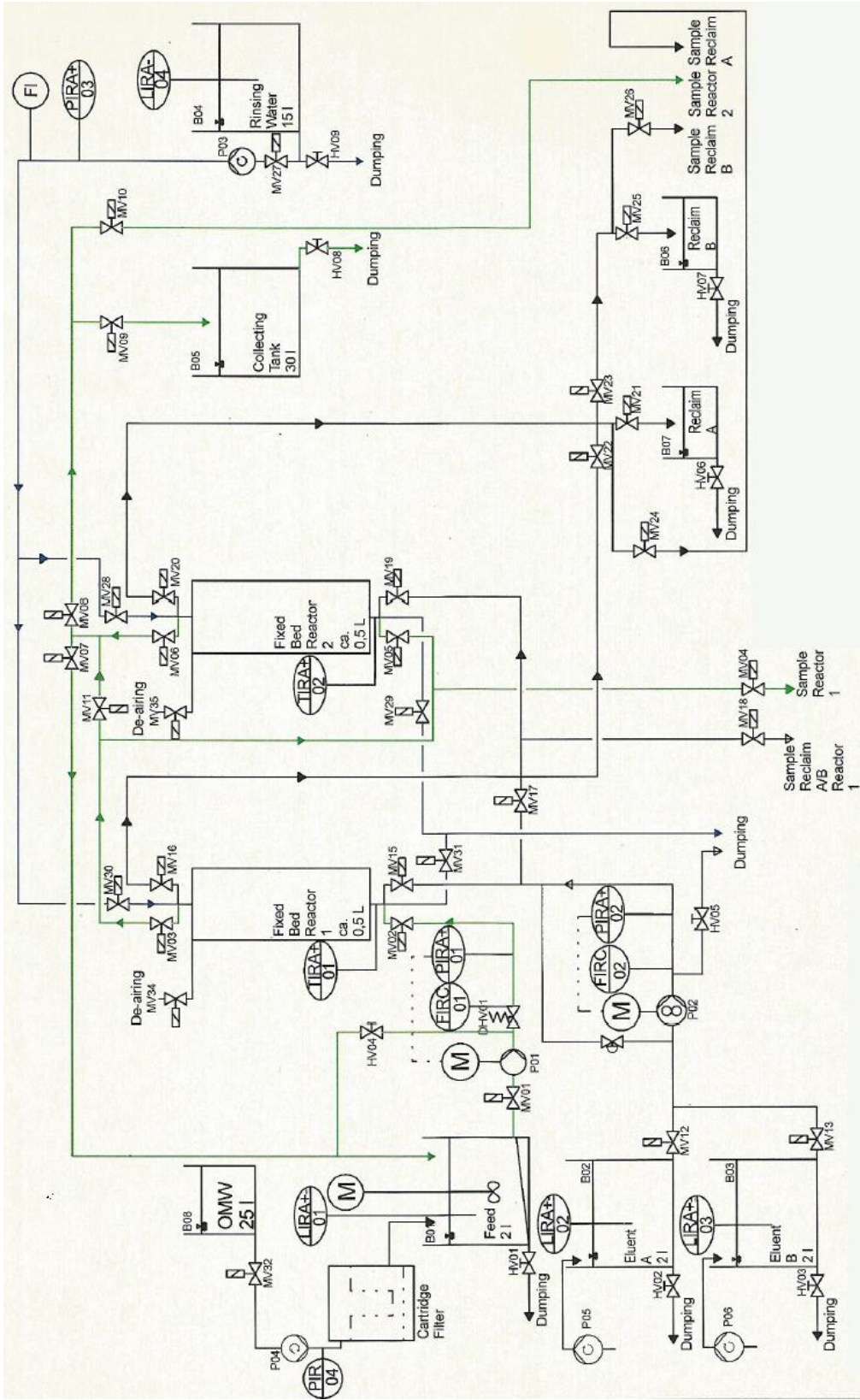


**Figure 81.** Process flow diagram of the pilot plant built by SIMA-Tec GmbH for TY and HT adsorption.

**Table 9**. Conditions for the optimization of the CDP scale up.

| Batch | β-CD (g) | Diisocyanate/mass (g) | DBTDL (µL) | Solvent/volume (mL) | Temperature (°C) | Yield (%) |
|---|---|---|---|---|---|---|
| 411 | 13.5879 | PDI/7.6864 | 1000 | DMF/360 | 75-85 | 46.5 |
| 417 | 3.5507 | PDI/2.0143 | 1000 | DMF/43 | - | 76.4 |
| 424 | 24.9400 | PDI/21.3561 | 3000 | DMF/250 | - | 54.8 |
| 428 | 76.2 | PDI/43.133 | 5600 | DMF/2000 | - | 100 |
| 431 | 1.2141 | PDI/1.0201 | 150 | - | - | 0 |
| 443 | 1.6208 | MDI/10.0209 | 50 | - | - | 0 |
| 446 | 1.3656 | MDI/1.2136 | 100 | DMF/36 | - | 96.2 |
| 448 | 13.6784 | MDI/12.2187 | 500 | DMF/260 | - | >100 |
| 449 | 4.5154 | TDI/2.76 | 300 | DMF/80 | - | 84.8 |
| 457-1 | 3.1589 | TDI/1.93 | 0 | DMF/11 | - | 88.5 |
| 457-2 | 3.1592 | TDI/6*1.93 | 25 | DMF/11 | - | 60.4 |
| 457-3 | 3.1536 | TDI/6*1.93 | 50 | DMF/11 | - | 60 |
| 457-4 | 3.1582 | TDI/6*1.93 | 100 | DMF/11 | - | 60 |
| 457-5 | 3.1558 | TDI/6*1.93 | 150 | DMF/11 | - | 60 |
| 457-6 | 3.1590 | TDI/6*1.93 | 231 | DMF/11 | - | 60 |
| 458-1 | 1.5141 | MDI/1.4086 | 0 | DMF/11 | - | 94.0 |
| 458-2 | 1.5189 | MDI/1.4032 | 10 | DMF/11 | - | 98.3 |
| 458-3 | 1.5136 | MDI/1.4048 | 20 | DMF/11 | - | 103.6 |
| 458-4 | 0.7560 | MDI/0.7054 | 0 | DMF/11 | - | 68.2 |
| 458-5 | 0.7586 | MDI/0.7059 | 10 | DMF/11 | - | 97.8 |
| 458-6 | 0.3831 | MDI/0.3522 | 0 | DMF/11 | - | 65.2 |
| 458-7 | 0.3871 | MDI/0.3515 | 10 | DMF/11 | - | 60.9 |
| 458-8 | 0.5070 | MDI/0.4611 | 10 | DMF/11 | - | 92.4 |
| 458-9 | 0.1954 | MDI/0.1823 | 10 | DMF/11 | - | 18.3 |
| 459-1 | 0.3272 | MDI/0.3011 | 10 | DMF/11 | - | 101.3 |
| 459-2 | 0.3251 | MDI/0.3049 | 10 | DMF/11 | - | 100.4 |
| 459-3 | 0.3270 | MDI/0.3027 | 10 | DMF/11 | - | 105.4 |
| 460-1 | 0.5061 | MDI/0.4652 | 10 | DMSO/11 | - | 58.0 |
| 460-2 | 0.7539 | MDI/0.7022 | 10 | DMSO/11 | - | 78.4 |
| 460-3 | 1.5127 | MDI/1.4007 | 10 | DMSO/11 | | 73.4 |
| 460-4 | 3.3361 | MDI/3.1091 | 10 | DMSO/11 | - | 97.9 |
| 460-5 | 2.0079 | MDI/18731 | 10 | DMSO/11 | - | 74.5 |
| 460-6 | 2.5035 | MDI/2.3370 | 10 | DMSO/11 | - | 84.8 |
| 461 | 60.1313 | MDI/56.1744 | 200 | DMSO/330 | - | |
| 462-1 | 2.0022 | MDI/1.8707 | 10 | DMSO/11 | - | 70.6 |
| 462-2 | 2.0021 | MDI/1.8716 | 10 | DMSO/11 | - | 85.9 |
| 462-3 | 2.0018 | MDI/1.8715 | 10 | DMSO/11 | - | 52.0 |
| 462-4 | 2.0040 | MDI/1.8717 | 10 | DMSO/11 | - | 50.8 |
| 463 | 1.3632 (HPBCD) | MDI/1.2010 | 100 | Acetone/30 | 50 | 49.4 |
| 464 | 1.3636 (MeBCD) | MDI/1.2008 | 100 | Acetone/35 | 50 | 74.5 |
| 465 | 1.3615 (MeBCD) | MDI/1.2078 | 100 | Acetone/80 | 50 | 68.1 |
| 466 | 6.8096 (MeBCD) | MDI/6.0072 | 500 | Acetone/35 | 50 | 74.7 |
| 467 | 20.4844 (MeBCD) | MDI/18.0128 | 500 | Acetone/45 | 50 | 66.4 |
| 468 | 34.1208 (MeBCD) | MDI/30.0020 | 500 | Acetone/100 | 50 | 68.4 |
| 469 | 21.2190 (MeBCD) | MDI/18.9023 | 200 | Acetone/35 | 50 | 75.4 |
| 470 | 21.2265 (MeBCD) | MDI/18.8675 | 50 | Acetone/35 | 50 | 87.6 |

| 471 | 13.2176 (MeBCD) | MDI/17.8368 | 200 | Acetone/35 | 42 | 93.2 |
| 472 | 13.0115 (MeBCD) | MDI/17.0066 | 100 | Acetone/35 | 42 | 90.3 |
| 473 | 100.9517 (MeBCD) | MDI/119.0042 | 700 | Acetone/350 | 42 | 93.9 |
| 474 | 440 (MeBCD) | MDI/567.3473 | 3000 | Acetone/1200 | 42 | 100 |

**Table 10.** Details of the gradient used for TY and HT desorption.

| | TY | HT | |
| --- | --- | --- | --- |
| Time (min) | Concentration (mg/L) | Concentration (mg/L) | Solvent |
| 3,00 | 3,27 | 9,03 | |
| 6,00 | 2,07 | 8,29 | **Acidified water** |
| 9,00 | 2,22 | 8,60 | |
| 12,00 | 2,66 | 8,56 | |
| 15,00 | 2,76 | 6,50 | |
| 18,00 | 2,88 | 4,85 | |
| 21,00 | 3,18 | 4,40 | **95% acid. water + 5% ACN** |
| 24,00 | 3,55 | 4,10 | |
| 27,00 | 4,44 | 4,15 | |
| 30,00 | 6,59 | 5,04 | **85% acid. water + 15% ACN** |
| 39,00 | 14,77 | 7,48 | |
| 42,00 | 16,31 | 8,80 | |
| 45,00 | 42,59 | 14,48 | |
| 48,00 | 54,51 | 17,55 | |
| 51,00 | 66,98 | 17,53 | |
| 54,00 | 93,59 | 17,78 | **75% acid. water + 25% ACN** |
| 57,00 | 137,13 | 20,27 | |
| 60,00 | 164,12 | 21,32 | |
| 63,00 | 175,08 | 18,59 | |
| 66,00 | 173,99 | 15,32 | |
| 69,00 | 172,49 | 13,17 | |
| 72,00 | 162,77 | 11,23 | |
| 75,00 | 153,11 | 8,46 | **80% acid. water + 20% MetOH** |
| 78,00 | 144,41 | 6,83 | |
| 81,00 | 135,19 | 5,45 | |
| 84,00 | 126,38 | 4,60 | |
| 87,00 | 107,15 | 3,63 | **40% acid. water + 60% MetOH** |
| 90,00 | 61,14 | 1,77 | |
| 93,00 | 30,73 | 0,83 | |
| 96,00 | 20,45 | 0,56 | |
| 99,00 | 23,88 | 0,62 | |
| 102,00 | 68,39 | 1,60 | |
| 105,00 | 83,68 | 1,71 | |
| 108,00 | 52,72 | 0,89 | |
| 111,00 | 65,43 | 1,19 | **100% MetOH** |
| 114,00 | 50,01 | 0,83 | |
| 117,00 | 45,40 | 0,70 | |

Mohamed EL IDRISSI

| | | |
|---|---|---|
| 120,00 | 43,87 | 0,54 |
| 123,00 | 20,63 | 0,35 |
| 126,00 | 7,60 | 0,18 |
| 129,00 | 4,46 | 0,32 |
| 132,00 | 2,87 | 0,30 |
| 135,00 | 1,16 | 0,21 |
| 138,00 | 0,57 | 0,12 |
| 141,00 | 0,26 | 0,07 |
| 144,00 | 0 | 0,04 |
| 147,00 | 0 | 0,02 |
| 150,00 | 0 | 0,02 |
| 153,00 | 0 | 0 |
| 156,00 | 0 | 0 |
| 159,00 | 0 | 0 |
| 162,00 | 0 | 0 |
| 165,00 | 0 | 0 |
| 168,00 | 0 | 0 |
| 171,00 | 0 | 0 |
| 174,00 | 0 | 0 |
| 177,00 | 0 | 0 |
| 180,00 | 0 | 0 |

## 2. Hierarchical self-assembly formation of pyrene derivative into nanorods
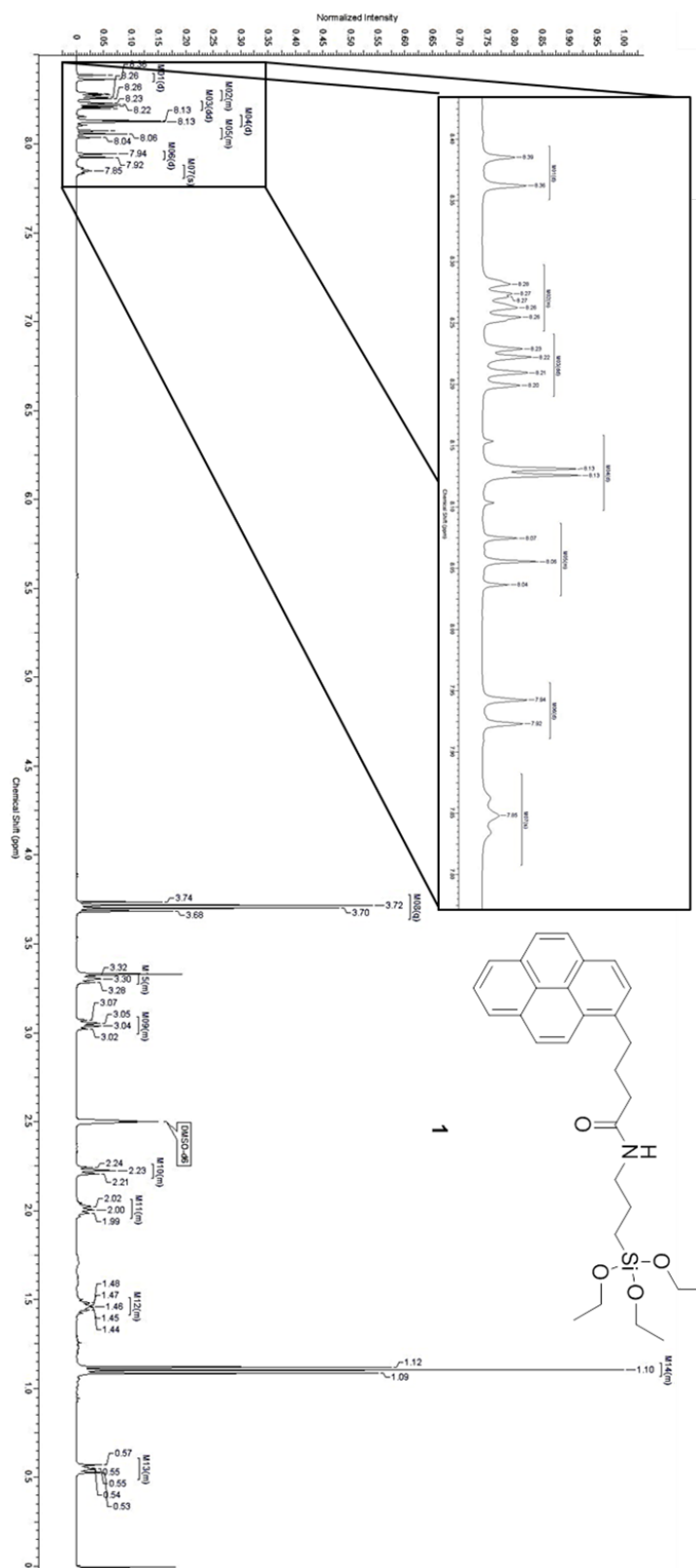


**Figure 82**. ^{1}H NMR spectra of 1.
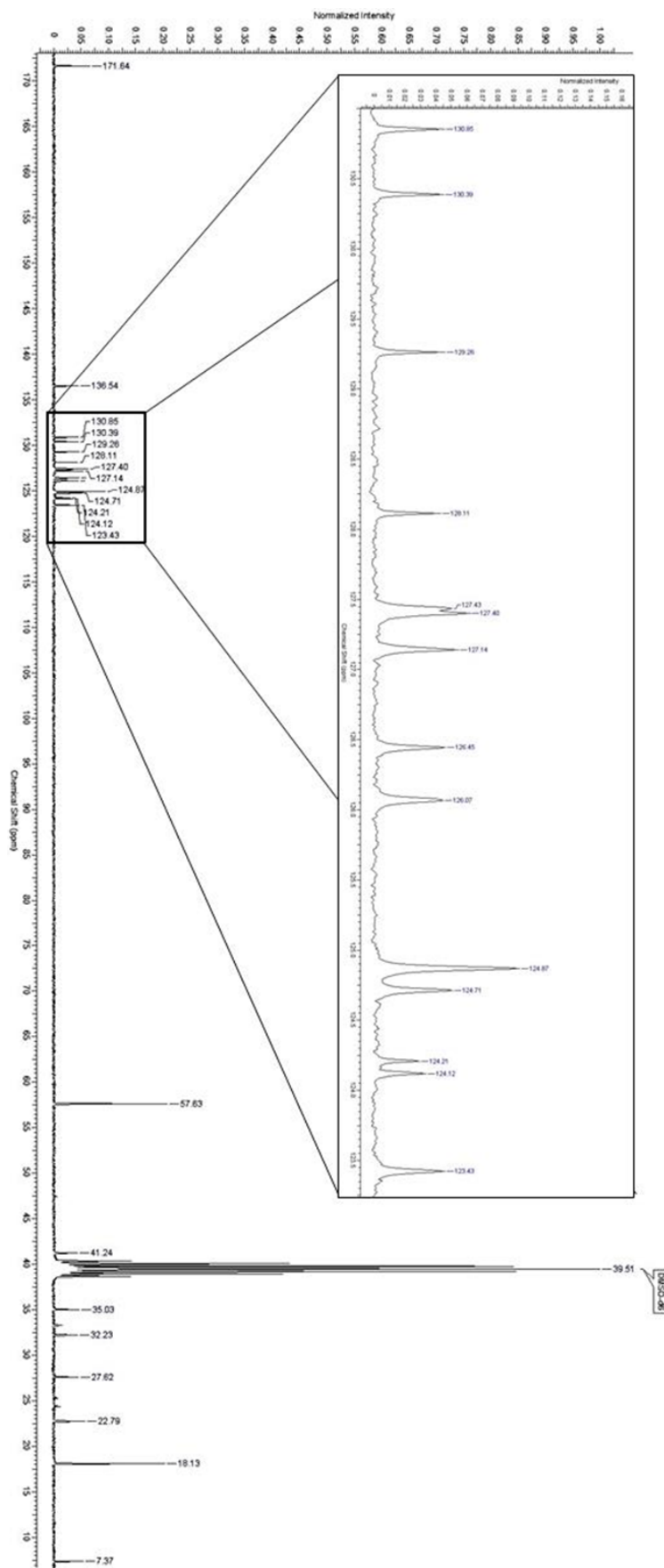
**Figure 83**. ^{13}C NMR spectra of 1.
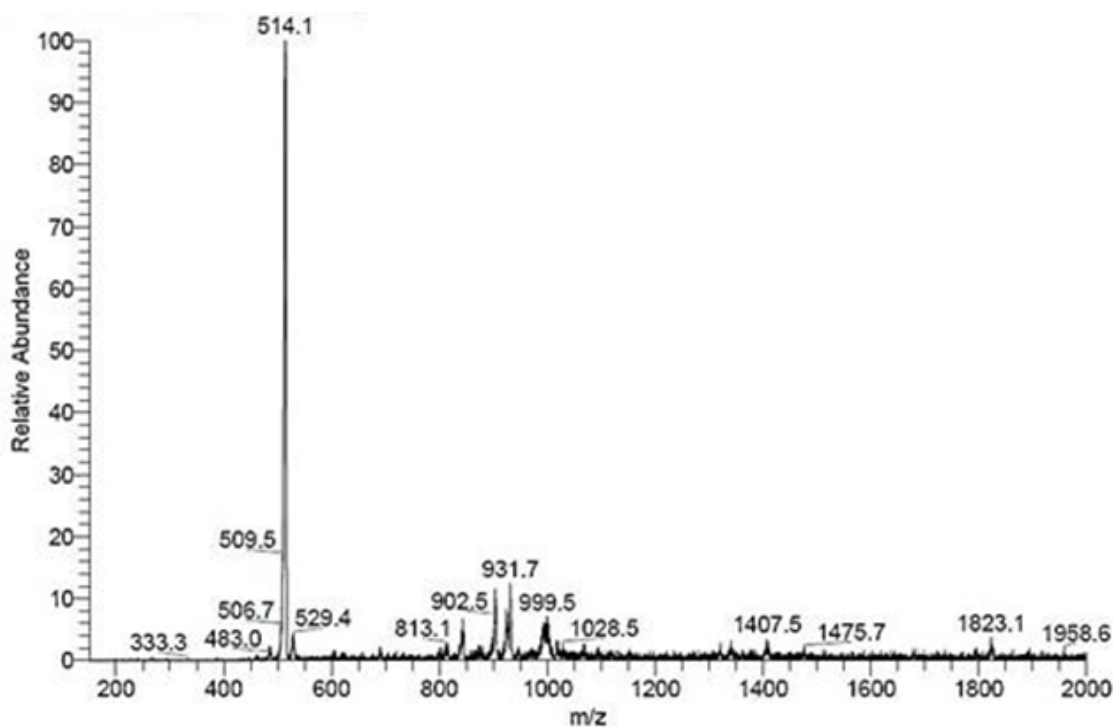
**Figure 84**. ESI mass chromatogram of the pyrene silane derivative **1**.
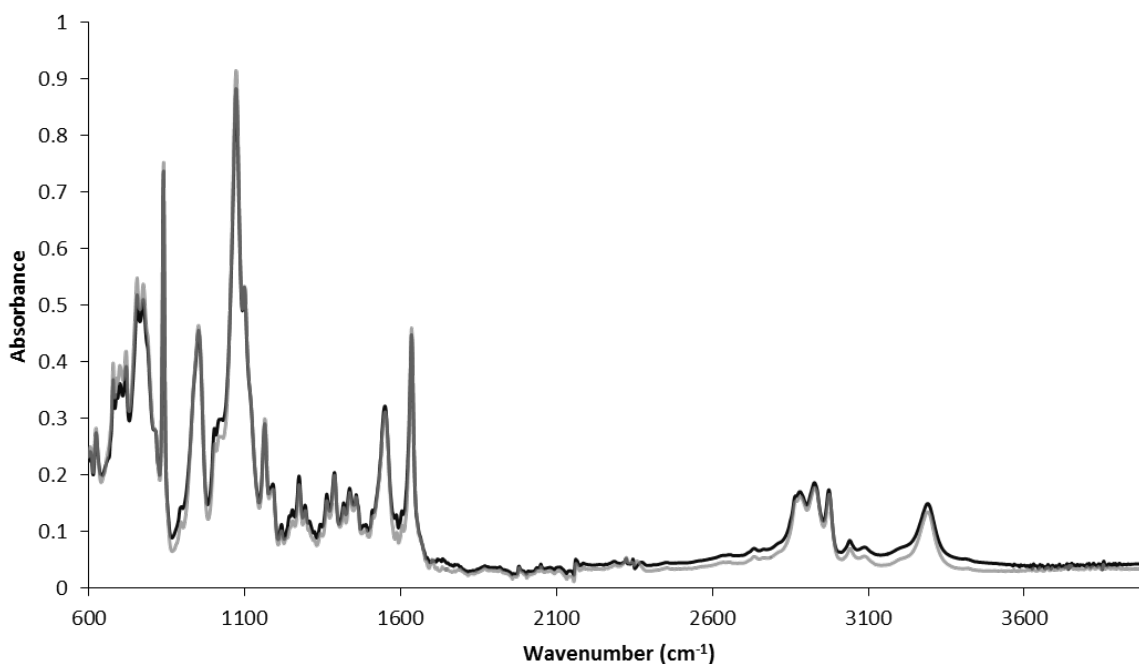


**Figure 85**. FTIR spectrum of powder of **1** (black line) and supramolecular rods of 1 (grey line). Both spectra from monomers and rods are superimposed on the graph, no differences were observed. Vibration bands of the main peaks: Si-O 1070 cm$^{-1}$, C=C aromatic 1550 cm$^{-1}$, C=O amide 1640 cm$^{-1}$, C-H alkane 2920 cm$^{-1}$, N-H amide 3050 cm$^{-1}$, C-H aromatic 3270 cm$^{-1}$.

**Table 11**. Peak-to-valley ratio values for **1** in ethanol and in aqueous medium (ethanol 10%). The peak-to-valley ratio values were obtained by considering the ratio of the absorption corresponding to each peak to that of the adjacent trough.

| Conditions | | | | | |
|---|---|---|---|---|---|
| **Ethanol** | Peak (nm) | 264 | 274 | 326 | 340 |
| | Peak-to-valley ratio | 1.4 | 2.42 | 1.68 | 2.22 |
| **Aqueous medium (ethanol 10%)** | Peak (nm) | 268 | 280 | 332 | 350 |
| | Peak-to-valley ratio | 1.27 | 1.45 | 1.16 | 1.38 |

**Table 12**. Crystal data and structure refinement for **1** (CCDC 1483530) and unit cell parameters for **1***.

| Identification code | PySi 1 | PySi 1* |
|---|---|---|
| **Empirical formula** | $C_{29}H_{37}NO_4Si$ | $C_{29}H_{37}NO_4Si$ |
| **Formula weight** | 491.68 | 491.68 |
| **Temperature/K** | 100(2) | 100(2) |
| **Crystal system** | monoclinic | monoclinic |
| **Space group** | Pc | Pc |
| **a/Å** | 19.1439(7) | 19.1717(18) |
| **b/Å** | 9.6535(3) | 9.6578(6) |
| **c/Å** | 30.1293(10) | 30.180(3) |
| **α/°** | 90 | 90 |
| **β/°** | 107.678(2) | 107.482(10) |
| **γ/°** | 90 | 90 |
| **Volume/Å$^3$** | 5305.1(3) | - |
| **Z** | 8 | - |
| **$\rho_{calc}$g/cm$^3$** | 1.231 | - |
| **μ/mm$^{-1}$** | 0.153 | - |
| **F(000)** | 2112.0 | - |
| **Crystal size/mm$^3$** | 0.3 × 0.05 × 0.02 | - |
| **Radiation** | Synchrotron (λ = 0.7749) | - |
| **2Θ range for data collection/°** | 4.48 to 51.166 | - |
| **Index ranges** | -21 ≤ h ≤ 21, -10 ≤ k ≤ 10, -33 ≤ l ≤ 33 | - |
| **Reflections collected** | 36515 | - |
| **Independent reflections** | 15242 [$R_{int}$ = 0.0503, $R_{sigma}$ = 0.0604] | - |
| **Data/restraints/parameters** | 15242/62/1102 | - |
| **Goodness-of-fit on F$^2$** | 1.034 | - |
| **Final R indexes [I>=2σ (I)]** | $R_1$ = 0.0975, $wR_2$ = 0.2590 | - |
| **Final R indexes [all data]** | $R_1$ = 0.1186, $wR_2$ = 0.2765 | - |
| **Largest diff. peak/hole / e Å$^{-3}$** | 0.83/-0.85 | - |
| **Flack parameter** | 0.60(6) | - |

# 3. Smart Gates Particles
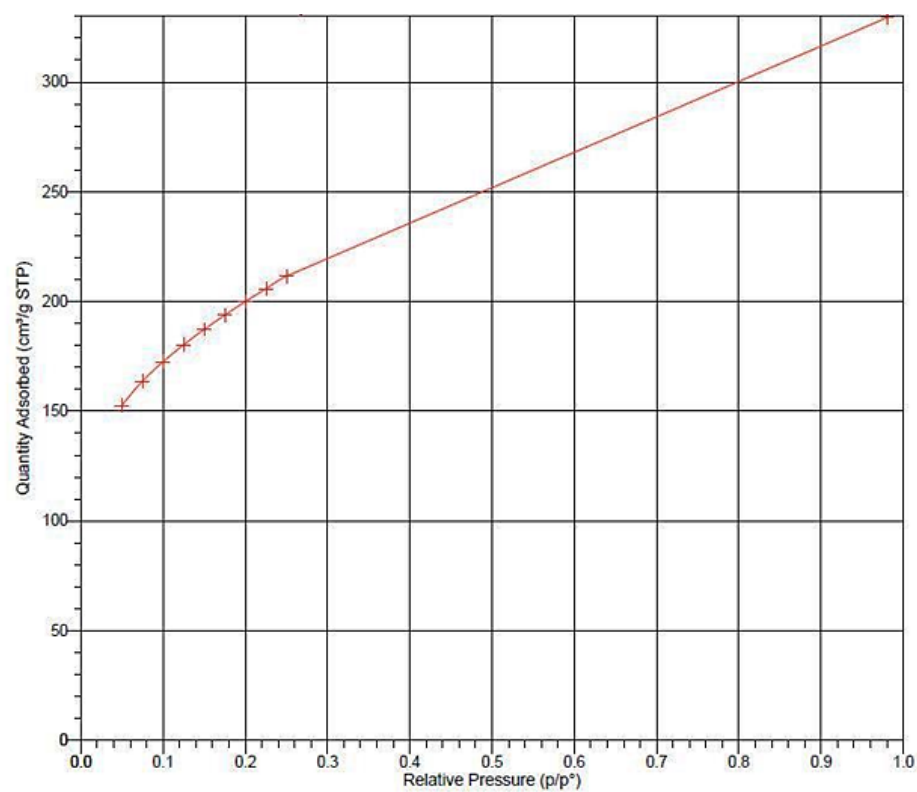


**Figure 86**. BET isotherm linear plot of the mesoporous particles.

# References

[1]     M. Tyagi, M. M. R. da Fonseca, C. C. C. R. de Carvalho, Bioaugmentation and biostimulation strategies to improve the effectiveness of bioremediation processes, *Biodegradation* **2011**, *22*, 231-241.

[2]     L. Pauling, The nature of the chemical bond. Application of results obtained from the quantum mechanics and from a theory of paramagnetic susceptibility to the structure of molecules, *J. Am. Chem. Soc.* **1931**, *53*, 1367-1400.

[3]     J.-M. Lehn, Supramolecular chemistry. Scope and perspectives molecules, supermolecules, and molecular Devices (Nobel lecture), *Angew. Chem., Int. Ed.* **1988**, *27*, 89-112.

[4]     R. M. Izatt, Charles J. Pedersen: Innovator in macrocyclic chemistry and co-recipient of the 1987 Nobel Prize in chemistry, *Chem. Soc. Rev.* **2007**, *36*, 143-147.

[5]     D. J. Cram, J. M. Cram, Host-guest chemistry: complexes between organic compounds simulate the substrate selectivity of enzymes, *Science* **1974**, *183*, 803-809.

[6]     J.-M. Lehn, Cryptates: the chemistry of macropolycyclic inclusion complexes, *Acc. Chem. Res.* **1978**, *11*, 49-57.

[7]     J.-M. Lehn, Supramolecular chemistry: receptors, catalysts, and carriers, *Science* **1985**, *227*, 849-856.

[8]     E. Fischer, Einfluss der Configuration auf die Wirkung der Enzyme, *Chem. Ber.* **1894**, *27*, 2985-2993.

[9]     L. Chen, X. Wang, W. Lu, X. Wu, J. Li, Molecular imprinting: perspectives and applications, *Chem. Soc. Rev.* **2016**, *45*, 2137-2211.

[10]    D. E. Koshland, The key-lock theory and the induced fit theory, *Angew. Chem., Int. Ed.* **1995**, *33*, 2375-2378.

[11]    J. F. Stoddart, The chemistry of the mechanical bond, *Chem. Soc. Rev.* **2009**, *38*, 1802-1820.

[12]    G. W. Gokel, W. M. Leevy, M. E. Weber, Crown ethers: sensors for ions and molecular scaffolds for materials and biological models, *Chem. Rev.* **2004**, *104*, 2723-2750.

[13]    D. J. Cram, M. E. Tanner, R. Thomas, The taming of cyclobutadiene, *Angew. Chem., Int. Ed.* **1991**, *30*, 1024-1027.

Mohamed EL IDRISSI

[14] D.-H. Qu, Q.-C. Wang, Q.-W. Zhang, X. Ma, H. Tian, Photoresponsive host–guest functional systems, *Chem. Rev.* **2015**, *115*, 7543-7588.

[15] C. Talotta, C. Gaeta, A. Soriente, M. De Rosa, C. Geraci, P. Neri, Large calixarenes in *Calixarenes and Beyond* (Eds.: P. Neri, J. L. Sessler, M.-X. Wang), Springer International Publishing, Cham, **2016**, 141-173.

[16] P. Thuéry, M. Nierlich, É. Lamare, J.-F. Dozol, Z. Asfari, J. Vicens, Bis(crown ether) and azobenzocrown derivatives of calix[4]arene. A review of structural information from crystallographic and modelling studies, *J. Inclusion Phenom. Macrocyclic Chem.* **2000**, *36*, 375-408.

[17] J. Szejtli, Introduction and general overview of cyclodextrin chemistry, *Chem. Rev.* **1998**, *98*, 1743-1754.

[18] G. Crini, Review: a history of cyclodextrins, *Chem. Rev.* **2014**, *114*, 10940-10975.

[19] A. L. Thakkar, P. V. Demarco, Cycloheptaamylose inclusion complexes of barbiturates: correlation between proton magnetic resonance and solubility studies, *J. Pharm. Sci.* **1971**, *60*, 652-653.

[20] D. C. Rideout, R. Breslow, Hydrophobic acceleration of Diels-Alder reactions, *J. Am. Chem. Soc.* **1980**, *102*, 7816-7817.

[21] K. Takahashi, Organic reactions mediated by cyclodextrins, *Chem. Rev.* **1998**, *98*, 2013-2034.

[22] C. Rest, R. Kandanelli, G. Fernandez, Strategies to create hierarchical self-assembled structures via cooperative non-covalent interactions, *Chem. Soc. Rev.* **2015**, *44*, 2543-2572.

[23] A. C. Mendes, E. T. Baran, R. L. Reis, H. S. Azevedo, Self-assembly in nature: using the principles of nature to create complex nanobiomaterials, *Wiley Interdiscip. Rev. Nanomed.* **2013**, *5*, 582-612.

[24] E. Buxbaum, *Fundamentals of Protein Structure and Function*, 2 ed., Springer International Publishing, Cham, **2015**.

[25] T. F. A. De Greef, M. M. J. Smulders, M. Wolffs, A. P. H. J. Schenning, R. P. Sijbesma, E. W. Meijer, Supramolecular Polymerization, *Chem. Rev.* **2009**, *109*, 5687-5754.

[26] P. Jonkheijm, P. van der Schoot, A. P. H. J. Schenning, E. W. Meijer, Probing the solvent-assisted nucleation pathway in chemical self-assembly, *Science* **2006**, *313*, 80-83.

[27]  W. L. Noorduin, A. Grinthal, L. Mahadevan, J. Aizenberg, Rationally designed complex, hierarchical microarchitectures, *Science* **2013**, *340*, 832-837.

[28]  E. Griffiths Kirsten, J. F. Stoddart, Template-directed synthesis of donor/acceptor [2]catenanes and [2]rotaxanes, *Pure Appl. Chem.* **2008**, *80*, 485-506.

[29]  E. Wasserman, The preparation of interlocking rings: a catenane[1], *J. Am. Chem. Soc.* **1960**, *82*, 4433-4434.

[30]  H. L. Frisch, E. Wasserman, Chemical topology[1], *J. Am. Chem. Soc.* **1961**, *83*, 3789-3795.

[31]  G. Schill, A. Lüttringhaus, The preparation of catena compounds by directed synthesis, *Angew. Chem., Int. Ed.* **1964**, *3*, 546-547.

[32]  I. T. Harrison, S. Harrison, Synthesis of a stable complex of a macrocycle and a threaded chain, *J. Am. Chem. Soc.* **1967**, *89*, 5723-5724.

[33]  T. J. Hubin, D. H. Busch, Template routes to interlocked molecular structures and orderly molecular entanglements, *Coord. Chem. Rev.* **2000**, *200*, 5-52.

[34]  C. O. Dietrich-Buchecker, J. P. Sauvage, J. P. Kintzinger, Une nouvelle famille de molecules : les metallo-catenanes, *Tetrahedron Lett.* **1983**, *24*, 5095-5098.

[35]  M. J. Whitcombe, N. Kirsch, I. A. Nicholls, Molecular imprinting science and technology: a survey of the literature for the years 2004–2011, *J. Mol. Recognit.* **2014**, *27*, 297-401.

[36]  C. Alexander, H. S. Andersson, L. I. Andersson, R. J. Ansell, N. Kirsch, I. A. Nicholls, J. O'Mahony, M. J. Whitcombe, Molecular imprinting science and technology: a survey of the literature for the years up to and including 2003, *J. Mol. Recognit.* **2006**, *19*, 106-180.

[37]  M. Polyakov, Adsorption properties and structure of silica gel, *Zhur. Fiz. Khim.* **1931**, *2*, 799-805.

[38]  J. E. Lofgreen, G. A. Ozin, Controlling morphology and porosity to improve performance of molecularly imprinted sol-gel silica, *Chem. Soc. Rev.* **2014**, *43*, 911-933.

[39]  A. Cumbo, B. Lorber, P. F. X. Corvini, W. Meier, P. Shahgaldian, A synthetic nanomaterial for virus recognition produced by surface imprinting, *Nat. commun.* **2013**, *4*, 1503.

[40]  A. Villiers, *Compt. Rend. Fr. Acad. Sci.* **1891**, *112*, 435-438.

[41]    H. Pringsheim, Twenty-five years of biochemistry, *Science* **1928**, *68*, 603-608.

[42]    H. Pringsheim, *A comprehensive survey of starch chemistry*, The Chemical Catalog Co., New York, **1928**.

[43]    K. Freudenberg, G. Blomquist, L. Ewald, K. Soff, Hydrolysis and acetolysis of starch and of the Schardinger dextrins, *Ber. Dtsch. Chem. Ges.* **1936**, *69*, 1258-1266.

[44]    D. French, R. E. Rundle, The molecular weights of the Schardinger alpha and beta dextrins[1], *J. Am. Chem. Soc.* **1942**, *64*, 1651-1653.

[45]    F. Cramer, *Einschlussverbindungen*, Springer, Heidelberg, **1954**.

[46]    T. Loftsson, D. Duchene, Cyclodextrins and their pharmaceutical applications, *Int. J. Pharm.* **2007**, *329*, 1-11.

[47]    G. Schmid, Preparation and industrial production of cyclodextrins in *Comprehensive supramolecular chemistry* (Eds.: J. L. Atwood, J. E. D. Davies, D. D. MacNicol, F. Vögtle), Pergamon, Oxford, **1996**, 41-56.

[48]    A. Biwer, G. Antranikian, E. Heinzle, Enzymatic production of cyclodextrins, *Appl. Microbiol. Biotechnol.* **2002**, *59*, 609-617.

[49]    S. Kobayashi, Cyclodextrin producing enzyme (CGTase), *Biotechnol. Prog.* **1996**, *12*, 23-41.

[50]    H. Bender, Production, characterization, and application of cyclodextrins, *Adv. Biotechnol. Proc.* **1986**, *6*, 31-71.

[51]    F. Shiraishi, K. Kawakami, H. Marushima, K. Kusunoki, Effect of ethanol on formation of cyclodextrin from soluble starch by bacillus macerans cyclodextrin glucanotransferase, *Starch /Stärke* **1989**, *41*, 151-155.

[52]    G. Schmid, Preparation and industrial production of cyclodextrins in *Comprehensive supermolecular chemistry*, Pergamon, Oxford, **1996**, 41-56.

[53]    A. Hedges, Cyclodextrin: production, properties, and applications in *Starch Hydrolysis Products* (Eds.: Fred W. Schenck, R. E. Hebeda), VCH Publishers, New York, **1992**, 319-333.

[54]    Y. Xiao, S. C. Ng, T. T. Y. Tan, Y. Wang, Recent development of cyclodextrin chiral stationary phases and their applications in chromatography, *J. Chromatogr. A* **2012**, *1269*, 52-68.

[55] J. Mosinger, V. Tomankova, I. Nemcova, J. Zyka, Cyclodextrins in analytical chemistry, *Anal. Lett.* **2001**, *34*, 1979-2004.

[56] E. Schneiderman, A. M. Stalcup, Cyclodextrins: a versatile tool in separation science, *J. Chromatogr. B* **2000**, *745*, 83-102.

[57] H. Nishi, Enantioselectivity in chiral capillary electrophoresis with polysaccharides, *J. Chromatogr. A* **1997**, *792*, 327-347.

[58] F. Bressolle, M. Audran, T. N. Pham, J. J. Vallon, Cyclodextrins and enantiomeric separations of drugs by liquid chromatography and capillary electrophoresis: Basic principles and new developments, *J. Chromatogr. B* **1996**, *687*, 303-336.

[59] P. Shahgaldian, U. Pieles, Cyclodextrin derivatives as chiral supramolecular receptors for enantioselective sensing, *Sensors* **2006**, *6*, 593-615.

[60] K. A. Connors, The stability of cyclodextrin complexes in solution, *Chem. Rev.* **1997**, *97*, 1325-1357.

[61] K. Harata, Crystallographic studies in *Cyclodextrins, Vol. 3* (Eds.: J. L. Atwood, J. E. D. Davies, D. D. MacNicol, F. Vögtle), Pergamon, Oxford, **1996**, 279-304.

[62] H.-J. Schneider, F. Hacket, V. Ruediger, H. Ikeda, NMR studies of cyclodextrins and cyclodextrin complexes, *Chem. Rev.* **1998**, *98*, 1755-1786.

[63] J. García, L. Martins, M. Pons, NMR spectroscopy in solution in *Supramolecular chemistry: from molecules to nanomaterials, Vol. 2* (Eds.: P. A. Gale, J. W. Steed), John Wiley & sons, Chichester, **2013**, 863.

[64] R. Singh, N. Bharti, J. Madan, S. N. Hiremath, Characterization of cyclodextrin inclusion complexes, *J. Pharm. Sci. Technol.* **2010**, *2*, 171-183.

[65] T. Loftsson, M. E. Brewster, Pharmaceutical applications of cyclodextrins: basic science and product development, *J. Pharm. Pharmacol.* **2010**, *62*, 1607-1621.

[66] T. Loftsson, Cyclodextrins and the biopharmaceutics classification system of drugs, *J. Incl. Phenom. Macrocyclic Chem.* **2002**, *44*, 63-67.

[67] A. Harada, R. Kobayashi, Y. Takashima, A. Hashidzume, H. Yamaguchi, Macroscopic self-assembly through molecular recognition, *Nat. Chem.* **2011**, *3*, 34-37.

Mohamed EL IDRISSI

[68]     A. Harada, Y. Takashima, H. Yamaguchi, Cyclodextrin-based supramolecular polymers, *Chem. Soc. Rev.* **2009**, *38*, 875-882.

[69]     A. Harada, L. Jun, K. Mikiharu, Synthesis of a tubular polymer from threaded cyclodextrins, *Nature* **1993**, *364*, 516-518.

[70]     M. Munteanu, S. Choi, H. Ritter, Cyclodextrin methacrylate via microwave-assisted click reaction, *Macromolecules* **2008**, *41*, 9619-9623.

[71]     S. Tamesue, Y. Takashima, H. Yamaguchi, S. Shinkai, A. Harada, Photoswitchable supramolecular hydrogels formed by cyclodextrins and azobenzene polymers, *Angew. Chem. Int. Ed.* **2010**, *49*, 7461-7464.

[72]     J. Solms, R. H. Egli, Harze mit Einschlusshohlräumen von Cyclodextrin-Struktur, *Helv. Chim. Acta* **1965**, *48*, 1225-1228.

[73]     F. van de Manakker, T. Vermonden, C. F. van Nostrum, W. E. Hennink, Cyclodextrin-based polymeric materials: synthesis, properties, and pharmaceutical/biomedical applications, *Biomacromolecules* **2009**, *10*, 3157-3175.

[74]     J. W. Zhou, H. Ritter, Cyclodextrin functionalized polymers as drug delivery systems, *Polym. Chem.* **2010**, *1*, 1552-1559.

[75]     P. Xiao, Y. Dudal, P. F. X. Corvini, U. Pieles, P. Shahgaldian, Cyclodextrin-based polyurethanes act as selective molecular recognition materials of active pharmaceutical ingredients (APIs), *Polym. Chem.* **2011**, *2*, 1264-1266.

[76]     P. Xiao, P. F. X. Corvini, Y. Dudal, P. Shahgaldian, Design and high-throughput synthesis of cyclodextrin-based polyurethanes with enhanced molecular recognition properties, *Polym. Chem.* **2013**, *4*, 942-946.

[77]     M. J. Kettel, F. Dierkes, K. Schaefer, M. Moeller, A. Pich, Aqueous nanogels modified with cyclodextrin, *Polymer* **2011**, *52*, 1917-1924.

[78]     P. Xiao, P. Corvini, Y. Dudal, P. Shahgaldian, Design of cyclodextrin-based photopolymers with enhanced molecular recognition properties: a template-free high-throughput Approach, *Macromolecules* **2012**, *45*, 5692-5697.

[79]     M. E. Davis, M. E. Brewster, Cyclodextrin-based pharmaceutics: past, present and future, *Nat. Rev. Drug Discov.* **2004**, *3*, 1023-1035.

[80]     P. Mura, M. T. Faucci, F. Maestrelli, S. Furlanetto, S. Pinzauti, Characterization of physicochemical properties of naproxen systems with amorphous β-cyclodextrin-epichlorohydrin polymers, *J. Pharm. Biomed. Anal.* **2002**, *29*, 1015-1024.

[81]     C. Rodriguez-Tenreiro, C. Alvarez-Lorenzo, A. Rodriguez-Perez, A. Concheiro, J. J. Torres-Labandeira, Estradiol sustained release from high affinity cyclodextrin hydrogels, *Eur. J. Pharm. Biopharm.* **2007**, *66*, 55-62.

[82]     J. J. Cheng, K. T. Khin, G. S. Jensen, A. J. Liu, M. E. Davis, Synthesis of linear, beta-cyclodextrin-based polymers and their camptothecin conjugates, *Bioconjugate Chem.* **2003**, *14*, 1007-1017.

[83]     J. Cheng, K. T. Khin, M. E. Davis, Antitumor activity of beta-cyclodextrin polymer-camptothecin conjugates, *Mol. Pharm.* **2004**, *1*, 183-193.

[84]     C. S. Su, C. P. Yang, Partial removal of various food components from aqueous-solution using cross-linked polymers of cyclodextrins with epichlorohydrin, *J. Sci. Food. Agric.* **1991**, *54*, 635-643.

[85]     M. Appell, M. A. Jackson, Sorption of ochratoxin A from aqueous solutions using beta-cyclodextrin polyurethane polymer, *Toxins* **2012**, *4*, 98-109.

[86]     A. Binello, B. Robaldo, A. Barge, R. Cavalli, G. Cravotto, Synthesis of cyclodextrin-based polymers and their use as debittering agents, *J. App. Polym. Sci.* **2008**, *107*, 2549-2557.

[87]     Z. T. Jiang, R. Li, J. C. Zhang, Determination of cobalt in foods using beta-cyclodextrin epichlorohydrin polymer functionalized with 1-(2-pyridylazo)-2-naphthol, *J. Food Drug Anal.* **2004**, *12*, 183-188.

[88]     N. Morin-Crini, G. Crini, Environmental applications of water-insoluble beta-cyclodextrin-epichlorohydrin polymers, *Prog. Polym. Sci.* **2013**, *38*, 344-368.

[89]     D. Bonenfant, P. Niquette, M. Mimeault, R. Hausler, Adsorption and recovery of nonylphenol ethoxylate on a crosslinked beta-cyclodextrin-carboxymethylcellulose polymer, *Water Sci. Technol.* **2010**, *61*, 2293-2301.

[90]     M. H. Mohamed, L. D. Wilson, D. Y. Pratt, R. Guo, C. Wu, J. V. Headley, Evaluation of the accessible inclusion sites in copolymer materials containing beta-cyclodextrin, *Carbohyd. Polym.* **2012**, *87*, 1241-1248.

[91]     Z. J. Yang, K. G. Chai, H. B. Ji, Selective inclusion and separation of cinnamaldehyde and benzaldehyde by insoluble beta-cyclodextrin polymer, *Sep. Purif. Technol.* **2011**, *80*, 209-216.

[92]     N. Li, X. L. Xiong, S. M. Chen, Studies on adsorption behaviors of aniline onto gamma-cyclodextrin polymer, *Prog. Envi. Sci. Technol.* **2009**, 1331-1336.

[93]     X. M. Zhang, C. S. Peng, G. C. Xu, Synthesis of modified beta-cyclodextrin polymers and characterization of their fuchsin adsorption, *J. Incl. Phenom. Macrocyclic Chem.* **2012**, *72*, 165-171.

[94]     K. Materna, J. Szymanowski, Separation of phenols from aqueous micellar solutions by cloud point extraction, *J. Colloid Interface Sci.* **2002**, *255*, 195-201.

[95]     R. Orprecio, C. H. Evans, Polymer-immobilized cyclodextrin trapping of model organic pollutants in flowing water streams, *J. Appl. Polym. Sci.* **2003**, *90*, 2103-2110.

[96]     J.-Y. Moon, H.-J. Jung, M. H. Moon, B. C. Chung, M. H. Choi, Inclusion complex-based solid-phase extraction of steroidal compounds with entrapped β-cyclodextrin polymer, *Steroids* **2008**, *73*, 1090-1097.

[97]     B. Sancey, G. Trunfio, J. Charles, P. M. Badot, G. Crini, Sorption onto crosslinked cyclodextrin polymers for industrial pollutants removal: an interesting environmental approach, *J. Incl. Phenom. Macrocyclic Chem.* **2011**, *70*, 315-320.

[98]     K. E. Riley, P. Hobza, On the importance and origin of aromatic interactions in chemistry and biodisciplines, *Acc. Chem. Res.* **2013**, *46*, 927-936.

[99]     R. Marty, R. Nigon, D. Leite, H. Frauenrath, Two-fold odd-even effect in self-assembled nanowires from oligopeptide-polymer-substituted perylene bisimides, *J. Am. Chem. Soc.* **2014**, *136*, 3919-3927.

[100]   Y. Chen, B. Zhu, F. Zhang, Y. Han, Z. Bo, Hierarchical supramolecular self-assembly of nanotubes and layered sheets, *Angew. Chem., Int. Ed.* **2008**, *47*, 6015-6018.

[101]   I. Radivojevic, I. Likhtina, X. Shi, S. Singh, C. M. Drain, Self-organized nanofibers and nanorods of porphyrins bearing hydrogen bonding motifs, *Chem. Commun.* **2010**, *46*, 1643-1645.

[102]   F. Würthner, Dipole-dipole interaction driven self-assembly of merocyanine dyes: from dimers to nanoscale objects and supramolecular materials, *Acc. Chem. Res.* **2016**, *49*, 868-876.

[103]   S. Fleming, R. V. Ulijn, Design of nanostructures based on aromatic peptide amphiphiles, *Chem. Soc. Rev.* **2014**, *43*, 8150-8177.

[104] F. J. M. Hoeben, M. Wolffs, J. Zhang, S. De Feyter, P. Leclère, A. P. H. J. Schenning, E. W. Meijer, Influence of supramolecular organization on energy transfer properties in chiral oligo(p-phenylene vinylene) porphyrin assemblies, *J. Am. Chem. Soc.* **2007**, *129*, 9819-9828.

[105] M. Vybornyi, A. V. Rudnev, S. M. Langenegger, T. Wandlowski, G. Calzaferri, R. Haner, Formation of two-dimensional supramolecular polymers by amphiphilic pyrene oligomers, *Angew. Chem., Int. Ed.* **2013**, *52*, 11488-11493.

[106] A. L. Nussbaumer, D. Studer, V. L. Malinovskii, R. Häner, Amplification of chirality by supramolecular polymerization of pyrene oligomers, *Angew. Chem., Int. Ed.* **2011**, *50*, 5490-5494.

[107] A. V. Rudnev, V. L. Malinovskii, A. L. Nussbaumer, A. Mishchenko, R. Häner, T. Wandlowski, Cooperative and noncooperative assembly of oligopyrenotides resolved by atomic force microscopy, *Macromolecules* **2012**, *45*, 5986-5992.

[108] F. Helmich, C. C. Lee, M. M. L. Nieuwenhuizen, J. C. Gielen, P. C. M. Christianen, A. Larsen, G. Fytas, P. E. L. G. Leclère, A. P. H. J. Schenning, E. W. Meijer, Dilution-induced self-assembly of porphyrin aggregates: a consequence of coupled equilibria, *Angew. Chem., Int. Ed.* **2010**, *49*, 3939-3942.

[109] E. Moulin, F. Niess, M. Maaloum, E. Buhler, I. Nyrkova, N. Giuseppone, The hierarchical self-assembly of charge nanocarriers: a highly cooperative process promoted by visible light, *Angew. Chem., Int. Ed.* **2010**, *49*, 6974-6978.

[110] Z. Wang, H. Möhwald, C. Gao, Nanotubes protruding from poly(allylamine hydrochloride)-graft-pyrene microcapsules, *ACS Nano* **2011**, *5*, 3930-3936.

[111] H. Wang, W. Zhang, C. Gao, Shape transformation of light-responsive pyrene-containing micelles and their influence on cytoviability, *Biomacromolecules* **2015**, *16*, 2276-2281.

[112] E. E. Jelley, Spectral Absorption and Fluorescence of Dyes in the Molecular State, *Nature* **1936**, *138*, 1009-1010.

[113] F. Würthner, T. E. Kaiser, C. R. Saha-Möller, J-aggregates: from serendipitous discovery to supramolecular engineering of functional dye materials, *Angew. Chem., Int. Ed.* **2011**, *50*, 3376-3410.

[114] F. Würthner, C. Bauer, V. Stepanenko, S. Yagai, A black perylene bisimide super gelator with an unexpected J-type absorption band, *Adv. Mater.* **2008**, *20*, 1695-1698.

[115]   S. Ghosh, X.-Q. Li, V. Stepanenko, F. Würthner, Control of H- and J-type π stacking by peripheral alkyl chains and self-sorting phenomena in perylene bisimide homo and heteroaggregates, *Chem. Eur. J.* **2008**, *14*, 11343-11357.

[116]   B. Jancy, S. K. Asha, Hydrogen-bonding-induced conformational change from J to H aggregate in novel highly fluorescent liquid-crystalline perylenebisimides, *Chem. Mater.* **2008**, *20*, 169-181.

[117]   S. Das, P. Heasman, T. Ben, S. Qiu, Porous organic materials: strategic design and structure-function correlation, *Chem. Rev.* **2016**.

[118]   W. Li, J. Liu, D. Zhao, Mesoporous materials for energy conversion and storage devices, *Nat. Rev. Mater.* **2016**, *1*, 16023.

[119]   C. T. Kresge, M. E. Leonowicz, W. J. Roth, J. C. Vartuli, J. S. Beck, Ordered mesoporous molecular sieves synthesized by a liquid-crystal template mechanism, *Nature* **1992**, *359*, 710-712.

[120]   R. L. Burwell, Manual of symbols and terminology for physicochemical quantities and units, *Pure and Appl. chem.* **1976**, *46*, 71-90.

[121]   J. Patarin, Mild methods for removing organic templates from inorganic host materials, *Angew. Chem., Int. Ed.* **2004**, *43*, 3878-3880.

[122]   J. S. Beck, J. C. Vartuli, W. J. Roth, M. E. Leonowicz, C. T. Kresge, K. D. Schmitt, C. T. W. Chu, D. H. Olson, E. W. Sheppard, S. B. McCullen, J. B. Higgins, J. L. Schlenker, A new family of mesoporous molecular sieves prepared with liquid crystal templates, *J. Am. Chem. Soc.* **1992**, *114*, 10834-10843.

[123]   F. Di Renzo, H. Cambon, R. Dutartre, A 28-year-old synthesis of micelle-templated mesoporous silica, *Microporous Mater.* **1997**, *10*, 283-286.

[124]   F. Hoffmann, M. Cornelius, J. Morell, M. Fröba, Silica-based mesoporous organic–inorganic hybrid materials, *Angew. Chem., Int. Ed.* **2006**, *45*, 3216-3251.

[125]   Q. Huo, D. I. Margolese, U. Ciesla, P. Feng, T. E. Gier, P. Sieger, R. Leon, P. M. Petroff, F. Schuth, G. D. Stucky, Generalized synthesis of periodic surfactant/inorganic composite materials, *Nature* **1994**, *368*, 317-321.

[126]   N. K. Mal, M. Fujiwara, Y. Tanaka, Photocontrolled reversible release of guest molecules from coumarin-modified mesoporous silica, *Nature* **2003**, *421*, 350-353.

[127] M. Fujiwara, S. Terashima, Y. Endo, K. Shiokawa, H. Ohue, Switching catalytic reaction conducted in pore void of mesoporous material by redox gate control, *Chem. Commun.* **2006**, 4635-4637.

[128] C. Park, K. Lee, C. Kim, Photoresponsive cyclodextrin-covered nanocontainers and their sol-gel transition induced by molecular recognition, *Angew. Chem., Int. Ed.* **2009**, *48*, 1275-1278.

[129] J. L. Vivero-Escoto, I. I. Slowing, C.-W. Wu, V. S. Y. Lin, Photo-induced intracellular controlled release drug delivery in human cells by gold-capped mesoporous silica nanosphere, *J. Am. Chem. Soc.* **2009**, *131*, 3462-3463.

[130] E. J. Kwon, T. G. Lee, Surface-modified mesoporous silica with ferrocene derivatives and its ultrasound-triggered functionality, *Appl. Surf. Sci.* **2008**, *254*, 4732-4737.

[131] R. Hernandez, H.-R. Tseng, J. W. Wong, J. F. Stoddart, J. I. Zink, An operational supramolecular nanovalve, *J. Am. Chem. Soc.* **2004**, *126*, 3370-3371.

[132] H. Meng, M. Xue, T. Xia, Y.-L. Zhao, F. Tamanoi, J. F. Stoddart, J. I. Zink, A. E. Nel, Autonomous in vitro anticancer drug release from mesoporous silica nanoparticles by pH-sensitive nanovalves, *J. Am. Chem. Soc.* **2010**, *132*, 12690-12697.

[133] K. Patel, S. Angelos, W. R. Dichtel, A. Coskun, Y.-W. Yang, J. I. Zink, J. F. Stoddart, Enzyme-responsive snap-top covered silica nanocontainers, *J. Am. Chem. Soc.* **2008**, *130*, 2382-2383.

[134] L. Bertin, F. Ferri, A. Scoma, L. Marchetti, F. Fava, Recovery of high added value natural polyphenols from actual olive mill wastewater through solid phase extraction, *Chem. Eng. J.* **2011**, *171*, 1287-1293.

[135] M. J. M. Rusan, A. A. Albalasmeh, S. Zuraiqi, M. Bashabsheh, Evaluation of phytotoxicity effect of olive mill wastewater treated by different technologies on seed germination of barley (Hordeum vulgare L.), *Environ. Sci. Pollut. Res.* **2015**, *22*, 9127-9135.

[136] A. Mekki, A. Dhouib, S. Sayadi, Polyphenols dynamics and phytotoxicity in a soil amended by olive mill wastewaters, *J. Environ. Manage.* **2007**, *84*, 134-140.

[137] M. El Idrissi, A. Molina, D. Frascari, P. F.-X. Corvini, P. Shahgaldian, Cyclodextrin-based polymeric materials for the specific recovery of polyphenolic compounds through supramolecular host-guest interactions, *J. Incl. Phenom. Macrocycl. Chem.* **2017**, (In Press).

[138] M. R. Meneghetti, S. M. P. Meneghetti, Sn(iv)-based organometallics as catalysts for the production of fatty acid alkyl esters, *Catal. Sci. Technol.* **2015**, *5*, 765-771.

[139] P. Changenet-Barret, A. Espagne, S. Charier, J. B. Baudin, L. Jullien, P. Plaza, K. J. Hellingwerf, M. M. Martin, Early molecular events in the photoactive yellow protein: role of the chromophore photophysics, *Catal. Sci. Technol.* **2004**, *3*, 823-829.

[140] P. T. Lee, J. C. Harfield, A. Crossley, B. S. Pilgrim, R. G. Compton, Significant changes in pKa between bulk aqueous solution and surface immobilized species: ortho-hydroquinones, *RSC Adv.* **2013**, *3*, 7347-7354.

[141] B. Kamm, Introduction of biomass and biorefineries in *The role of green chemistry in biomass procesing and conversion* (Eds.: H. Xie, N. Gathergood), Wiley, Hoboken, **2013**, 1-26.

[142] L. Bertin, F. Ferri, A. Scoma, L. Marchetti, F. Fava, Recovery of high added value natural polyphenols from actual olive mill wastewater through solid phase extraction, *Chem. Eng. J.* **2011**, *171*, 1287-1293.

[143] M. El Idrissi, S. J. Teat, P. F. X. Corvini, M. J. Paterson, S. J. Dalgarno, P. Shahgaldian, Template-free hierarchical self-assembly of a pyrene derivative into supramolecular nanorods, *Chem. Commun.* **2017**, 1973 - 1976.

[144] P. A. Gale, J. W. Steed, *Self-assembly and supramolecular devices*, Wiley-VCH, Chichester, **2012**.

[145] L. Cademartiri, K. J. M. Bishop, Programmable self-assembly, *Nat. Mater.* **2015**, *14*, 2-9.

[146] J.-M. Lehn, Toward complex matter: supramolecular chemistry and self-organization, *Proc. Natl. Acad. Sci. U.S.A.* **2002**, *99*, 4763-4768.

[147] H. Siu, J. Duhamel, Molar absorption coefficient of pyrene aggregates in water, *J. Phys. Chem. B* **2008**, *112*, 15301-15312.

[148] Y. Shiki, G. Yusaku, L. Xu, K. Takashi, K. Akihide, K. Daiki, Y. Hiroko, K. Yoshihiro, S. Akinori, S. Shu, Self-organization of hydrogen-bonding naphthalene chromophores into J-type nanorings and H-type nanorods: impact of regioisomerism, *Angew. Chem., Int. Ed.* **2012**, *51*, 6643-6647.

[149] T. Förster, Excimers, *Angew. Chem., Int. Ed.* **1969**, *8*, 333-343.

[150] L. Gai, H. Chen, B. Zou, H. Lu, G. Lai, Z. Li, Z. Shen, Ratiometric fluorescence chemodosimeters for fluoride anion based on pyrene excimer/monomer transformation, *Chem. Commun.* **2012**, *48*, 10721-10723.

[151]  Z. Xu, N. J. Singh, J. Lim, J. Pan, H. N. Kim, S. Park, K. S. Kim, J. Yoon, Unique sandwich stacking of pyrene-adenine-pyrene for selective and ratiometric fluorescent sensing of ATP at physiological pH, *J. Am. Chem. Soc.* **2009**, *131*, 15528-15533.

[152]  Z. An, C. Zheng, Y. Tao, R. Chen, H. Shi, T. Chen, Z. Wang, H. Li, R. Deng, X. Liu, W. Huang, Stabilizing triplet excited states for ultralong organic phosphorescence, *Nat. Mater.* **2015**, *14*, 685-690.

[153]  M. Nikolopoulou, N. Kalogerakis, Biostimulation strategies for fresh and chronically polluted marine environments with petroleum hydrocarbons, *J. Chem. Technol. Biotechnol.* **2009**, *84*, 802-807.

[154]  S. Huh, J. W. Wiench, J.-C. Yoo, M. Pruski, V. S. Y. Lin, Organic functionalization and morphology control of mesoporous silicas via a co-condensation synthesis method, *Chem. Mater.* **2003**, *15*, 4247-4256.

[155]  P. Horcajada, A. Rámila, J. Pérez-Pariente, R. Vallet, amp, x, M., Influence of pore size of MCM-41 matrices on drug delivery rate, *Microporous Mesoporous Mater.* **2004**, *68*, 105-109.

[156]  Z. Liu, Y. Wei, Y. Qi, S. Zhang, Y. Zhang, Z. Liu, Synthesis of MCM-41 type materials with remarkable hydrothermal stability from UTM-1, *Microporous Mesoporous Mater.* **2006**, *93*, 205-211.

# Curriculum Vitae

# Mohamed EL IDRISSI

Klingentalstrasse 87, 4057 Basel
mohamed.elidrissi@unibas.ch

## EDUCATION

| | |
|---|---|
| **Nov. 2012 – Feb. 2017** | PhD thesis in nanosciences, chemistry, **FHNW/University of Basel**, (Muttenz-Basel) |
| **Sept. 2011- July 2012** | Master *Sciences et technologies*, speciality molecular chemistry, **Université Pierre et Marie Curie**, (Paris) |
| **Sept. 2010 - July. 2011** | Master *Sciences et technologies,* **University of Bristol**, (Bristol) |
| **Sept. 2007 - June. 2010** | Bachelor *Sciences, Technologie, Sante Mention Chimie et procédés*, **Université Grenoble 1**, (Grenoble) |

## PROFESSIONAL EXPERIENCE

| | |
|---|---|
| **Nov. 2012 - Feb. 2017** | PhD thesis in nanochemistry *"Design of supramolecular nanomaterials"* **FHNW/University of Basel**, (Muttenz-Basel) |
| **Jan. 2011- June 2012** | Internship *"Synthesis of pillararene like structure from cyclodextrin unit block"*, **Université Pierre et Marie Curie**, (Paris) |
| **Jan. 2010- June 2011** | Internship *"Synthesis of a potential antibiotic, inhibitor of ASADH enzyme"* **Université of Bristol**, (Bristol) |

## TECHNICAL SKILLS

Extensive and strong organic synthesis skills

| | |
|---|---|
| Analytical techniques | 1D and 2D NMR, HPLC, MALDI and ESI-Mass spectrometry, FT-IR and UV-Vis spectroscopy, X-ray powder diffraction, Brunauer-Emmet-Teller adsorption |
| Surface analysis methods | Scanning Electron Microscopy (SEM)<br>Transmission Electron Microscopy (TEM)<br>Atomic Force Microscopy (AFM) |

## IT SKILLS

- Extensive knowledge of Microsoft Office Pack
- Able to produce reviews from PubMed and SciFinder search
- Proficient in chemistry software: ChemBioDraw Suite, NMR software and Mercury
- Photoshop, InDesign

Mohamed EL IDRISSI

## LANGUAGES

| | | | |
|---|---|---|---|
| -French | Native language | -Spanish | Basic knowledge |
| -English | Fluent | -Arab | Basic knowledge |
| -Berber | Native language | | |

## MANAGEMENT RELATED SKILLS

- Management (partly) and elaboration of collaborative research reports for European projects
- Supervision and scientific formation of trainees
- Experience of assistant lecturer for bachelor students
- Excellent interpersonal skills and strong team spirit

## PUBLICATIONS, BOOK CHAPTER AND AWARD

El Idrissi, M.; Molina, A.; Frascari, D.; Corvini, P. F.-X.; Shahgaldian, P.; Cyclodextrin-based polymeric materials for the specific recovery of polyphenolic compounds through supramolecular host-guest interactions, *J. Incl. Phenom. Macrocycl. Chem.,* **2017***,* 1-8.

El Idrissi, M.; Paterson, J. M.; Corvini, F.-X.; Teat, J. S.; Dalgarno, J. S.; Shahgaldian, P.; Template-free hierarchical self-assembly of a pyrene derivative into supramolecular nanorods, *Chem. Commun.,* **2017**, 53, 1973-1976.

El Idrissi, M.; Moridi, N.; Shahgaldian, P., Function-Oriented Molecular Design of Cyclodextrins In *Encyclopedia of Physical Organic Chemistry*, W. Zherong, Ed. Wiley-VCH, Weinheim: **2017,** DOI: 10.1002/9781118468586.

Award from the Swiss Nanoscience Institute (SNI) for best scanning electron microscope micrograph, **2015.**

## ORAL AND POSTER PRESENTATIONS AT CONFERENCES

| | |
|---|---|
| **September 2016** | Poster presentation at the Swiss Chemical Society Meeting, (Zurich). |
| **June 2016** | Poster presentation at the Swiss Nano Convention, (Basel). |
| **October 2015** | Talk at the ICID2015 event, (Montpellier). |
| **April 2014** | Poster presentation at the Clariant Chemistry Day, (Basel). |
| **May 2013** | Poster presentation at the Swiss Nano Convention, (Basel). |

## INTERESTS

**Sport**
Running
Play football and golf
**Literature and Art**
Book aficionado
Painting and photography
**Philanthropic Activities**
President and founder of Selsebil (association promoting education and culture for children in remote places)